Molecular Engineering Approaches against Germs, Spores and Biofilm Formation

Luo Mi

A dissertation

submitted in partial fulfillment of the

requirements for the degree of

Doctor of Philosophy

University of Washington

2014

Reading Committee:

Shaoyi Jiang, Chair

Daniel M. Ratner

James D. Bryers

Program Authorized to Offer Degree:

Chemical Engineering

University of Washington

Abstract

Molecular Engineering Approaches against Germs, Spores and Biofilm Formation

Luo Mi

Chair of the Supervisory Committee:
Professor Shaoyi Jiang
the Department of Chemical Engineering

Bacterial surface adhesion, colonization and related infections have been major issues plaguing many industrial and biomedical applications. In fact, the very subject has posed engineering challenges and incented scientific questioning for as long as the history of modern day microbiology and materials science themselves. With the rapid advances of molecular engineering in the past few decades, engineers as well as scientists are now equipped with new tools to study and solve these age-old problems. In the wake of these recent developments, the central goal of this thesis is essentially three-fold: first, to expand the existing zwitterionic nonfouling polymer platform for the search of novel and pragmatic solutions to bacterial surface adhesion and subsequent proliferation; second, to adopt a chemical biology approach to understand and potentially combat the extreme

survivability of bacterial endospores; and lastly to explore the possible new routes and targets for future anti-virulence small molecules against biofilm formation. This dissertation is thus divided into these three sections accordingly:

Traditional zwitterionic polymers have been widely accepted and routinely applied because of their biocompatibility and nonfouling property. However, less recognized are their responsiveness to environmental stimuli, their chemical malleability, their ease to be integrated into more complex systems as well as the biological significance of this polymer structural diversity. It is the intention to the first part of this dissertation to expand our current capacity and understanding of zwitterionic-based materials to cater to more complicated or more specific biomedical scenarios. Four aspects of molecular engineering were presented in this section: (1) first, to exploit the pH responsive property of traditional carboxylbetaine zwitterionic polymers for bacteria detection; (2) one step further, on a monomer level, to design novel hydrolysable zwitterionic molecules that are simultaneously nonfouling and antimicrobial; (3) on a polymeric level, to integrate an antimicrobial zwitterionic derivative portion into wound dressing block copolymers that can undergo both monomer hydrolysis as well as polymer temperature-induced *in situ* gelation; (4) and finally to investigate how different molecular structures impact zwitterionic polymer performance in complex biological environments, and, in particular, their interactions with bacterial extracellular polysaccharides (EPS).

Bacterial endospores are among the most tenacious life forms on earth, and are highly resistant to traditional antibiotic compounds and disinfection procedures. For this reason, in the second part of this thesis, the focus was shifted from normal vegetative bacterial cells to dormant bacterial endospores: first, to unveil the mechanism behind spore

extreme survivability by studying dodecylamine (DDA) lethal germination process as a model system; and second, to apply this newly acquired fundamental understanding in the design of new environmentally benign and easily implementable anti-spore strategies.

Perhaps the most urgent challenge and threat facing clinical microbiology at the moment is the rapid emergence of antibiotic-resistant strains due to decades of extensive usage of antibiotic drugs. One promising strategy to circumvent this problem of rapid evolution under strong antibiotic selection pressure is the development of so-called “anti-virulence” drugs that seeks to disarm bacteria by limiting their virulent phenotypes instead of directly killing bacteria. The last part of this thesis explore the feasibility of using bacterial osmoprotectant analogues as such anti-virulence metabolites to interfere with glycine betaine homeostasis and potentially impair *P.aeruginosa* biofilm formation without causing a detrimental effect on planktonic bacterial cells.

Table of Contents

List of Figures v

List of Schematics vii

List of Tables vii

Chapter 1. Introduction 1

Chapter 2. pH Responsive Properties of Nonfouling Mixed-Charge Polymer Brushes Based on Quaternary Amine and Carboxylic Acid Monomers 4

2.1 Introduction 4

2.2 Materials and Methods 7

2.2.1 Chemicals: 7

2.2.2 Preparation of initiator-coated SPR Chips: 7

2.2.3 Atom transfer radical polymerization (ATRP) of TMA:CAA mixed-charge and pSBMA surfaces: 8

2.2.4 Film thickness measurement and surface characterization: 9

2.2.5Measurement of protein adsorption on gold substrates coated with TMA:CAA and pSBMA by surface plasmon resonance (SPR) sensors: 10

2.2.6 Bacteria species and culture conditions: 10

2.2.7 Bacteria attachment assay under flow condition: 11

2.2.8 Bacteria detachment by hydrodynamic methods: 12

2.2.9 Atomic force microscope force curves: 12

2.3 Results and Discussion 13

2.4 Conclusions 17

2.5 Acknowledgements 17

2.6 Chapter Figures 18

Chapter 3. Synchronizing Nonfouling and Antimicrobial Properties in a Zwitterionic Hydrogel 26

3.1 Introduction 26

3.2 Materials and Methods 29

3.2.1 Chemicals: 29

3.2.2 Hydrolysis of CBSA monomer 31

3.2.3 Hydrogel synthesis and drug release 31

3.2.4 Protein fouling test 32
3.2.5 Bacteria surface adsorption test 33
3.2.6 Bacteria growth inhibition test 34
3. 3 Results and discussion 34
3. 4 Conclusions 38
3.5 Acknowledgements 38
3.6 Chapter Figures 39
Chapter 4. A Thermo-responsive Antimicrobial Wound Dressing Hydrogel Based on a Cationic Betaine Ester 48
4.1 Introduction 48
4.2 Materials and Methods 51
4.2.1 Chemicals: 51
4.2.2 Synthesis of triblock copolymer NIPAM-co-CBAA-1-C2SA: 52
4.2.3 Gel permeation chromatography: 53
4.2.4Measurements of polymer phase transition temperature: 53
4.2.5 In vitro SA^- release and HPLC analysis: 54
4.2.6 Bacteria growth inhibition: 54
4.2.7 Mammalian fibroblast COS-7 cell culture and cytotoxicity assay: 55
4.2.8 COS-7 cell surface attachment assay: 56
4.3 Results and Discussion 56
4.3.1 Synthesis of triblock copolymer via RAFT 56
4.3.2 LCST and gelation property of triblock copolymer solution 57
4.3.3 Drug release and antimicrobial activity 58
4.3.4 Mammalian cell cytotoxicity 59
4.3.5 Initial attachment of mammalian fibroblast onto hydrogel surface 60
4.4 Conclusions 61
4.5 Acknowledgements 61
4.6 Chapter Figures 62
Chapter 5. Divalent Cation-mediated Polysaccharide Interactions with Zwitterionic Surfaces 73
5.1 Introduction 73
5.2 Materials and Methods 76

5.2.1 Chemicals 76
5.2.2 Preparation of self-assembled monolayers 77
5.2.3 Surface-initiated atom transfer radical polymerization 77
5.2.4 Measurements of polysaccharide adsorption 78
5.2.5 Quantum chemical calculations 79
5.3 Results and Discussion 79
5.3.1 Mg^{2+} mediated alginate binding on PSBMA, PCBMA-2 and PCBAA-1 79
5.3.2 Quantum chemical calculations on CBMA-2 and CBAA-1 head groups 82
5.3.3 Effect of polysaccharide molecular weight and chemical structure on Mg^{2+} mediated surface adsorption 83
5.4. Conclusions 83
5.5 Acknowledgements 84
5.6 Chapter Figures 85
Chapter 6. Chemical Insights into Dodecylamine Spore Lethal Germination 92
6.1 Introduction 92
6.2 Materials and Methods: 94
6.2.1 Chemicals 94
6.2.2 RAFT Polymerization of AMA Monomer 96
6.2.3 Spore Lethal Germination Assay 97
6.2.4 Molecular Dynamic Simulations 98
6.3 Results and Discussions 99
6.3.1 DDA primary ammonium head group. 99
6.3.2 DDA alkyl tail. 101
6.3.3 Structural determinants for antispore compounds 103
6.4 Conclusions 106
6.5 Acknowledgements 106
6.6 Chapter Figures 107
Chapter 7. A Green-Chemistry-Oriented Sporicidal Cocktail 113
7.1 Introduction 113
7.2 Materials and Methods 114
7.2.1 Chemicals 114
7.2.2 Evaluating chemical antispore potency in solution 115

7.2.3 Evaluating chemical antispore potency on surface 115
7.2.4 Phase contrast microscopy 116
7.3 Results and Discussions 116
7.4 Conclusion 119
7.5 Chapter Figures 121
Chapter 8 Reducing *Pseudomonas aeruginosa* Biofilm Formation with Osmoprotectant Analogues as Anti-virulence Metabolites 126
8.1 Introduction 126
8.2 Materials and Methods 129
8.2.1 Chemicals: 129
8.2.2 Bacterial strains and culture conditions: 129
8.2.3 Growth curve measurement and biofilm quantification: 130
8.3 Results and Discussion 131
8.3.1 Anti-biofilm effects of osmoprotectant analogues 131
8.3.2 Ethylcholine and bacterial antibiotic susceptibility 132
8.3.3 Metabolic fate of ethylcholine and its genetic-level impact 133
8.4 Conclusions 134
8.5 Chapter Figures 135
Chapter 9. Conclusions 141
Acknowledgements 144
Curriculum Vitae 145
References 147

List of Figures

Figure 2.1 SPR sensorgram detecting adsorption of 1 mg/mL fibrinogen and lysozyme to TMA:CAA copolymer coated surfaces at pH 7.4. 20
Figure 2.2 Representative fluorescence microscopy images of *S.epidermidis* attachment to uncoated Au, TMA:CAA copolymer, and pSBMA surfaces..... 21
Figure 2.3 Quantitative analysis of *S.epidermidis* attachment to bare Au, TMA:CAA copolymer, and pSBMA surfaces..... 22
Figure 2.4 Representative fluorescence microscopy images showing *S.epidermidis* pH 4.5 initial attachment to uncoated Au, TMA:CAA copolymer, pSBMA surfaces and detachment at higher pH. 23
Figure 2.5 Quantitative analysis of *S.epidermidis* pH 4.5 initial attachment to bare Au, TMA:CAA copolymer, pSBMA surfaces and and detachment at higher pH.. 24
Figure 2.6 Average adhesion forces of $HS(CH_2)_{11}SO_3$ SAM modified AFM tips scanning over pSBMA and TMA:CAA copolymer surfaces in high and low pH aqueous buffer solutions. 25
Figure 3.1 (a) Chemical structure of PCBSA PCBMA-2 and PCBMA-1-C2 SA (b) A hydrogel made up of the PCBSA polymer that is able to keep the surface free from bacteria and inhibit bacterial growth in bulk..... 40
Figure 3.2 Reaction scheme for the synthesis of the CBSA monomer and subsequent radical polymerization..... 41
Figure 3.3 (a) The monomer hydrolysis curve of CBSA monomer in PBS 20^oC (b) The cumulative drug release of three hydrogels each. 42
Figure 3.4 The monomer hydrolysis curve of CBSA monomer in pH~4 H_2O at 4 ^oC and 20^oC..... 44
Figure 3.5 Hydrogel protein nonfouling property as determined by incubation in 0.1mg/ml FITC labeled Fg protein solution..... 45
Figure 3.6 (a) Bacterial surface adhesion on PCBSA, PCBMA-1-C2 SA, PCBMA-2 hydrogels as well as on the polystyrene control surface. (b) The growth inhibition of PCBSA, PCBMA-1-C2 SA and PCBMA-2 hydrogels against *S. epidermidis*..... 47
Figure 4.1 ^1H- NMR spectra of three polymers: Triblock I, Triblock II and PNIPAM in D_2O..... 64
Figure 4.2 GPC trace of $PNIPAM_{218}$ and $PNIPAM_{454}$ in DMF running at 0.5ml/min and 60^oC. PDI for both polymers are below 1.1. 65
Figure 4.3 GPC trace of PNIPAM and Triblock II in water with 0.5M $NaNO_3$ running at 0.5ml/min and 25^oC..... 66
Figure 4.4 Hydrodynamic radius change of 0.1wt% (a) Triblock I, (c) Triblock II and (e) PNIPAM in water as temperature ramps from 20^oC to 50^oC together with representative pictures of three polymer solutions: (b) 20 wt% Triblock I (d) 20wt% Triblock II and (f) 5 wt% PNIPAM in a gelation test at 37^oC..... 68
Figure 4.5 Release profile of Salicylate from the 20wt% Triblock II hydrogel disc in PBS at 37^oC as determined from reverse phase HPLC..... 69
Figure 4.6 OD 600 of *E.coli* K12 inoculated LB liquid media after 12 h coincubation with various hydrogels. 70

Figure 4.7 Normalized number of COS-7 cells remaining in the cell culture supernatant after 2-hour cell incubation on various surfaces. 71
Figure 4.8 Cytotoxicity of Triblock II (SA) hydrogel leach-out on COS-7 cell..... 72
Figure 5.1. High molecular weight alginate adsorption onto PSBMA, PCBMA-2, and PCBAA-1 polymer surfaces as Mg^{2+} concentration changes from 0 to 20 mM in the PBS running buffer..... 87
Figure 5.2 Comparison between protein fouling (undiluted human plasma) and polysaccharide adsorption at 20mM Mg^{2+} on three zwitterionic polymer coated surfaces..... 88
Figure 5.3 Electron density surfaces of CBMA-2 (a) and CBAA-1 (b) 89
Figure 5.4 (a) Representative SPR sensorgrams of high molecular weight alginate, low molecular weight alginate, and dextran adsorption on PCBMA-2 surfaces with a PBS running buffer supplemented with 0mM, 5mM and 20mM Mg^{2+}. (b) Statistical results of high molecular weight alginate, low molecular weight alginate, and dextran adsorption on PCBMA-2 surfaces with a PBS running buffer supplemented with 0mM or 20mM Mg^{2+}..... 91
Figure 6.1 The role of primary ammonium head groups in DDA lethal germination.. 109
Figure 6.2. The role of DDA alkyl tail in spore germination studied using primary ammonium monomers and polymers. 110
Figure 6.3 The loss of spore viability after exposure to DMAG 112
Figure 7.1 *B. megaterium, B. atrophaeus* and *B. cereus* spore survival percentage after exposure to various chemical conditions at 40^{o}C for 30 min..... 122
Figure7.2 a) Representative phase contrast microscopy photos of dormant and nutrient-germinated *B. megaterium* spores as well as spores exposed to pH 2 10mM SDS solution at 40^{o}C for 30min. D **b)** *B. megaterium* spore survival percentage after exposure to 10mM SDS solution with 10% ethanol under different pH. **c)** *B. megaterium* spore survival percentage after exposure to 10mM SDS solution with 10% ethanol at neutral pH but supplemented with various metal cations. **d)** *B. megaterium* spore survival percentage after exposure to pH 2 buffer with 10% ethanol at various SDS concentrations. **e)** *B. megaterium* spore survival percentage after exposure to pH 2 buffer with 10% ethanol supplemented with anionic surfactant SDS and SHS, cationic surfactant DTAC, metal chelating agent EDTA and protein denaturing agent urea. All incubation conditions from **b-e** were identical at 40^{o}C and 30 min..... 124
Figure7.3 The proposed antispore mechanism of low pH and SDS.. 125
Figure 8.1: Chemical structures of osmoprotectant analogues together with glycine betaine and choline tested in this study. 135
Figure 8.2 24 h biofilm formation of *P.aeruginosa* PAO1 supplemented with various chemical compounds at 10mM in LB media.. 136
Figure 8.3 Growth curves of *P.aeruginosa* PAO1 in LB media **a)**; LB media supplemented with 10mM compound 4 ethylcholine **b)**; LB media supplemented with 10mM compound 17 trigonelline **c)** and LB media supplemented with 10mM potassium iodide **d)**. 137
Figure 8.4 24 h biofilm formation of *P.aeruginosa* PAO1 and *P.aeruginosa* MPAO1 at 10mM, 5mM and 1mM ethylcholine concentration..... 138

Figure 8.5 *P.aeruginosa* PAO1 survival after exposure to tobramycin (20ug/ml), gentamicin (10ug/ml) or nalidixic acid (60ug/ml) with or without additional ethylcholine at 10mM..... 139
Figure 8.6: **a)** Conversion of choline and ethylcholine into their respective zwitterionic forms in *P.aeruginosa* by BetAB. **b)** 24 h biofilm formation of *P.aeruginosa* MPAO1 and various isogenic mutants with or without additional 1mM ethylcholine in the growth media.. 140

List of Schematics

Scheme 2.1: Chemical structures of TMA and CAA monomers and the TMA:CAA random copolymer..... 18
Scheme 2.2 A surface switching from fouling to non-fouling in response to environmental pH change..... 19
Scheme 4.1 Synthesis route of thermo-responsive wound dressing copolymers. 62
Scheme 5.1 Chemical structures of PSBMA, PCBMA-2 and PCBAA-1 polymers. 85
Scheme 5.2 Scheme 2: Mg^{2+} mediated alginate adsorption onto zwitterionic polymer coated surfaces monitored by SPR. 96
Scheme 6.1. Proposed model of interactions between DDA and spores..... 107

List of Tables

Table 4.1 PNIPAM homopolymer and triblock copolymer DP and PDI..... 63
Table 4.2 Gelation property of triblock copolymers at 37^{o}C with different concentrations 63

Chapter 1. Introduction

The tendency to bind to abiotic surfaces and the resistance to environmental adversities are evolutionary adaptation strategies central to bacteria survival [1, 2]. The ability to intercept bacteria surface association and to eliminate bacteria, both planktonic as well as surface bound, have become important themes in the field of molecular engineering [3, 4]. Because of the gravity of the issue, related technological advances can potentially bring profound biomedical and social impacts. In addition to the aforementioned bacterial surface adhesion, bacterial sporulation and post-adhesion biofilm development are also pressing issues hindering current clinical and industrial applications, this work seeks to address these three challenges in three corresponding sections:

The first part of the dissertation focuses on providing pragmatic solutions to specific biomedical scenarios, and, through chapters 2~5, to show the capability to detect, repel and eliminate bacteria by the use of zwitterionic polymers and their derivatives. In chapter 2, a carboxylate-based mixed-charge copolymer surface coating was designed to enhance the pH-response property of more traditional carboxybetaine zwitterionic polymers [5]. The pH-dependent sticky/nonfouling surface transition of the resulting biomaterial was shown to be potentially useful in various bacterial detection applications. Chapter 3 aims to combine the two popular strategies against bacterial surface fouling, i.e. antimicrobial [6-8] and nonfouling [9-11], into one single zwitterionic platform via monomer design. To this end, an antibacterial zwitterionic homopolymer coating was synthesized and demonstrated to simultaneously prevent bacterial surface adhesion as

well as bulk-phase proliferation. In chapter 4, the successful integration of zwitterionic ester precursor with the thermo-responsive poly(N-isopropylacrylamide) (PNIPAM) moiety created a clinical hydrogel that caters to the various aspects of a wound healing process including the reduction in bacterial infection risk [12] and the promotion of tissue regeneration [13]. Finally, in chapter 5, an effort was made to go beyond the current notion of equating bacterial nonfouling with non-protein adsorption [14] and unveiled the structural parameters critical for zwitteroinic polymer nonfouling performance in repelling polysaccharide-rich bacterial species [15].

Many chemical or physical procedures have been developed over the years to successfully eliminate vegetative bacterial cells. However, such antibacterial methods usually have little effects on bacterial endospores as a result of their metabolically dormant state. The second part of this thesis attempts to address this long-standing bioengineering challenge from two different aspects. In chapter 6, a fundamental study was conducted to understand the chemical basis for dodecylamine (DDA), the most potent antispore agent known [16], lethal germination process. Furthermore, the structural determinants underlying DDA unusual bioactivity was also discovered in this this study. Based on this newly acquired understanding, the first green-chemistry-oriented antispore tri-component chemical system was presented and evaluated in chapter 7, with the aim to ultimately replace the current spore chemical sterilization procedures that typically require environmentally-damaging oxidizing agents.

The third part (chapter 8) explores the possibility of targeting bacterial glycine betaine homeostasis to specifically reduce *P.aeruginosa* biofilm formation without the necessity to kill planktonic bacterial cells. The main motivation behind this anti-virulence approach

is to seek an alternative strategy against biofilm phenotype and not incur the strong evolutionary selection pressure for resistant strains as typically associated with conventional antibiotic drugs.

Chapter 9, the last chapter, summarizes those studies presented in previous chapters.

Chapter 2. pH Responsive Properties of Nonfouling Mixed-Charge Polymer Brushes Based on Quaternary Amine and Carboxylic Acid Monomers

In this work, we report a tunable mixed-charge copolymer surface containing positively-charged quaternary amine monomers ([2-(Acryloyloxy)ethyl] trimethyl ammonium chloride, TMA) and negatively-charged carboxylic acid monomers (2-carboxy ethyl acrylate, CAA). The nonfouling properties of this copolymer coating depend on environmental pH. The surface has charge neutrality under neutral and basic conditions, and is positively charged under acidic conditions due to the protonation of the carboxylic acid group. This transition in surface charge with respect to pH allows the surface to be switched from bacteria-adhesive to bacteria-resistant. We demonstrate that the bacteria adhered to the surface under acidic conditions can be easily released as bulk pH increases. This tunable surface can be used to collect a contaminant and then be externally stimulated to release the contaminant, to allow for analysis of its composition. Its bacteria attraction and release property makes it very promising for decontamination and biomedical applications.

2.1 Introduction

Bacterial contamination and infection are critical issues in both industry and medicine [17-21]. Materials or surface coatings which can be used in collecting, detecting, analyzing, and cleaning bacterial contamination are under increasing demand. It is of

great interest to develop a material that can be used to collect a contaminant (e.g., biomacromolecules or bacterial cells) and then be stimulated with an external signal to release the contaminant, to allow for an analysis of its composition. The whole-cell isoelectric point of most bacteria strains are usually in the pH range of 1.5 to 4.5 [22] and under pH conditions above their isoelectric point, the bacterial cells are negatively charged and can be attracted by cationic materials [23]. On the other hand, in order to release the contaminant, a non-fouling material is required and an overall neutral charge is necessary [24-25]. Our previous studies demonstrated that zwitterionic surface coatings such as poly(carboxybetaine methacrylate) (pCBMA) and poly(sulfobetaine methacrylate) (pSBMA) can efficiently prevent protein adsorption and bacterial adhesion/biofilm formation [11, 26]. We have further reported that surface coatings and hydrogels formed from mixtures of positively charged [2-(methacryloyloxy)ethyl] trimethyl ammonium chloride (TM) and negatively charged 3-sulfopropyl methacrylate potassium salt (SA) monomers show similar non-fouling properties to zwitterionic surface coatings, as long as the overall charge is kept neutral [27-29]. It is very important and challenging to develop a surface which can switch between fouling and nonfouling properties by changing its surface charge. The tunable properties of these zwitterionic or mixed-charge materials will allow for their broad applications in protection (enhanced protective activity), decontamination (physical wipe), and detection (agent recovery). pCBMA has been shown to have this type of responsive behavior based on the protonation state of the carboxylic acid group in the zwitterionic side chain [5]. pCBMA surfaces were shown to be nonfouling in intermediate to high ionic strength solutions and at pH values that ranged from neutral to basic. These same pCBMA surfaces were shown to be slightly

fouling at lower salt concentrations and under acidic pH conditions, but the observed changes in this surface property was too insignificant to have any impact on practical applications. Thus, a material which is more sensitive to pH changes under a wider range is highly desirable.

Herein we report a mixed-charge copolymer surface composed of positively-charged quaternary amine ([2-(Acryloyloxy)ethyl] trimethyl ammonium chloride, TMA) and negatively-charged carboxylic acid (2-carboxy ethyl acrylate, CAA) monomers, as shown in Scheme 2.1. Under neutral and basic conditions, the copolymer has an overall neural charge that gives the copolymer its nonfouling property. The carboxylic acid group becomes protonated under low pH conditions, making the copolymer positively charged. This pH responsive surface chemistry gives rise to distinct bacteria attraction and release properties under different pH conditions as shown conceptually in Scheme 2.2 and confirmed in this study. The transition in surface charge was further characterized and verified with force curve measurements using atomic force microscopy (AFM). The improvement in the pH responsiveness of the TMA:CAA copolymer over the previously reported pCBMA polymer brush coating results from a reduction in the interference caused by the proximity of the oppositely charged groups. pSBMA is used as a negative control surface in this pH responsive study because the sulfo group of pSBMA is completely deprotonated within a wide range of pH values, keeping the nonfouling properties of pSBMA independent of pH changes.

2.2 Materials and Methods

2.2.1 Chemicals:

Fibrinogen, fraction I from bovine plasma (Fg) and lysozyme from chicken egg white (Lyz) were purchased from Sigma-Aldrich (Milwaukee, WI). Anhydrous sodium acetate, 1,1,4,7,10,10-hexamethyltriethylenetetramine (HMTETA 97%), TMA (80 wt.% solution in water), CAA, *N*-(3-sulfopropyl)-*N*-(methacryloxyethyl)-N,N-dimethylammonium betaine (SBMA, 97%), copper(I) bromide (99.999%), copper(II) bromide (99.999%), 2,2'-bipyridine (BPY, 99%), tetrahydrofuran (THF, HPLC grade), and 0.15M phosphate-buffered saline (PBS) were also purchased from Sigma-Aldrich. Ethanol (absolute 200 proof) was purchased from AAPER Alcohol and Chemical Co. Methanol was obtained from Omnisolv, EMD Chemicals Inc. Glacial acetic acid was purchased from Mallinckrodt Baker, Inc. Water used in the experiments was purified using Simplicity 185 water purification system from Millipore Co. THF for reactions and washings was dried by sodium before use.

Mercaptoundecyl bromoisobutyrate was synthesized through the reaction of bromoisobutyryl bromide and 11-mercapto-1-undecanol using a method published previously[30]. Bromoisobutyryl bromide and 11-mercapto-1-undecanol were purchased from Sigma-Aldrich.

2.2.2 Preparation of initiator-coated SPR Chips:

Electron beam evaporation under vacuum was used to coat glass samples with a layer of titanium (2 nm) to promote the adhesion of a subsequent layer of gold (48 nm). Before self-assembled monolayer (SAM) preparation, the substrates were washed with pure

ethanol, cleaned with a UV-ozone cleaner (Jelight, model 42) for 20 min, and then washed with water and pure ethanol. The initiator SAMs were formed by soaking gold-coated substrates in a pure ethanol solution containing 0.1mM ω-mercaptoundecyl bromoisobutyrate at room temperature for 24 h. Before polymerization, substrates were rinsed with pure ethanol, followed by THF, and dried with a stream of nitrogen.

2.2.3 Atom transfer radical polymerization (ATRP) of TMA:CAA mixed-charge and pSBMA surfaces:

The optimal TMA:CAA mixed-charge copolymer polymerization conditions determined in this study were as follows: SPR gold chips and gold coated Si wafers immobilized with initiators were placed in a reaction tube with Cu(I)Br (1.0mmol) and purged with nitrogen. TMA (7.0mmol) and CAA (7.0mmol) were mixed in 5 ml water, and then the pH of this mixture was adjusted to 6.0 with concentrated base (3.0 M NaOH) before adding 5ml of deoxygenated methanol. HMTETA (0.27ml) was added into 10ml deoxygenated methanol. The HMTETA solution and monomer mixtures were separately purged with nitrogen for 20 minutes. Following the purging, the monomer and HMTETA solutions were moved into the reaction vessel using a deoxygenated syringe. The 20ml ATRP reaction solution was further purged with nitrogen for 20 minutes. The reaction was allowed to proceed for 24 hours in a shaker at room temperature. Following the reaction, the samples were removed from the reaction tube and immersed in PBS overnight before use.

SBMA was grafted to the Au coated SPR chips via ATRP following a method reported previously [31]. Water and methanol were deoxygenated by passing a continuous stream of dry N_2 through the solution for 15 minutes at room temperature. Initiator-coated

samples were sealed in a glass tube with BPY (1.34 mmol), CuBr (0.54 mmol), and $CuBr_2$ (0.05 mmol), deoxygenated for 15 minutes, dissolved in methanol (10.0 ml), and left at room temperature under N_2. SBMA (26.75 mmol) was sealed in a separate glass tube, deoxygenated for 15 minutes, dissolved in a mixture of water (5.0 ml) and methanol (10.0 ml), and left at room temperature under nitrogen protection. The monomer solution was then transferred into the sample tube with a syringe under nitrogen protection. After overnight polymerization, the samples were removed, washed with warm PBS solution (60^o C), and dried under a stream of N_2. The samples were then immersed in PBS overnight before use.

2.2.4 Film thickness measurement and surface characterization:

The thickness of the polymer brushes formed on a substratum surface was measured by atomic force microscopy (AFM) in the contact mode using a Dimension 3100 AFM (Digital Instruments/Veeco, Woodbury, NY) operated in air. Commercial Si_3N_4 cantilevers (DI) with an elastic modulus of 0.56N/m were used. Gold-coated Si wafers were patterned using standard photolithography techniques to obtain lines of Au with a width and line spacing of ~25 μm and a measured step height of 48.2 ± 1.4 nm. These patterned wafers were then subjected to ATRP reaction together with the regular SPR chips and the step height was measured again to determine the thickness of the polymer brush coating. The polymer surfaces were blown dry with filtered air before analysis. For each polymer brush modified surface, 5 height measurements were performed.

2.2.5Measurement of protein adsorption on gold substrates coated with TMA:CAA and pSBMA by surface plasmon resonance (SPR) sensors:

In this study, a custom-built SPR sensor was used to measure protein adsorption on the coated substrata. An SPR chip was attached to the base of the prism and optical contact was established using refractive index matching fluid (Cargille). A flow cell with four independent parallel flow channels was used to contain liquid samples during experiments. A peristaltic pump (Ismatec) was used to deliver liquid samples to the four channels of the flow cell. Fibrinogen and lysozyme solutions of 1.0 mg/mL in PBS (0.15 M, pH 7.4) were delivered to the surfaces at a flow rate of 0.05 ml/min. A surface-sensitive SPR detector was used to monitor protein-surface interactions in real time. In this work, the wavelength shift between buffer baselines established before and after protein injection was used to quantify the change in surface concentration (mass per unit area). For the SPR sensor used in the study, a 1 nm SPR wavelength shift at 750 nm represents a surface coverage of ~15 ng/cm^2 adsorbed proteins.

2.2.6 Bacteria species and culture conditions:

S*taphylococcus epidermidis* ATCC 14990 was used in the bacteria attachment assay in this study. The optimal growth temperature for *S.epidermidis* is 37^{o}C. *S.epidermidis* was first cultured overnight at 37^{o}C on Luria-Bertani (LB) (BD, USA) agar plates. Cultures on agar plates can be used for two weeks, if kept at 4^{o}C. Several colonies from a plate were used to inoculate 25ml of LB media. These initial cultures were incubated at 37^{o}C with shaking at 200 rpm for 18 hours and then 100ul was used to inoculate a second LB medium that was used in the bacteria attachment assay described below.

2.2.7 Bacteria attachment assay under flow condition:

The second LB inoculated bacteria culture was incubated at 37 ^{o}C, with shaking at 200 rpm until the optical density as measured at 600 nm reached 1.0. At this point, the bacteria from the culture was collected by centrifugation, washed 3 times with sterile, neutral PBS solution, and subsequently diluted into buffers of different pH values to a concentration of 1x10^{8} cells/ml. In this study, sodium acetate buffer was used to obtain a pH ~4.5 solution and PBS was used to obtain solutions with pH values ~7.4 and 10.0. All three buffer solutions were prepared at the same ionic strength of 150mM.

The cell suspension was delivered into a custom built flow chamber (75 mm x 25 mm x 3 mm) by a peristaltic pump at a volumetric flow rate of 6 ml/min (corresponding to a shear stress of 0.0027 Pa) for 3 hours. Gold coated Si wafers covered with polymer brushes composed of pSBMA, TMA:CAA or without any polymer brush modification were mounted into the flow chamber and were allowed to soak in buffer solutions with a pH of 4.5, 7.4, or 10.0 for at least 30 minutes before the cell suspension in an identical buffer was introduced.

After 3 hours of continual cell suspension exposure, the flow chamber was washed with the sterile buffer of an identical pH for 15 minutes at flow rate of 6 ml/min for 15 minutes to remove loosely attached bacteria. The wafer chips were then carefully removed from the flow chamber without causing air bubble formation inside the chamber [32]. After this, all of the wafer chips were stained with Baclight (Molecular Probes, Inc.) for 10 minutes and then imaged using a CCD-CoolSNAP camera mounted on a Nikon Eclipse 80i microscope using a 100x oil lens and epifluorescent illumination through a FITC filter.

2.2.8 Bacteria detachment by hydrodynamic methods:

An *S.epidermidis* cell suspension was prepared in a similar fashion to that in the attachment assay. After 3 times washes with neutral PBS, the concentrated cell suspension was diluted in sodium acetate buffer with a pH of 4.5 to a final cell concentration of $6x10^8$ cells/ml. The suspension was then delivered into the flow chamber at flow rate of 8 ml/min for 30 min to allow bacteria attachment to the surface. Following this, sterile sodium acetate buffer was used to rinse the surface at the same flow rate for 15 minutes, to remove loosely attached bacteria. Several substrates with different surface modifications were carefully removed from the flow chamber at this stage in order to determine the bacteria cell density before performing the hydrodynamic detachment study. The remaining samples in the flow cell were then exposed to an increased volumetric flow rate corresponding to a shear stress of 0.2 Pa of buffer solutions with a pH of 4.5 or 10.0. The hydrodynamic detachment process was allowed to proceed for 30 minutes before the remaining wafer chips were removed, stained, and imaged for bacteria cell counting.

2.2.9 Atomic force microscope force curves:

TMA:CAA copolymer and pSBMA ATRP coated SPR chips were used in force curve experiments. Measurements were performed using Dimension 3100 AFM in aqueous contact mode. Before measurements were performed, AFM tips (DNP-S20, Veeco) with a spring constant of 0.06N/m were coated with a 2 nm chromium adhesive layer and a 20 nm gold layer using a thermal-evaporator (Auto 306, Edwards) to allow for subsequent SAM formation. The gold coated AFM tips were modified with $HS(CH_2)_{11}SO_3Na$

(ProChimia ,Sopot, Poland) SAMs in order to give the tips a constant negative charge within the pH range tested in the force measurements. The force curve measurements were carried out in pH 4.5 and pH 10.0 buffer solutions with an ionic strength of 150 mM. Both approach and retraction curves were recorded.

2.3 Results and Discussion

In this work, TMA:CAA mixed-charge copolymers and pSBMA were prepared via surface initiated ATRP [31]. After surface initiated polymerization, the dry thickness of the polymer brushes was determined by AFM. The measured thickness of the mixed-charge copolymer brush was 23.8 nm $\pm$ 6.1 nm and the pSBMA brush was 76.5 nm $\pm$ 5.0 nm.

In our previous study, we demonstrated that a mixed-charge statistical copolymer grafted surface would have similar nonfouling properties to polybetaine coated surfaces as long as the charged groups are uniformly mixed and the overall surface charge is neutral [29]. In this work, we tested the nonfouling property of our mixed-charge surface using SPR. Fg and Lyz were used as model proteins due to their overall negative and positive charges under neutral pH conditions, respectively. Figure 2.1 shows one representative SPR sensorgram for Fg and Lyz adsorption to TMA:CAA coated surface at 25 ^{o} C. Following the PBS buffer wash, the nonspecific Fg adsorption was 1.6 ng/cm^2 and the Lyz adsorption was 0.3 ng/cm^2 (below the sensor limit of detection) [26]. The adsorption amount for both proteins is below the commonly accepted ultra-low fouling surface criteria of <5 ng/cm^2 nonspecific protein adsorption [33]. This result also indicates that the ratio of the oppositely charged monomer species in the copolymer is close to 1:1, because there is no preferential adsorption of either protein [25].

The pH responsive properties of the various polymer brush coated surfaces were tested by using a 3-hour bacteria adhesion assay under flow conditions with a model bacteria, gram positive *S.epidermidis*. The low pH testing condition of 4.5 was chosen for two reasons. First, surface-confined carboxylic acid groups commonly have a pKa ranging from 4.5~7.7 [34]. Under a pH of 4.5, a significant portion of the carboxylic acid groups in the polymer brush are expected to be in a protonated state, resulting in a positively charged surface. Second, this pH value is higher than most bacteria whole cell isoelectric points (typical range of 1.0~4.5) [22] and thus would not drastically alter the natural bacteria surface charge. The reported whole cell isoelectric point for *S.epidermidis* is in the range of 2.3~2.6 [35], which is significantly lower than the low pH condition tested in this work. Thus, any changes in adhesion properties would be unlikely to be caused by changes in the bacteria surface charge. This was further verified by monitoring adhesion properties of bacteria on uncoated gold and pSBMA surfaces as positive and negative controls, respectively. The results for the bacteria adhesion experiments under flow conditions are shown in Figures 2.2 and 2.3. The TMA:CAA mixed-charge copolymer coated surface displayed a drastic change in its nonfouling property with respect to changes in the pH as anticipated. The greater responsive behavior of the TMA:CAA surface as compared to that previously reported for pCBMA [5] can be attributed to the increased spatial freedom and reduced interference of the oppositely charged groups in the TMA:CAA copolymer. In this coating, the oppositely charged groups are located on different side chains , while the different charged regions are located within the same side chain in the pCBMA coating. In this work, no bactericidal effects were observed from the TMA:CAA copolymer coated surface either, as confirmed through Baclight viability

staining under all conditions. This must be confirmed because of the known potential for cationic surfaces to be bactericidal, and the expected moderate positive charge of the TMA:CAA surface in the low pH environment [36].

After showing the bacteria adhesion/collection property of TMA:CAA when at pH 4.5, we proceeded to test if a subsequent increase of the bulk solution pH would lead to the release of the surface-attached bacteria cells by returning the surface to a mixed-charge nonfouling state. Before examining the bacteria detachment by means of hydrodynamic force, a high concentration suspension of bacteria cells in a pH 4.5 buffer were placed in contact with the test surfaces for 30 minutes to facilitate bacteria attachment. Following this, sterile buffer solutions of different pH values (pH 4.5 and 10.0) were pumped through the flow chamber at a rate that applied a shear stress of 0.2 Pa to the surfaces. The results shown in Figures 2.4 and 2.5 indicate that a significant decrease in the amount of surface attached bacteria is only observed for the TMA:CAA copolymer surface after the pH 10.0 rinse. Under these conditions, only 13% of the original bacteria cells were retained by the surface. The 0.2 Pa shear stress applied in this experiment is comparable to the reported lower limit of critical shear stress to remove *S.epidermidis* from a hydrophilic surface and it is significantly lower than that needed for a hydrophobic surface [37-38].

To further characterize the surface pH responsive properties and to better understand our bacteria detachment results, we obtained force curves between our polymer brush surfaces and SO_3^- terminated SAM coated AFM tips using AFM. Force curve measurements were performed in contact mode and aqueous solutions. The buffer pH and ionic strength in these measurements were the same as those used in the bacteria

detachment assay, i.e., 4.5 for the low pH condition and 10.0 for the high pH condition with an ionic strength of 150 mM for both cases. In order to maintain a relatively unvaried surface property under two pH conditions tested, AFM tips used were coated with SO_3^- terminated SAMs, whose charge is considered to be insensitive to changes in pH. The modified AFM tips are expected to be subjected to a force change similar to the bacteria cells in different pH buffer solutions because of their negative charge. Figure 2.6 showed the average adhesion forces for pSBMA and TMA:CAA mixed-charge surfaces at the two different pH conditions. A long-range acid-base attraction force is not seen in the approach curves (data not shown) due to relatively high ionic strength (150 mM), thus short Debye lengths, used in the experiment [39-40]. The vertical distance between the minima of the approach curve and the retract curve is reported as the adhesion force between tip-polymer interaction, i.e. the force required to remove the tip from the modified surface. From the force curve measurement, a strong surface adhesion force was observed between the tip and the TMA:CAA modified surface under acidic conditions, while the force is dramatically lower under the basic pH conditions. This difference can be a concerted effect of an increase of acid-base interaction and a reduction of polymer solvation after protonation at low pH for mixed-charge surfaces. As for the pSBMA control surface, no significant surface adhesion forces were observed under either pH condition. These results agree well with those from the bacteria experiments, suggesting that the TMA:CAA surface changes from a positively charged adhesive surface at pH 4.5 to a mixed-charge, nonfouling surface at pH 7.4 and 10.0.

2.4 Conclusions

In this work, we report a highly pH responsive mixed-charge copolymer surface that exhibits distinct bacterial fouling and nonfouling properties, depending on the environmental pH value. The number of bacterial cells that adhered to the TMA:CAA polymer brush coated surface showed a six-fold difference between acidic and neutral pH test conditions, while no significant differences were observed in both the positive (bare gold) and negative (pSBMA) controls. Furthermore, the adherent bacteria could be easily removed by changing the environmental pH conditions. As the environmental cue, i.e. pH change, for this surface chemistry transition is relative mild, multiple cycles of bacterial surface attachment and release should be realized without permanently damaging the mixed-charge material. The results from the bacteria adhesion/detachment assay were well supported by AFM force curve measurements obtained under different pH conditions. These results suggest that the TMA:CAA mixed-charge copolymer is very promising for effective surface enrichment, removal and detection of microorganisms.

2.5 Acknowledgements

This work is supported by the Defense Threat Reduction Agency / Joint Science and Technology Office through Grant HDTRA 1-07-1-0033. The AFM work was completed at the University of Washington Center for Nanotechnology, one of the twelve nodes of the National Nanotechnology Infrastructure Network supported by the National Science Foundation.

2.6 Chapter Figures

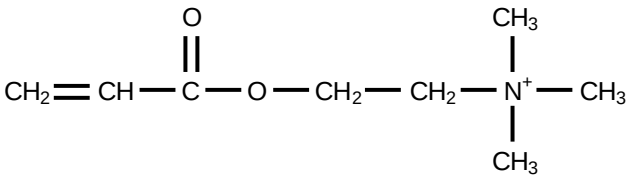

[2-(acryloyloxy) ethyl] trimethyl ammonium chloride (TMA)

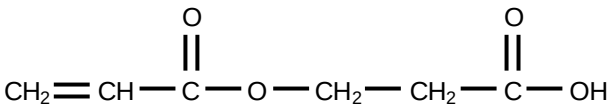

2 carboxy ethyl acrylate (CAA)

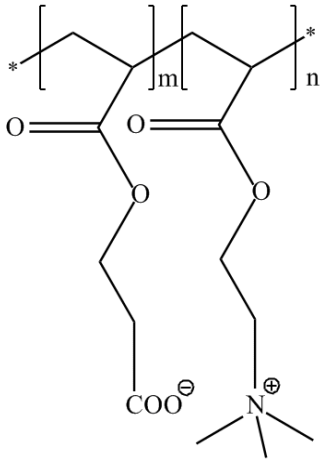

Scheme 2.1: Chemical structures of TMA and CAA monomers and the TMA:CAA random copolymer.

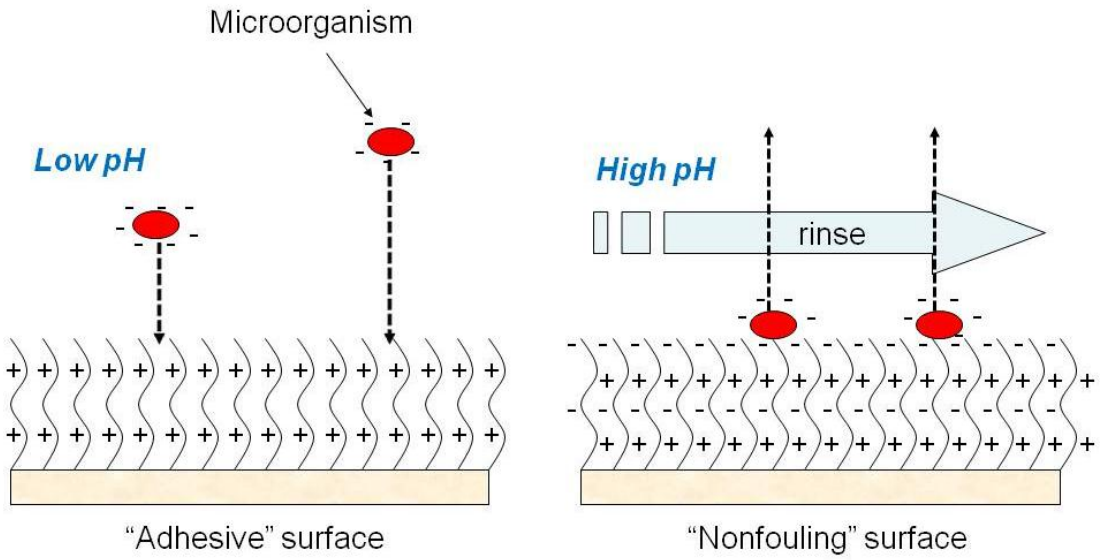

(a) **(b)**

Scheme 2.2 A surface switching from fouling to non-fouling in response to environmental pH change (a) in low pH solutions, the surface bears a moderately positive charge, favoring the attachment of bacteria cells (b) in neutral or higher pH solutions, the surface becomes non-fouling, releasing the bacteria cells.

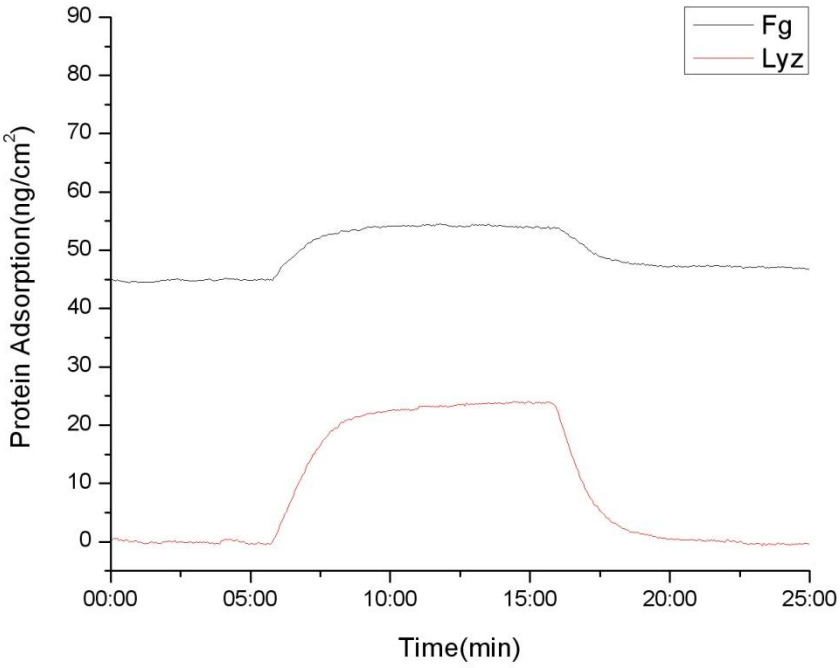

Figure 2.1 Representative SPR sensorgram showing the adsorption of 1 mg/mL fibrinogen and lysozyme to TMA:CAA copolymer coated surfaces at pH 7.4.

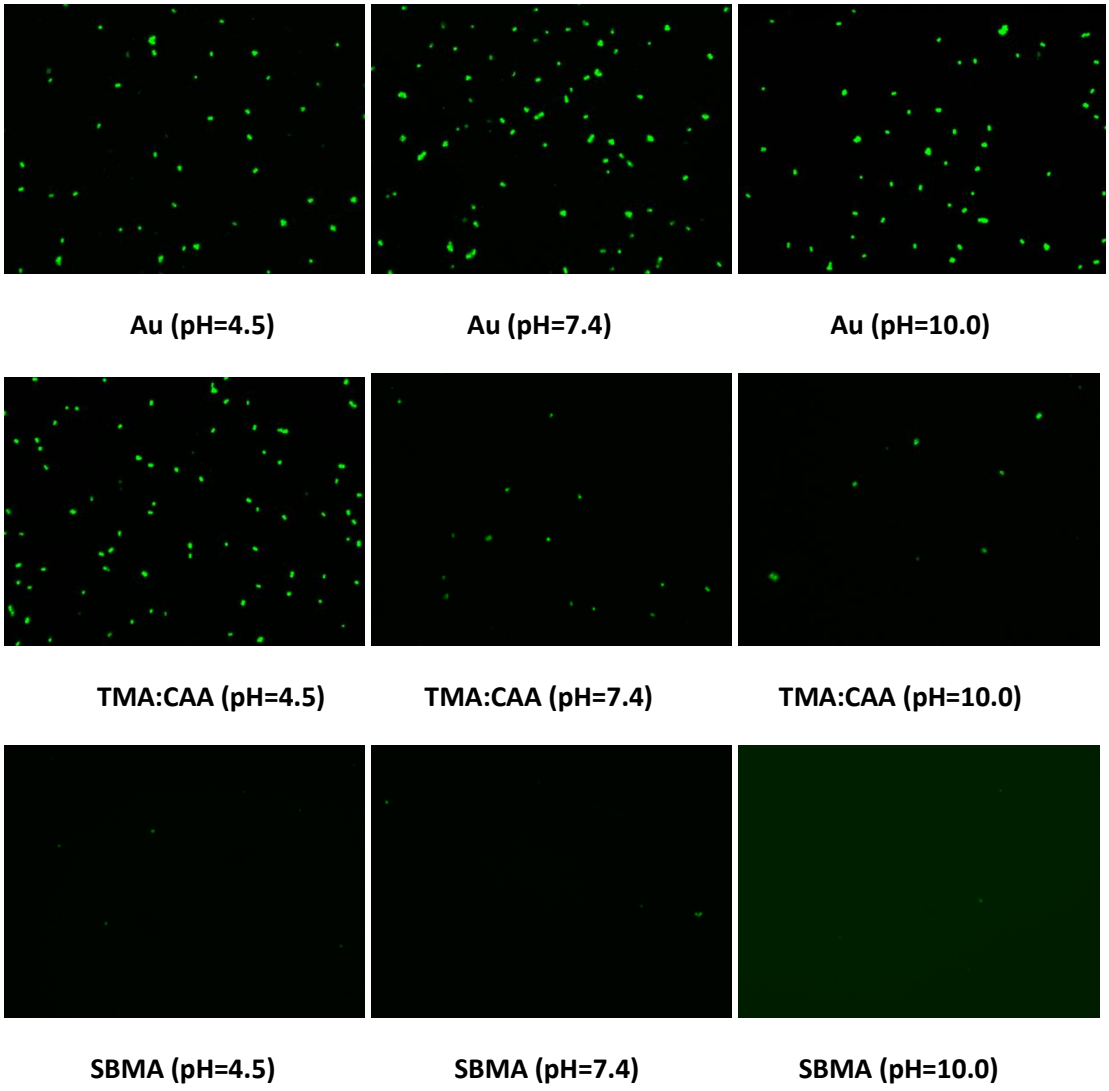

Figure 2.2 Representative fluorescence microscopy images showing *S.epidermidis* attachment to uncoated Au, TMA:CAA copolymer, and pSBMA surfaces under pH 4.5, 7.4 and 10.0 following a 3 h flow-chamber adhesion assay under room temperature. 1 x10^8cell/ml was used as the bacteria exposure concentration for the surface attachment study.

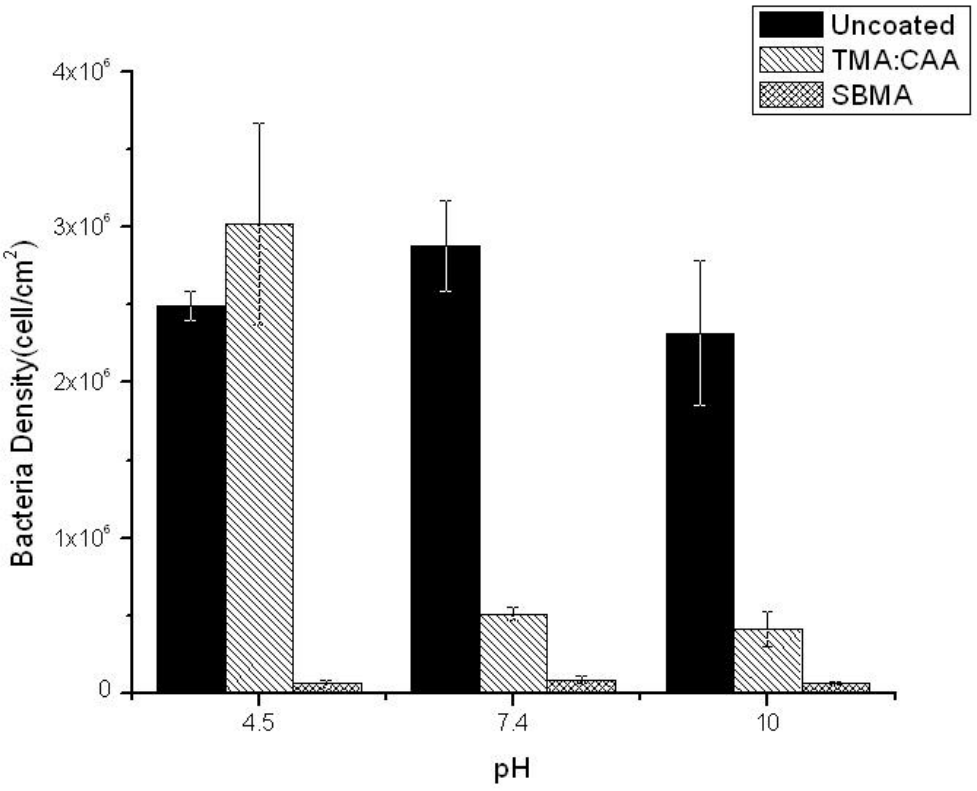

Figure 2.3 Quantitative analysis of *S.epidermidis* attachment to bare Au, TMA:CAA copolymer, and pSBMA surfaces following a 3 h flow-chamber adhesion assay. The data are reported as the mean ± standard deviation (n=10).

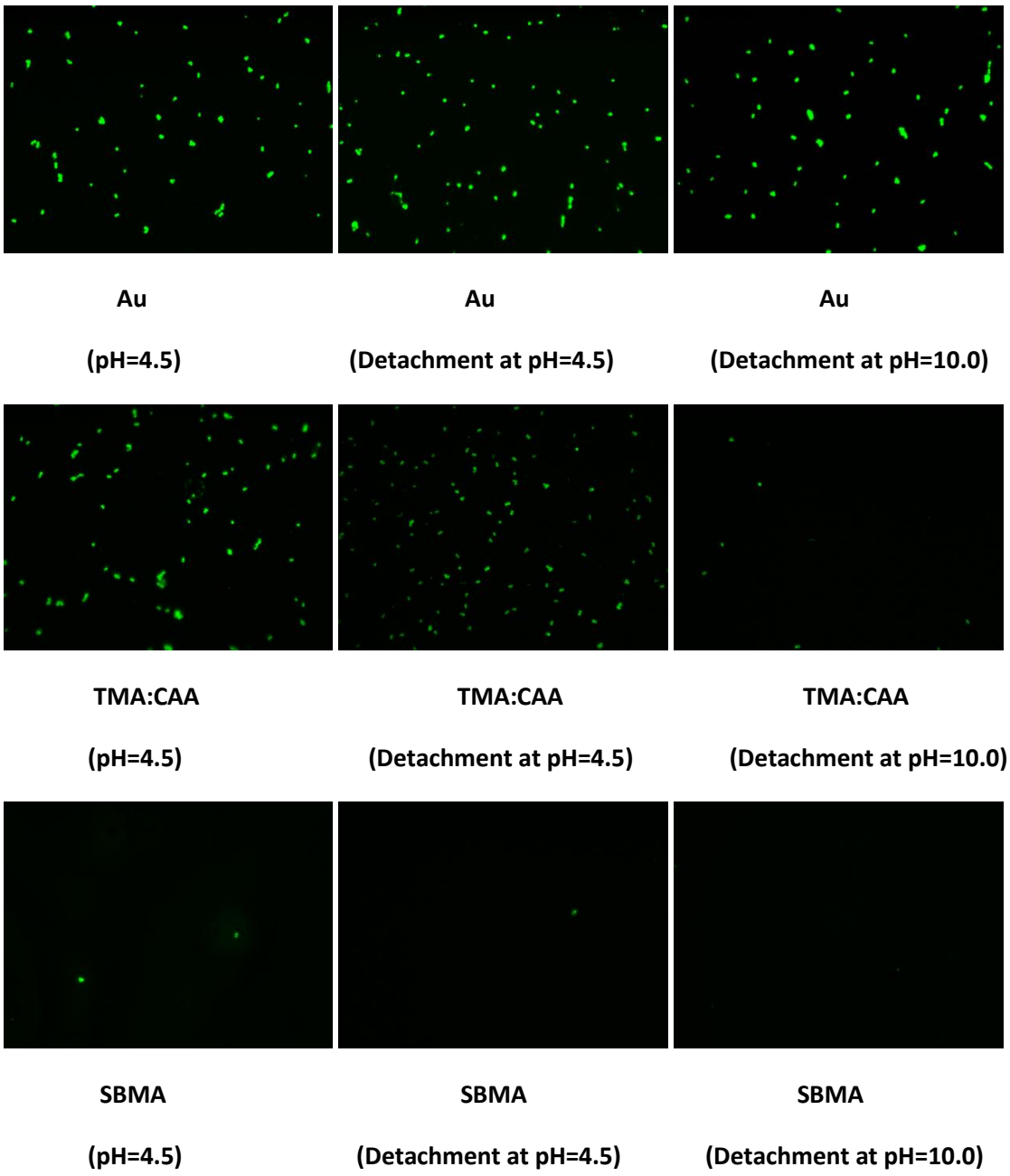

Figure 2.4 Representative fluorescence microscopy images showing *S.epidermidis* pH 4.5 initial attachment to uncoated Au, TMA:CAA copolymer, pSBMA surfaces and after a 30-min hydrodynamic detachment at pH 4.5 and pH 10.0 conditions. $6x10^8$cell/ml was used as the bacteria exposure concentration for the initial surface attachment.

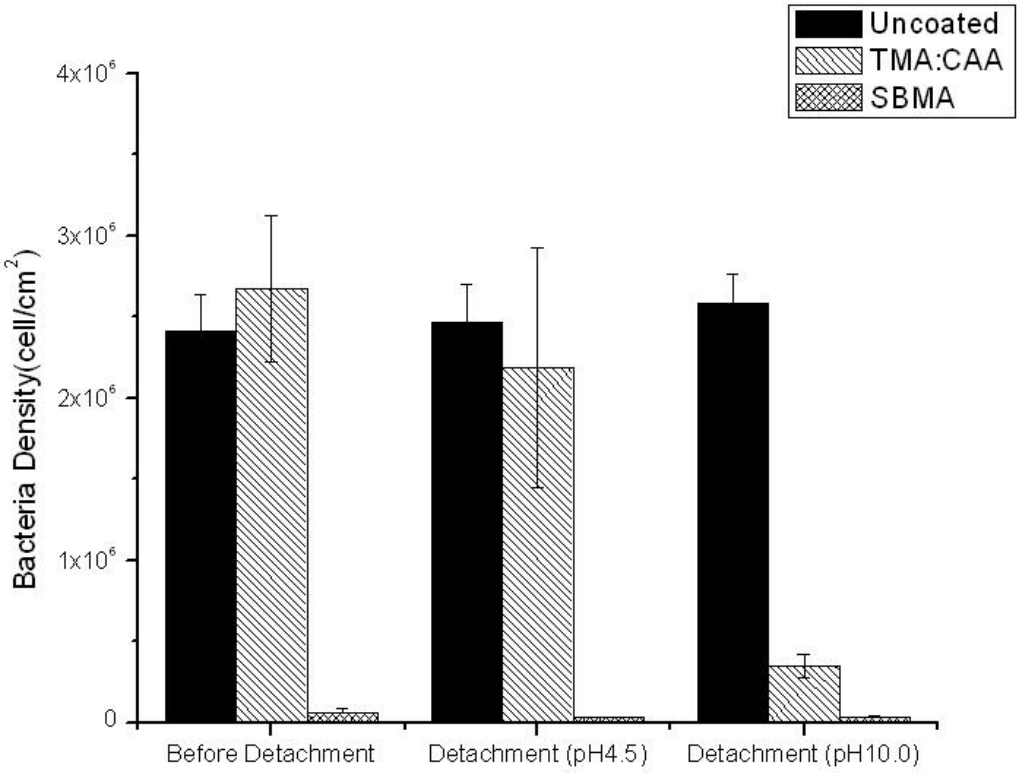

Figure 2.5 Quantitative analysis of *S.epidermidis* pH 4.5 initial attachment to bare Au, TMA:CAA copolymer, pSBMA surfaces and after a 30 min hydrodynamic detachment assay at pH 4.5 and pH 10 conditions. The data are reported as the mean ± standard deviation (n=10).

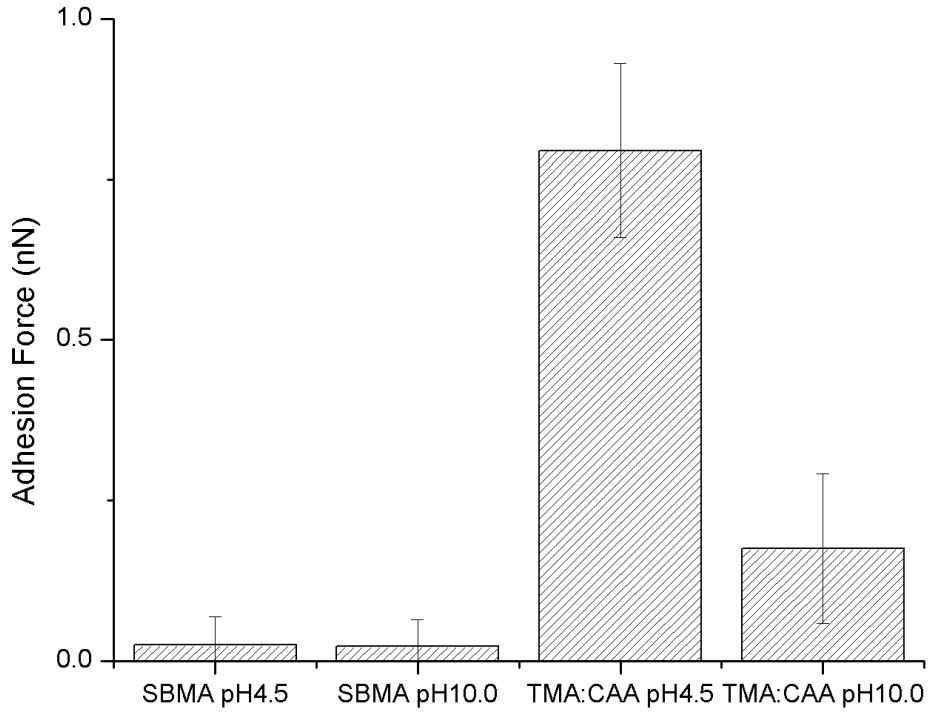

Figure 2.6 Average adhesion forces of $HS(CH_2)_{11}SO_3$ SAM modified AFM tips scanning over pSBMA and TMA:CAA copolymer surfaces in high and low pH aqueous buffer solutions. The vertical distance between the minima of the approach and retract curves from AFM measurement is recorded as the surface adhesion force. The data are reported as the mean ± standard deviation (n=20).

Chapter 3. Synchronizing Nonfouling and Antimicrobial Properties in a Zwitterionic Hydrogel

In this work, we report a new approach to integrate antimicrobial and nonfouling properties into a single platform without compromising each other. To achieve this, a zwitterionic hydrogel is conjugated with an antimicrobial agent as a leaving group in a way that maintains the zwitterionic form of the hydrogel before, during and after drug release, preventing bacteria surface adhesion and bulk proliferation simultaneously. The antibacterial salicylate anion contributes the negative charge to the initial zwitterionic state and is released through the ester linkage hydrolysis. The hydrogel then switches to its final zwitterionic state with the carboxylate as its new negatively charged group. We prove that this hydrogel can reach one-salicylate-per-monomer drug loading while still retaining the nonfouling property at protein and bacteria levels. It was also shown that its drug release profile was dictated by the hydrolysis rate of the monomer, making it possible to control and tailor the release rate of small hydrophilic drugs from the highly hydrated nonfouling polymer matrix.

3.1 Introduction

Bacterial surface adhesion and subsequent colonization have been among the major issues for many biomedical applications, causing device failure as well as tissue infections [41-43]. Traditionally, two common approaches exist to combat such threats. The first approach utilizes antimicrobial agents, particularly quaternary ammonium compounds and small molecular weight antibiotics, to actively kill the bacteria [6-8]. The

second approach uses nonfouling coatings such as poly (ethylene glycol) (PEG) and zwitterionic materials to fend off bacteria from adhering onto the surface [9-11]. Despite their popularity, each has its own significant drawbacks. One major concern for the "attacking" approach is the surface accumulation of dead microorganisms blocking antibiotic functional groups, whereas the key problem associated with "defending" approach lies in its incapability to inhibit bacterial proliferation both on surface and in bulk. Many efforts have hence been made to combine these two features into a single system. The direct immobilization of an antimicrobial agent onto a nonfouling polymer background, though straightforward, usually compromises one property in the pursuit of the other [44]. An alternative route is to prepare switchable polymers that undergo separate stages of functionality. In recent years, we have reported three such approaches capable of switching between the cationic antimicrobial form and the zwitterionic nonfouling form of the material through reversible lactonization, ester hydrolysis, and ester hydrolysis coupled with an antimicrobial counter ion [45-47]. However, in all three cases, it inevitably involves a positively charged state at the bactericidal stage of their action. Such cationic states are subject to severe biofouling, making them unsuitable for many applications in complex media. Ideally, a material or surface shall be able to carry a certain biological function (e.g. antimicrobial activity) with minimal interference to its nonfouling property. We envision that a good way to accomplish this is to create a polymer-drug complex, whose conjugate form as well as the unconjugated polymer itself are zwitterionic and nonfouling, thus achieving effective bacteria surface resistance and bulk growth inhibition simultaneously.

Herein, we demonstrate this concept through the design, synthesis and characterization of a new polymer that will meet this criterion and provide the capabilities aforementioned. In this system, poly (2-(2-((2-(methacryloyloxy) ethyl) dimethylammonio) acetoxy) benzoate) (PCBSA) polymers consist of an antimicrobial leaving group salicylic acid (SA) conjugated to a carboxyl betaine (CB) zwitterionic unit through a hydrolysable ester linkage (Figure 3.1a) [48]. This drug conjugate enjoys a high drug loading capacity unattainable via post-polymerization modification and a controllable drug release rate. More importantly, this resulting functional polymer maintains its zwitterionic state and nonfouling property both before and after the SA release, keeping the surface free from bacteria and inhibiting bacterial growth in bulk. Before hydrolysis, the negative charge on the SA carboxyl group balances with the cationic quaternary amine group on the polymer side chain, rendering the whole polymer zwitterionic and nonfouling. Our study shows that the PCBSA polymer has a nonfouling property comparable to that of the benchmark zwitterionic nonfouling polymer, poly (3-((2-(methacryloyloxy)ethyl) dimethylammonio) propanoate) (PCBMA-2) at the protein and bacterial levels. During the hydrolysis process, SA was released from the polymer matrix via the breaking of the ester bond, inhibiting bacterial growth in the surrounding environment. For every molecule of SA released, one negatively charged carboxylate is formed on the polymer side chain, maintaining the overall charge neutrality. After complete hydrolysis, the polymer then turns into poly (2-((2-(methacryloyloxy)ethyl) dimethylammonio)acetate) (PCBMA-1) with the hydrolysis-generated carboxyl betaine serving as a zwitterionic moiety further providing long-term bacterial resistance (Figure 3.1b).

3.2 Materials and Methods

3.2.1 Chemicals:

2-(dimethylamino)ethyl methacrylate (DMAEMA), 4-(dimethylamino)pyridine (DMAP), ethylene glycol dimethacrylate (EGDMA), 2-hydroxy-2-methylpropiophenone, bromoacetyl bromide, salicylic acid (SA), and phosphate buffered saline (PBS) were purchased from Sigma-Aldrich Chemical Co. (MO, USA). Pyridine and $MgSO_4$ were purchased from EMD Chemicals Inc. (NJ, USA). H_2SO_4 was purchased from Macron Fine Chemicals (PA, USA). Tert-butanol was purchased from J.T. Baker (PA, USA). BacLight® bacterial staining kit was purchased from Invitrogen Co. (NY, USA).

3-((2-(methacryloyloxy)ethyl) dimethylammonio) propanoate (CBMA-2) and 2-ethoxy-N-(2-(methacryloyloxy)ethyl)-N,N-dimethyl-2-oxoethanaminium-2-hydroxybenzoate (CBMA-1-C2 SA) monomers were synthesized as previously described [47, 49].

(2-(2-((2-(methacryloyloxy) ethyl) dimethylammonio) acetoxy) benzoate) (CBSA) monomer was synthesized in this work via a four-step reaction: (1) 2-(2-bromoacetoxy) benzoic acid was synthesized following a previously described procedure with a minor adaptation [50]. SA (10g, 72.4mmol), DMAP (0.054g, 0.44mmol) and pyridine (5.86ml, 72.4mmol) were first added into 100ml anhydrous diethyl ether (DEE). The diethyl ether solution was subsequently stirred and cooled to 0^oC on an ice bath. Bromoacetyl bromide (7.56ml, 86.88mmol) was then dropwise added into the mixture over 30 minutes. The reaction was stirred vigorously overnight at 0^oC to room temperature. After 16 hour reaction, the insoluble product of the reaction (largely pyridinium salt) was filtered out. The liquid phase was dried on a rotary vacuum evaporator, subsequently dissolved in

ethanol and precipitated in H_2O. The precipitate was dried in vacuum and analyzed, giving 2-(2-bromoacetoxy) benzoic acid at a quantitative yield. (2) The tert-butyl 2-(2-bromoacetoxy) benzoate was prepared based on a previously published method [51]. In a typical reaction, $MgSO_4$ (4.81g) and H_2SO_4 (0.55ml) were first added to 40ml dichloromethane (DCM). The resulting solution was stirred at room temperature for at least 15min. 2-(2-bromoacetoxy) benzoic acid (2.6g, 10mmol) from the first step and tert-butanol (4.78ml, 50mmol) were added into the stirring DCM solution sequentially. The reaction mixture was then stirred at 25^oC for 18h. After 18 h reaction, 75ml saturated bicarbonate solution was added to quench the reaction. The mixture was further stirred until all $MgSO_4$ dissolved into the aqueous phase. The DCM organic phase was subsequently washed three times with brine to remove any remaining $MgSO_4$, H_2SO_4 and 2-(2-bromoacetoxy) benzoic acid. After the extraction, the organic phase was dried overnight with Na_2SO_4. Finally, DCM was removed on a rotary vacuum evaporator. The solid was analyzed on ^{1}HNMR. The reaction yield was 70%. (3) 2-(2-bromoacetoxy) benzoic acid synthesized in the second step was used to react with DMAEMA at a 1:1 molar ratio in acetonitrile at 70^oC overnight. The solvent was then removed on a rotary vacuum evaporator and DEE was added into the resulting product to precipitate out 2- (2-(tert-butoxycarbonyl) phenoxy)-N- (2-(methacryloyloxy) ethyl) -N,N-dimethyl-2-oxoethanaminium bromide. The resulting white powder was further washed three times with DEE, dried and analyzed. The reaction gives a quantitative yield. (4) The tert-butanol deprotection was carried at a strong acidic condition: the product from step 3 was dissolved in 4 N HCl solution (H_2O: dioxane ~1:2). The reaction solution was stirred vigorously overnight at room temperature. The solvent was subsequently removed on

vacuum. The final product (CBSA monomer) was washed sequentially with excessive amount of acetone and DEE. ^{1}HNMR (300MHz, MeOD): δ8.04 (m. 1H), δ 7.60 (m. 1H), δ7.40 (m. 1H), δ7.17 (m. 1H), δ 6.10 (s. 1H), δ 5.66 (s. 1H), δ 4.78 (s. 2H), δ 4.64 (m, 2H), δ4.05 (m. 2H), δ 3.40 (s. 6H), δ 1.90 (s. 3H).

3.2.2 Hydrolysis of CBSA monomer

The CBSA monomer hydrolysis was measured *in situ* in an NMR tube. CBSA monomer was dissolved in PBS deuterium oxide solution and kept at 20^{o}C. ^{1}HNMR of the CBSA sample was taken at predetermined time points. The hydrolyzed percentage of CBSA in PBS at any given time was calculated based on the characteristic peak integrations belonging to hydrolyzed and unhydrolyzed SA moiety: particularly, the proton ortho to the SA carboxyl group was chosen for the calculation as they were the most deshielded protons and thus experience the least interference from other proton peaks in the NMR spectrum. The chemical shift of this proton changed from δ 7.63 to δ 7.72 as the ester linkage hydrolyzed in PBS solution.

3.2.3 Hydrogel synthesis and drug release

PCBMA, PCBMA-1-C2 SA, and PCBSA hydrogels were synthesized using the following procedure: 1mmol monomer in 1ml solvent (DMSO for CBSA and CBMA-1-C2 SA; methanol for CBMA) was mixed with 30ul EGDMA crosslinker and 20ul 2-hydroxy-2-methylpropiophenone photo-initiator. The reaction was carried out between a pair of glass substrates, separated with a poly-(tetrafluoroethylene) (PTFE) spacer with a thickness of 0.76 mm. The reaction mixture was then exposed to 302nm wavelength UV radiation for 2 hours to allow photo-initiated radical polymerization and gelation. The hydrogels were then hydrated for 24h before characterization. For PCBMA-2 hydrogel,

the hydration proceeded at room temperature in water (PCBMA-2) or 0.5 M sodium salicylate solution (SA infused PCBMA-2). For hydrolysable PCBMA-1-C2 SA and PCBSA hydrogels, the hydration was performed under 4^{o}C pH~4 aqueous condition. This condition was experimentally confirmed to stabilize PCBSA and minimize the premature hydrolysis. Water was changed every 8 hours for all three hydrogels.

Hydrated hydrogel disks (5mm in diameter and 1mm in thickness) of PCBMA-1-C2 SA, PCBSA, and SA infused PCBMA were placed in 10ml PBS solution. The hydrolysis was carried out at 20^{o}C and 90 rpm. 1ml PBS was removed for HPLC characterization at a desired time point and replaced by a 1ml fresh PBS solution. The amount of salicylate released was monitored using a high performance liquid chromatography system (HPLC) (Waters, MA) consisting of a separation module (Model 2695) and a UV/Visible Detector (Model 2489). All separations were performed on an Econosil C18 5µ column (4.6mm X 250mm) (Alltech, USA) using a mixture of 60% acetonitrile and 40% water. The flow rate of the mobile phase was 0.5ml/min. The elution was monitored at 280 nm.

3.2.4 Protein fouling test

After hydration, PCBMA-2, PCBMA-1-C2 SA and PCBSA hydrogels were washed three times with PBS solution in a 24-well tissue culture plate, 2 minutes per wash. Hydrogels were then immersed in 1ml 0.1mg/ml FITC labeled Fibrinogen PBS solution at room temperature for 30 minutes to allow protein surface adsorption. After the protein incubation, hydrogel samples were then rinsed gently with PBS buffer to remove any loosely bound surface Fg. Finally, hydrogel surface fluorescence was visualized using a CCD-CoolSNAP camera (Roper Scientific, Inc., Trenton,NJ) mounted on Nikon Eclipse 80i with a 60X lens through FITC filter. The excitation light intensity and exposure time

for all samples were manually set constant to ensure the observed difference in fluorescent intensity was only a result of the difference in nonspecific protein surface adsorption. All pictures were taken on the edge of hydrogel samples as a way of making sure the microscope focal plane fell on the upper surface of the hydrogel.

3.2.5 Bacteria surface adsorption test

S.epidermidis ATCC 14990 single colonies were used to inoculate 25ml Luria-Bertani medium (LB) and the inoculated growth media was then cultured at 37^{o}C, 125rpm. Exponential phase *S.epidermidis* were harvested and subsequently washed three times with sterile PBS buffer through cycles of centrifugation and resuspension. After the final wash, *S.epidermidis* suspension in PBS was diluted to reach OD_{600}~0.1 ready for hydrogel surface adhesion test.

All hydrogel samples were place in a 24-well plate soaked in PBS solution for 10 minutes before the assay. After the PBS pretreatment, hydrogels were immersed in 1 ml *S.epidermidis* suspension. The incubation was carried out at room temperature with 60 rpm shaking for 2 h. The bacteria suspension was then replaced by sterile PBS. Hydrogel samples were further incubated in PBS for an additional 10 min with gentle shaking to remove any loosely bound bacteria. Finally, the hydrogel samples were stained with BacLight® bacterial staining kit for 10 minutes before visualization. The surface density of bacteria cells was determined with a CCD-CoolSNAP camera (Roper Scientific, Inc., Trenton,NJ) mounted onNikon Eclipse 80i with a 100X oil lens through FITC filter. It is worth pointing out the released SA was not found to directly kill bacteria in this assay, as evidenced by a lack of fluorescent signal for bacteria cells under the Texas Red stain. SA

was observed in this work as a bacteriostatic agent by the inhibition of bacteria growth. (See below)

3.2.6 Bacteria growth inhibition test

S.epidermidis single colonies were used to inoculate 25 ml of LB liquid media cultured at 37^{o}C. Exponential phase bacteria was later harvested and diluted with fresh LB to yield OD600~0.001. Diluted bacteria culture was then added into a 24-well plate at the volume of 1ml/well. One hydrogel disc (5mm in diameter and 1 mm in thickness) was added into each well. After 16h incubation at 37^{o}C, 100μl bacteria culture was carefully removed from each well for OD600 reading with a spectrophotometer Smartspet^{TM} 3000 (Biorad, USA). The final solution concentration of salicylate in the solution for PCBSA hydrogel is estimated to be approximately 300ug/ml based on initial hydrogel monomer loading, size of the hydrogel disc, typical swelling ratio of zwitterionic hydrogels and by assuming a complete drug release after incubation.

3. 3 Results and discussion

CBSA monomer was synthesized via the route shown in Figure 3.2. The synthesized monomer then underwent radical polymerization with a di-functional crosslinker to form the hydrogels tested in this study. Two other polymers were used as control groups in this work and were synthesized as previously reported: PCBMA-2 as the conventional nonfouling material without any antimicrobial function [11], and 2-ethoxy-N-(2-(methacryloyloxy)ethyl)-N,N-dimethyl-2-oxoethanaminium-2-hydroxybenzoate (PCBMA-1-C2 SA) as the cationic zwitterionic-precursor bearing SA as the counter ion [47]. (Figure 3.1a)

The hydrolysis rate of the CBSA monomer was expected to strongly affect the drug release and antimicrobial activity of the final hydrogel, and was measured using ^{1}HNMR. The hydrolyzed monomer percentage at any time point was calculated based on the ratio between the characteristic peak integrations belonging to the hydrolyzed and unhydrolyzed salicylate moieties (Figure 3.3 a). The half-life of the ester linkage in CBSA was observed to be approximately 5 hours in PBS at 20^{o}C. Leaving group being the same, the ester alkaline hydrolysis rate is greatly affected by neighboring group inductive effect and can be reflected by the deprotonation tendency of the carboxyl group formed. A lower pKa of the carboxyl group would indicate a more stable carboxylate anion, and, in turn, a less stable ester form during hydrolysis. Unsurprisingly, a previous report also showed that the acidity of the carboxyl group on the carboxyl betaine (CB) unit varies greatly with the proximity of the strong electron-withdrawing quaternary amine: the pKa of carboxyl groups in CB were 1.8, 3.25, 3.96 and 5.12 respectively for CB molecules with 1, 2, 3, and 5 carbon atoms between the two oppositely charged groups [52]. This strong correlation between carbon spacer length and ester bond stability explains the relatively short half-life of CBSA monomer (one carbon spacer) and also offers a way to tailor the SA hydrolysis rate to future applications.

Reverse phase high-performance liquid chromatography (RP-HPLC) was used to determine the drug release kinetics of PCBSA hydrogel. PCBSA hydrogels were prepared in DMSO and later hydrated at 4^{o}C under acidic conditions for 24h. Such conditions were experimentally verified to stabilize the hydrolysable ester bond and result in negligible premature hydrolysis (Figure 3.4). SA infused PCBMA-2 hydrogel and PCBMA-1-C2 SA hydrogel were also included in the experiment to help compare

the performance of various drug release mechanisms. The mechanisms by which drugs are released from a hydrogel matrix can be generally divided into three categories: free diffusion, physical association (particularly electrostatic attraction), as well as degradable covalent bonding [53-54]. SA infused zwitterionic PCBMA-2 hydrogel represents the free diffusion mechanism. The complete drug depletion within the first 5 minutes highlights the ineffectiveness of this strategy when it comes to small, hydrophilic drugs (Figure 3.3 b). The electrostatic attraction approach was exemplified in this work by the PCBMA-1-C2 hydrogel using SA as the counter ion. Under physiological ionic strength, ion exchange can play a major role in this mechanism, typically leading to a quick release. Among the three hydrogels tested, a relatively prolonged drug release was only observed for PCBSA hydrogel with a cumulative release curve resembling the monomer hydrolysis curve. An observed slightly faster rate of the cumulative release likely results from additional shaking and initial hydration. It is also worth pointing out that PCBSA hydrogel does not require any chemical modification of the drug SA with an additional linker often necessary in PEG hydrogel drug release platforms, thus eliminating the risk of losing bioactivity in the "pro-drug" state [54].

To test the ability of PCBSA hydrogels to resist protein fouling before hydrolysis, a protein adsorption assay was carried out to qualitatively probe the nonfouling property of the hydrogels [55]. Zwitterionic PCBMA-2 hydrogels and cationic PCBMA-1-C2 SA hydrogels were used as controls in the assay. Hydrogels were briefly rinsed with PBS, and then soaked in 0.1mg/ml Fluorescein Isothiocyanate labeled fibrinogen (FITC-Fg) solution for 30 minutes. After the soaking, hydrogels were gently washed again with PBS. Finally, the pictures of three hydrogels were taken under a fluorescent microscope

with the same excitation light intensity and exposure time. Among the three species of hydrogels tested, PCBSA and PCBMA-2 hydrogel showed similar fluorescent signal and both were significantly lower than that of PCBMA-1-C2 hydrogel (Figure 3.5). The Fg fouling of PCBMA-1-C2 hydrogel can be attributed to its surface hydrophobicity and electrostatic interaction. The fact that PCBSA hydrogel showed a fluorescent intensity similar to that of PCBMA-2 hydrogel, which has been previously proven to effectively reduce protein fouling and cell adhesion, serves as a strong indication for its good nonfouling property at the protein level [56].

On the bacterial level, the PCBSA hydrogel was designed to exert antimicrobial property without sacrificing the nonfouling surface chemistry, thus effectively combining the advantages of both PCBMA-1-C2 SA and PCBMA hydrogels. The ability of PCBSA hydrogel to resist surface bacterial adhesion was tested by incubating PCBSA hydrogel with *Staphylococcus epidermidis* suspension (O.D.600~0.1) in PBS. The assay was performed at room temperature with 2 hour incubation time and gentle shaking (60 rpm). After incubation, the hydrogels were briefly washed with sterile PBS solution to remove the unbound bacteria. Finally, surface-attached bacteria were stained and visualized under fluorescent microscope. The results showed that PCBSA hydrogel has a bacteria surface density of $2.7*10^5$ cells/cm^2, which was less than 10% of the bacteria surface accumulation on PCBMA-1-C2 hydrogels and was only marginally higher than that of PCBMA-2 nonfouling hydrogels (Figure 3.6 a). Note that the majority of the hydrolysable ester linkage remained intact in the timespan of bacterial adhesion assay, as can be deduced from monomer hydrolysis curve.

The antimicrobial property of PCBSA hydrogels was tested in a 16 h growth inhibition assay using *S. epidermidis*. PCBMA-2 and PCBMA-1-C2 SA hydrogels were also evaluated in parallel for comparison. One hydrogel disk 5mm in diameter and 1mm in thickness was placed in a well of a 24-well cell culture plate and then submerged in 1ml Luria Broth (LB) growth media inoculated with exponential phase *S. epidermidis* to reach OD600~0.001. After 16h incubation at 37^{o}C, the OD600 of the supernatant of each well was measured and recorded as an indication for bacteria population density (Figure 3.6 b). Both PCBSA hydrogel and PCBMA-1-C2 SA hydrogel showed complete *S. epidermidis* growth inhibition (>99%), while PCBMA-2 hydrogel, expectedly, displayed no antimicrobial activity compared to the negative control. Thus, as seen from Figure 3.6, PCBSA is the only system able to maintain the surface free from bacteria and to inhibit bacterial growth in the bulk.

3. 4 Conclusions

In conclusion, a new approach of integrating biological functionality and nonfouling property was demonstrated through the design and characterization of PCBSA polymer hydrogels, which are able to keep the surface free from bacteria and simultaneously inhibit bulk bacteria growth in a controllable manner. Incorporating charged bioactive molecules as a part of the zwitterionic moiety opens a door to the design and development of stealth materials and coatings with built-in biological functions.

3.5 Acknowledgements

This work has been supported by the Defense Threat Reduction Agency (HDTRA1-10-1-0074) and the Office of Naval Research (N000141210441). We thank Dr.Hong Xue and Dr. Jean-Rene Ella-Menye for stimulating discussions related to this project.

3.6 Chapter Figures

(a)

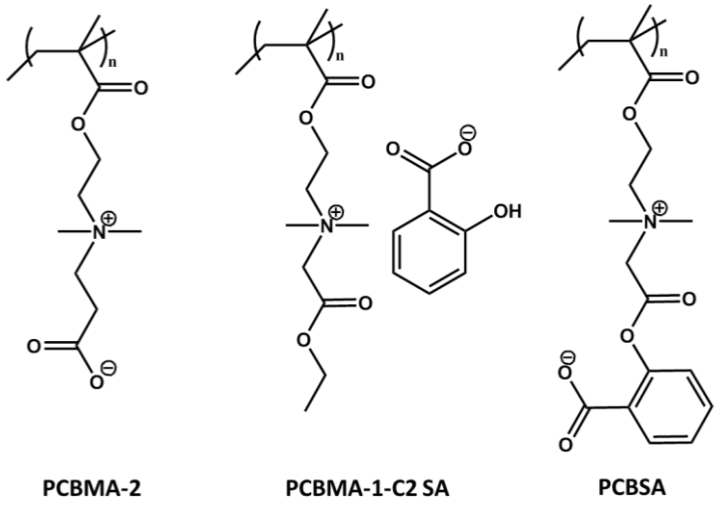

(b)

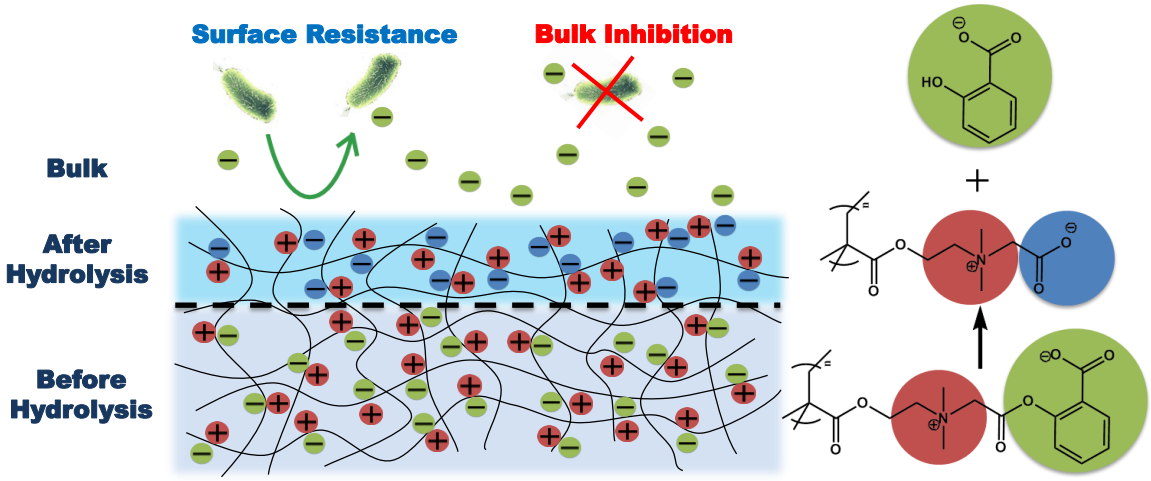

Figure 3.1 (a) Chemical structure of PCBSA (a zwitterionic polymer with built-in antimicrobial properties reported in this work) along with two reference systems of PCBMA-2 (conventional zwitterionic polymer) and PCBMA-1-C2 SA (cationic zwitterionic-precursor with an antimicrobial counter ion). (b) A hydrogel made up of the PCBSA polymer that is able to keep the surface free from bacteria and inhibit bacterial growth in bulk. For every antimicrobial salicylate anion released upon hydrolysis, one

carboxylate anion is formed at the hydrolysis site to maintain its zwitterionic nonfouling state.

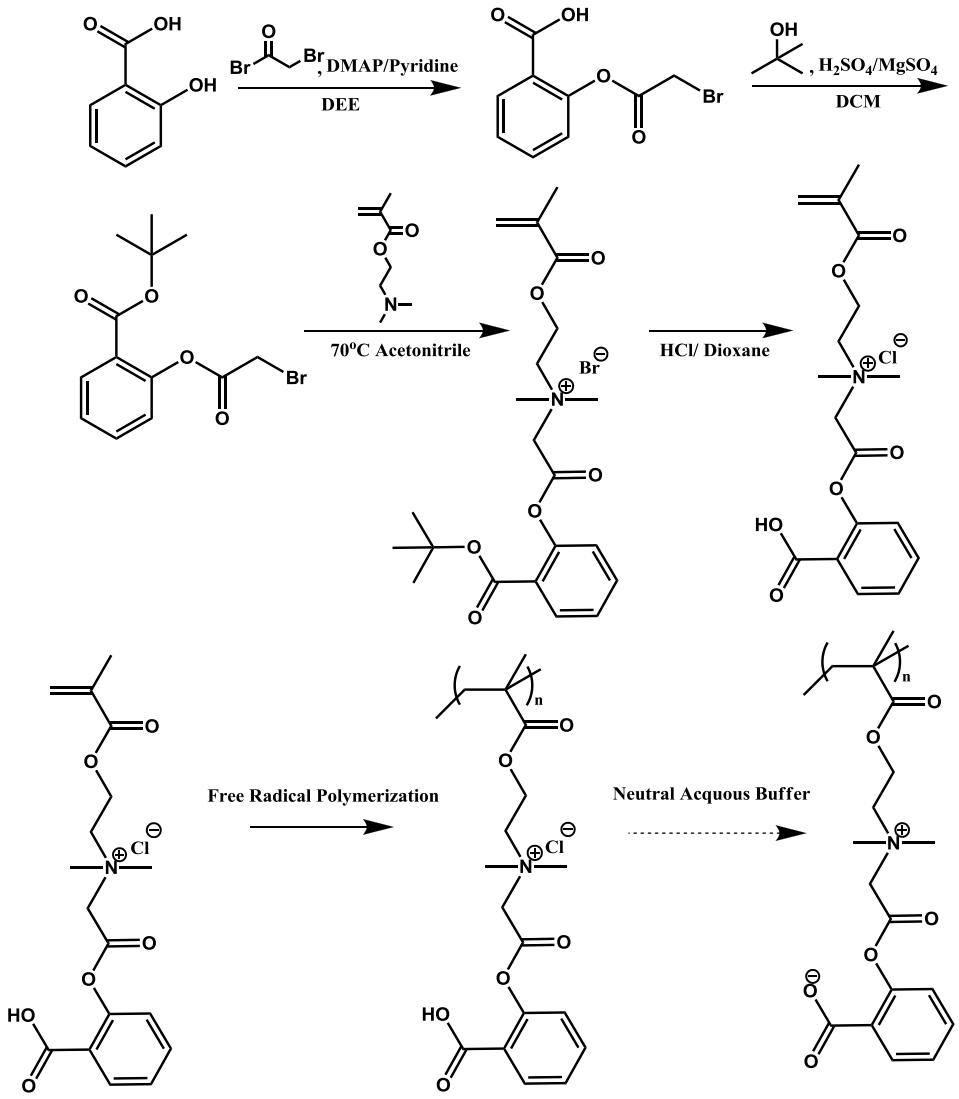

Figure 3.2 Reaction scheme for the synthesis of the CBSA monomer and subsequent radical polymerization.

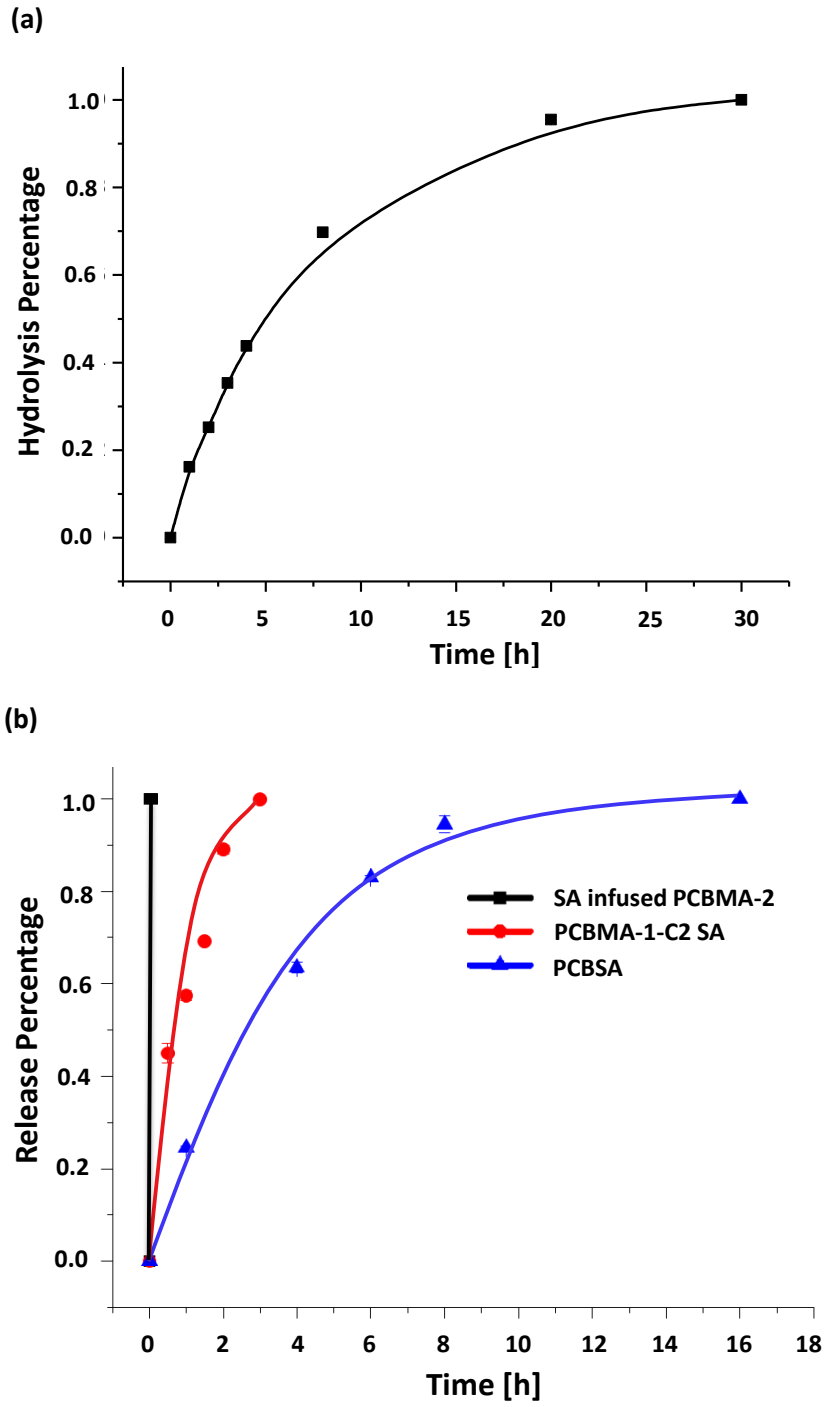

Figure 3.3 (a) The monomer hydrolysis curve of CBSA monomer in PBS 20^{o}C as determined by the ratio of peak integrations characteristic to hydrolyzed and unhydrolyzed SA moieties using ^{1}HNMR. (b) The cumulative drug release of three hydrogels each representing a typical controlled release mechanism: SA infused

PCBMA-2 hydrogel (free diffusion); PCBMA-1-C2 SA hydrogel (electrostatic interaction) and PCBSA (hydrolysable covalent bonding). The experiments were carried out under pH 7.4, 20^{o}C and 90 rpm shaking.

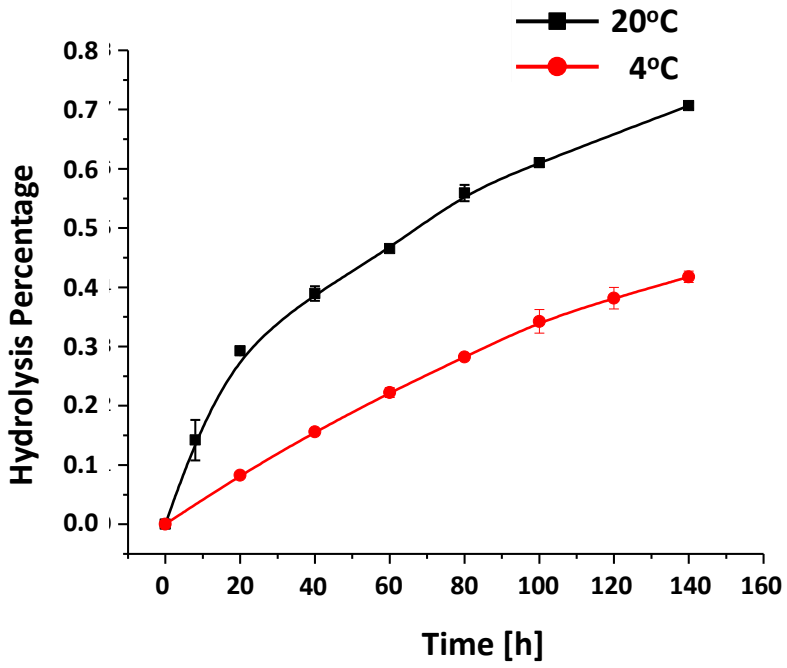

Figure 3.4 The monomer hydrolysis curve of CBSA monomer in pH~4 H_2O at 4 ^oC and 20^oC as determined by the ratio of peak integrations characteristic to hydrolyzed and unhydrolyzed SA moieties using ^{1}HNMR. The low temperature and acidic condition was to minimize premature hydrolysis.

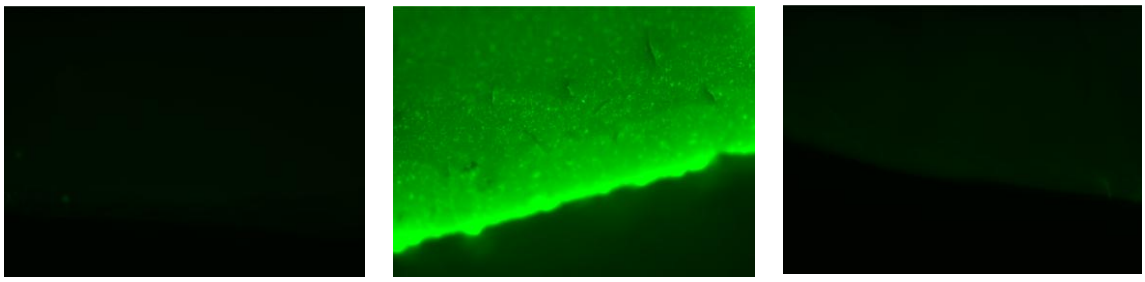

PCBMA-2 PCBMA-1-C2 SA PCBSA

Figure 3.5 Hydrogel protein nonfouling property as determined by incubation in 0.1mg/ml FITC labeled Fg protein solution and subsequently visualized under fluorescent microscope with the same excitation light intensity and exposure time. The pictures were taken on the edge of the hydrogel to ensure the focal plane falls on the upper surface of each hydrogel sample.

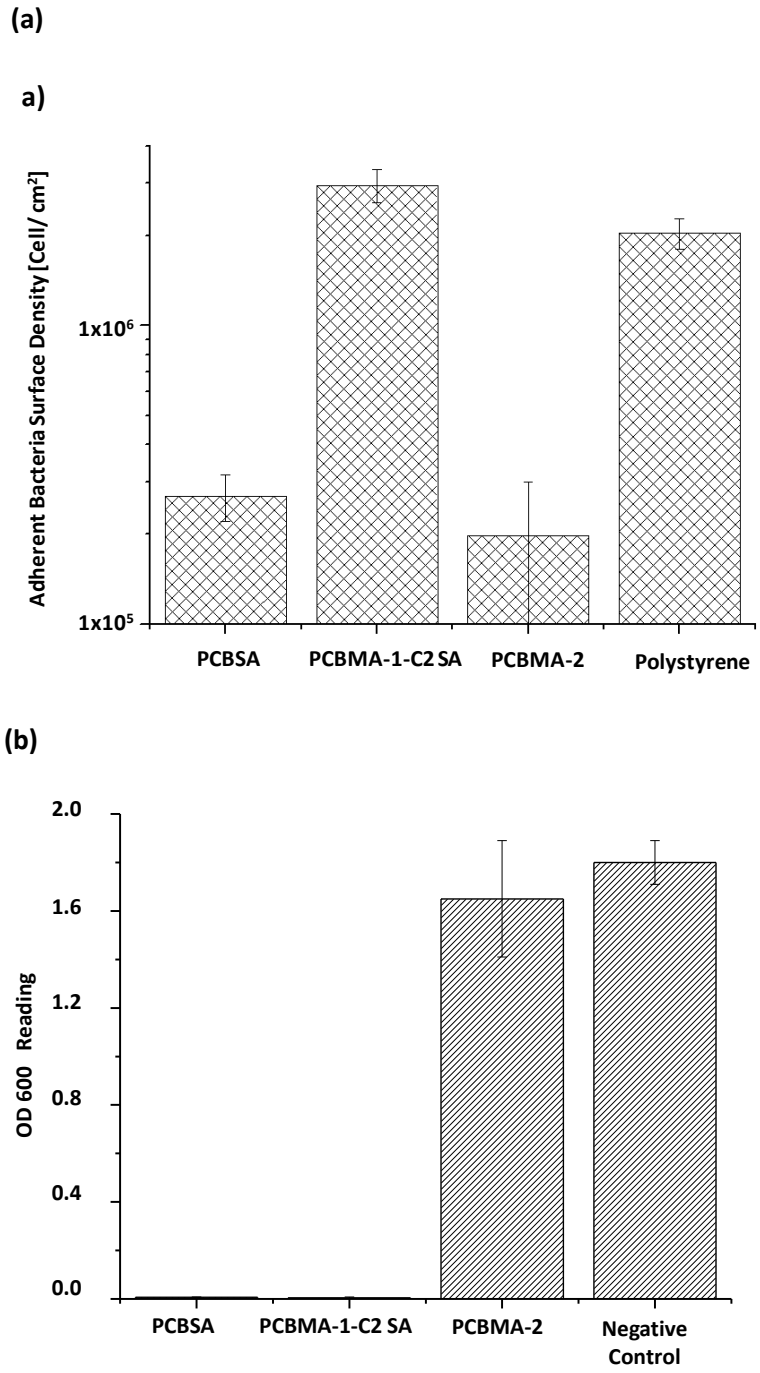

Figure 3.6 (a) Bacterial surface adhesion on PCBSA, PCBMA-1-C2 SA, PCBMA-2 hydrogels as well as on the polystyrene control surface. The four surfaces were subject to bacteria *S. epidermidis* (ATCC 14990) suspension in PBS (OD600~0.1) at room temperature and mild shaking condition for 2 h before visualization. (b) The growth

inhibition of PCBSA, PCBMA-1-C2 SA and PCBMA-2 hydrogels against *S. epidermidis*. The supernatant OD600 reading was recorded 16 hours after initial inoculation as an indication for bacteria bulk density. The final concentration of salicylate is calculated to be approximately 300ug/ml (see Materials and Methods). The Baclight® staining of surface attached *S.epidermidis* showed green fluoresce, suggesting the growth inhibition of salicylate is resulted from the bacteriostatic rather than the bactericidal activity of the molecule.

Chapter 4. A Thermo-responsive Antimicrobial Wound Dressing Hydrogel Based on a Cationic Betaine Ester

In this work, we report a thermo-responsive multifunctional wound dressing hydrogel based on ABA triblock copolymers synthesized via reversible addition fragmentation chain transfer (RAFT) polymerization. The inner B block consists of a positively-charged hydrolysable betaine ester loaded with an antimicrobial drug as its counter ion and the B block is flanked by two outer A blocks of thermo-responsive poly (N-isopropylacrylamide) (PNIPAM). A solution containing the triblock copolymers can be applied to wound sites and immediately turns into a physical gel at the body temperature. This wound dressing can reduce the risk of wound infection by releasing small-molecular-weight antimicrobial drug and facilitate the attachment of mammalian cells during tissue regeneration through its positive surface charge. The cationic betaine ester can then hydrolyze at the wound site to its zwitterionic form, which is known to be biocompatible and nonsticky. The thermo-responsive *in situ* gelation feature along with controlled drug release, enhanced tissue-hydrogel interactions as well as long-term biocompatibility make this hydrogel a very promising material for antimicrobial wound dressing applications.

4.1 Introduction

Serious wounding, typically incurred from armed conflicts as well as industrial accidents, can be a major contributor to the total loss of manpower and must be treated with

specialized wound dressing materials. Despite its urgent demand, the state of art wound dressing technology today is still well behind, and the main challenge comes from the intrinsic complexity of wound healing process itself. Hydrogels have been studied and used as wound dressing materials for decades [57]. This is largely due to the fact that the moist and occlusive environment provided by a hydrogel has been proven to significantly facilitate the wound healing process [58, 59]. Moreover, a hydrogel offers a much more versatile platform that allows for functional manipulation as compared to traditional gauze dressings. Good tissue conformity, easy application, reduced risk of infection and accelerated tissue healing rate are all desirable properties for wound dressings.

A wound dressing hydrogel that gelates at the wound site usually offers good tissue conformity by accommodating the irregular substrate interface. To date, most *in situ* gelation wound dressing hydrogels use chemical crosslinking approach, which requires either time-consuming premixing step or exposure to a specific light source [60-62]. In contrast, spray-on thermo-responsive hydrogels that gel at physiological temperature are desirable due to their ease of application. However, previously reported hydrogels exhibit an undesirably wide temperature range for phase transition and an inability to form a mechanically useful gel [63].

A second concern for wound dressing hydrogels is the high risk of infection, as the moist condition provided by a hydrogel is equally ideal for pathogen proliferation and colonization [64]. To solve this problem, inclusion of silver particles is routinely used to kill bacteria. Unfortunately, they have limited efficacy and exert a detrimental effect on mammalian cells when a large quantity is used [65]. Thus, the impregnation of the wound

dressing material with an antimicrobial agent, that is more cytocompatible and can be released in a controllable fashion, is highly preferred.

A third desirable function of wound care is to accelerate hemostasis and tissue regeneration. A cationic polyelectrolyte dressing has been known to fulfill this requirement. Chitosan, one popular positively-charged wound dressing material, for example, is shown to cause strong hemagglutination by attracting negatively charged residues on red blood cell membranes [66]. The attachment of fibroblasts, another cell type crucial for wound repair [67, 68], has also been reported to be highly favored on cationic hydrogels [69]. One drawback of cationic polymers is their relatively high cytotoxicity [70]. Thus, instead of permanently cationic polymers, it is beneficial to use a hydrolysable positively charged polymer that is able to switch from its functional cationic form to tissue-friendly zwitterionic form.

In short, the ideal hydrogel must combine all features mentioned above (*in situ* gelation, antimicrobial activity, accelerating wound healing and long-term biocompatibility) into one single design to address the different aspects of a dynamic wound healing process. To this end, for the next-generation wound dressing materials, a multifunctional hydrogel with *in situ* forming capability is needed to accommodate irregular deep wounds and simultaneously eliminate bacterial infection risks as well as to promote reepithelialization of the damaged tissue.

Herein, we report the synthesis and characterization of an ABA triblock copolymer as a thermo-responsive wound dressing hydrogel. The inner B block consists of a positively-charged betaine ester loaded with an antimicrobial drug, salicylate, as its counter ion [poly(N-1-(ethoxycarbonylmethyl)-N-(3-acryloylamino-propyl)-N,N-dimethyl

ammonium salicylate)] (PCBAA-1-C2 SA). The B block is flanked by two outer A blocks of thermo-responsive poly(N-isopropylacrylamide)(PNIPAM) (Scheme 4.1 a). PNIPAM has a low critical solution temperature (LCST) close to human physiological temperature [71]. Above its LCST, PNIPAM quickly turns from water soluble to insoluble in a very narrow temperature window, enabling the block copolymer solution to immediately form a hydrogel through physical crosslinking [72]. The inner hydrophilic block PCBAA-1-C2 SA can release salicylate as a mild antimicrobial counter ion, while the cationic polymer backbone is designed to promote negatively charged fibronectin adsorption and thus, in turn, accelerate fibroblast cell adhesion and tissue regeneration (Scheme 4.1 b) [73]. Furthermore, the PCBAA-1-C2 polymers used in this study have been experimentally shown to be able to hydrolyze to its ziwtterionic form in a well-controlled fashion [46, 74]. The LCST of a PNIPAM copolymer is known to vary with respect to the copolymerization ratio and hydrophilicity of the second monomer [75]. In this study, the phase transition temperatures of block copolymers with different compositions were measured using dynamic light scattering (DLS). The antimicrobial activity and biocompatibility of the hydrogel after gelation were characterized with *E.coli* K12 growth inhibition assay and mammalian COS-7 cell MTT assay, respectively.

4.2 Materials and Methods

4.2.1 Chemicals:

Ethyl bromoacetate (98%), N-[3-(dimethylanimo) propyl] acrylamide (99%), salicylic acid sodium salt (NaSA) (99%), and dimethylformamide (DMF, HPLC grade) were purchased from ACROS, and were used without further purification. N-isopropylacrylamide (NIPAM) (99%) was purchased from Sigma-Aldrich and was

recrystalized before use. 2,2'-Azobis(4-methoxy-2.4-dimethyl valeronitrile) (V-70) initiator was purchased from WAKO. Ethanol (absolute 200 proof) was purchased from Decon. Water used in experiments was purified by a Millipore purification system.

(N-1-(ethoxycarbonylmethyl)-N-(3-acryloylamino-propyl)-N,N-dimethyl ammonium bromide (CBAA-1-C2 Br) was synthesized by reacting ethyl bromoacetate with N-[3-(dimethylanimo) propyl] acrylamide in dry acetonitrile at 60^{o}C, the formed product precipitation was further washed with diethylether. ^{1}H NMR (D_2O 300M Hz, 25^{o}C) : 6.57 (m, 2H), 5.96 (m,1H), 4.41(m,4H), 3.72 (t,2H), 3.44 (t,2H), 3.31(s,6H),2.42 (m, 2H), 1.55(t,3H).

Difunctional RAFT chain transfer agent (CTA) 2-(1-carboxy-1-methylethylsulfanyl thiocarbonylsulfanyl)-2-methylpropionic acid was synthesized using a previously published method [76].

4.2.2 Synthesis of triblock copolymer NIPAM-co-CBAA-1-C2SA:

NIPAM macroCTA was synthesized by RAFT, following a previously published method [30]. Briefly, deoxygenated NIPAM monomer (33 wt%) was polymerized with CTA and V-70 at 30^{o}C for 24h in DMF. CTA amount was changed to obtain homopolymers with different degrees of polymerization (DP), while [CTA]/[I] was kept at 3 :1 due to the relatively low reaction temperature. The resulting polymer was purified by dialysis against MilliQ water at 4^{o}C for 72h. The purified product was then lyophilized and stored at 4^{o}C before use. MacroCTA chain extension with CBAA-1-C2 Br was carried out in deoxygenated monomer ethanol solution (0.5M) with macroCTA and V-70. [M]/[CTA] was varied in order to yield different DP values while [CTA]/[I] was kept constant at 3 :1

for each reaction. Synthesized NIPAM-co-CBAA-1-C2Br was mixed with 20 times over-amount of NaSA in 1:1 mixed solvent of water and ethanol. The solution was stirred for 3h and then dialyzed against MilliQ water at 4^{o}C for 120 h. Water was changed every 12 h. The dialyzed product was lyophilized and stored at 4^{o}C before use.

4.2.3 Gel permeation chromatography:

Gel Permeation Chromatography (GPC) was used to determine *M*n, *M*w and PDI. GPC analysis of PNIPAM homopolymer samples was obtained using a triple detection method (with angular correction) using a Viscotek I-Series Mixed Bed low-MW and mid-MW column running at 60^{o}C DMF flow rate of 0.5ml/min, having refractive index, viscometer, and right angle laser light scattering (RALLS) detectors, the wavelength of the laser being 670nm. A previously published dn/dc value of 0.074 was used for all PNIPAM homopolymer samples [77]. The DP of the inner block was calculated based on comparison between integration of characteristic peaks from two copolymer blocks in NMR. Unfortunately, triblock copolymer aggregates in DMF and cannot be analyzed using the previous method. Alternatively, an aqueous phase GPC system, Waters Alliance 2695 Separations Module equipped with a Waters Ultrahydrogel 1000 column and a Waters 2414 reflex detector, was used to verify the successful extension for macroCTA. The mobile phase was $NaNO_3$ (0.5M) running at 25^{o}C with a flow rate of 0.5ml min^{-1}. The relatively high salt concentration was used to help solubilize the positively charged polymer.

4.2.4Measurements of polymer phase transition temperature:

The phase transition behavior of the polymer was characterized using a dynamic light scattering (DLS) particle sizer (Nano ZS, Zetasizer Nano, Malvern). 0.1wt% triblock

copolymer was dissolved in water, and the hydrodynamic radius of the polymer was measured continuously as the temperature being ramped from 20^{o}C to 50^{o}C.

4.2.5 In vitro SA^- release and HPLC analysis:

20wt% triblock copolymer solution was heated to 37^{o}C to form a gel in a 10mm diameter circular mold. Then, the hydrogel disk was immediately transferred to 10ml prewarmed PBS solution (37^{o}C) shaking at 40rpm. 1ml PBS was removed for HPLC characterization at a desired time point and replaced by a 1ml prewarmed fresh PBS solution.

The amount of salicylate released was monitored using a high performance liquid chromatography system (HPLC) (Waters, MA) consisting of a separation module (Model 2695) and a UV/Visible Detector (Model 2489). All separations were performed on an Econosil C18 5μ column (4.6mm X 250mm) (Alltech, USA) using a mixture of acetonitrile (60%) and water (40%). The flow rate of the mobile phase was 0.5ml min^{-1}. The elution was monitored at 280 nm. The cumulative fractional release at time t was then calculated based on a freshly prepared calibration curve (R^2>0.999).

4.2.6 Bacteria growth inhibition:

E. coli K12 single colonies were used to inoculate 25 ml of LB (BD, Franklin Lakes, NJ) (20 g L^{-1}) liquid media cultured at 37^{o}C. Exponential phase bacteria was later harvested and diluted with fresh LB to yield OD600~0.001. Diluted bacteria culture was then added into a 24-well plate at the volume of 1ml/well. Different wells contain 0 or 100ul hydrogel prewarmed to 37^{o}C with different weight concentrations and counter ions to be tested for antibacterial activity. After 12h incubation at 37^{o}C, bacteria culture (100μl) was

carefully removed from each well for OD600 reading with a spectrophotometer Smartspet^{TM} 3000 (Biorad, USA). Each measurement had three replicate wells.

4.2.7 Mammalian fibroblast COS-7 cell culture and cytotoxicity assay:

COS-7 cells (African Green Monkey fibroblast cells, American Tissue Culture Collection; Manassas, VA) used in this study were cultured in Dulbecco's Modified Eagle Medium (Gibco, Invitrogen; Carlsbad, CA) supplemented with Fetal Bovine Serum (10%), 1× non-essential amino acids, and penicillin streptomycin. Cells were incubated at 37^{o}C and 5% CO_2.

Since hydrogel can potentially absorb the chromophore used in a regular MTT assay leading to inaccurate measurements, the MTT assay protocol was adapted similar to a previously published method [78]. Briefly, a solution containing triblock polymer (20wt%) was added into a 24-well tissue culture plate at 100µl per well and incubated briefly at 37^{o}C to help solidification. Then 1ml cell culture media (without phenol red) was added into each well to incubate with hydrogel. Medium from each well was collected after 12h culture and diluted to give 25%, 50% and 100% leach from the hydrogel to be tested in a standard MTT assay [79]. The MTT assay was carried out using a Vybrant MTT cell proliferation assay kit (Invitrogen, Carlsbad, CA). COS-7 cells (100µl) were seeded into 96 well tissue culture plates at a density of $1x10^4$ cells ml^{-1} for 48 h. At the end of 48 h, regular cell medium was replaced with the hydrogel-infused medium collected previously and incubated for 8 h. Then, fresh medium (100µl) (without phenol red) supplemented with MTT (10 µl, 1.2mg ml^{-1}) was changed to incubate for another 4 h. Finally, cell medium was removed and DMSO (50µl) was added into each well to completely dissolve the crystal formed. The absorbance at 570 nm was read with

a 96-well plate reader (SpectraMax M5, Molecular Devices, Sunnyvale, CA). Cell viability was expressed as the percentage of absorbance of leach-out treated cells relative to the absorbance of cells that were incubated with fresh cell culture medium. Each measurement had five replicate wells.

4.2.8 COS-7 cell surface attachment assay:

A thermo-responsive hydrogel quickly dissolves into cell culture medium at room temperature, making it difficult to directly count surface bound cells. An indirect method was used to characterize COS-7 cell adhesion onto various surfaces: prewarmed COS-7 cell culture (1ml) at the density of $1x10^5$ cells ml^{-1} was seeded onto a 24-well plate of (1) tissue culture polystyrene (TCPS), (2) regular polystyrene (PS) and (3) regular PS coated with gelled thermo-responsive hydrogel (100ul) at 37^oC. After 2 h culture, the supernatant was carefully removed from each well and unattached cells were counted with Nikon Eclipse TE2000-U microscope. Each measurement had three replicate wells.

4.3 Results and Discussion

4.3.1 Synthesis of triblock copolymer via RAFT

ABA triblock copolymers were synthesized via a two-step RAFT polymerization using a difunctional CTA. The GPC results in DMF showed a very low Polydispersity Index (PDI) and good control over Degree of Polymerization (DP) for the PNIPAM first block (Table 4.1). The DP for the second block (PCBAA-1-C2) was calculated based on the integration ratio of characteristic NMR monomer peaks, and also agrees well with the theoretical molecular weight. (Figure 4.1) Unfortunately, the triblock copolymer after extension aggregates in DMF, as indicated by a more than two orders of magnitude

increase in MW compared to the theoretical MW. For this reason, an aqueous phase GPC system with a relatively high ionic strength eluent was used to verify that the macro CTA can indeed reinitiate the second step of polymerization. The GPC results (Figure 4.2 and 4.3) in water with 0.5M $NaNO_3$ does strongly suggest a successful polymer extension, although a significant peak broadening effect was also observed in the new system (with PNIPAM first block PDI >1.5 in aqueous system).

The SA^- counter ion is found to severely interfere with the living polymerization system used in this study. To counter this, the SA^- was incorporated into the polymer as a counter ion through ion exchange with over-amount of NaSA after the polymerization process. The replacement of Br^- with SA^- was followed by dialysis against MilliQ water at 4^oC to remove any excessive SA^- or Na^+. The NMR results after dialysis showed a 1:1 ratio between SA^- and CBAA-1-C2 in the final polymer.

4.3.2 LCST and gelation property of triblock copolymer solution

Many previous studies have reported that copolymerization of NIPAM with other monomers can cause significant shift of the original LCST of PNIAPM homopolymer at 32^oC [75]. Because the temperature-induced phase transition behavior is crucial for the new polymer's *in situ* crosslinking and wound dressing application, we use DLS to monitor the copolymer critical solution temperature in water with varying proportions of hydrophilic and hydrophobic blocks as well as the PNIPAM homopolymer. The results (Figure 4.4 a, c, e) shows that the phase transition temperatures, as marked by the sudden increase in the particle size caused by hydrophobic aggregation, for Triblock I $[(NIPAM)_{109}(CBAA\text{-}1\text{-}C2\ SA)_{214}(NIPAM)_{109}]$, Triblock II $[(NIPAM)_{227}(CBAA\text{-}1\text{-}C2\ SA)_{121}(NIPAM)_{227}]$, and PNIPAM $[(NIPAM)_{218}]$ are 41^oC, 37^oC and 30^oC respectively.

This upshift of LCST for the new block copolymer was indeed expected as the proportion of hydrophilic fragment increases.

In addition to a phase transition behavior at desired temperatures, the formation of a mechanically useful hydrogel also requires the hydrophobic domain in the polymer to hold a strong physical network while the hydrophilic domain bind water and prevent phase separation from occurring [80, 81]. To this end, a direct gelation test at 37^{o}C is carried out for Triblock I, Triblock II and PNIPAM (Figure 4.4 b, d, f) and the results are summarized in Table 4.2. These results show that even at similar DP (~500), Triblock I and Triblock II exhibit drastically different gelation behavior from PNIPAM and from each other. Triblock I, obviously suffering from its too short hydrophobic block, does not have sufficient physical crosslinking even when heated well above its LCST. In contrast, for PNIPAM, though the polymer is able to form a gel at 5% weight concentration, a phase separation follows within an hour owing to the hydrophobic nature of the homopolymer above its LCST. Alone among the three, Triblock II is able to form a physically free-standing hydrogel at 10 and 20 wt% and remains stable after prolonged incubation at 37^{o}C. For this reason, Triblock II is used for further biological characterization.

4.3.3 Drug release and antimicrobial activity

Figure 4.5 shows the release profile of SA^- from the 20 wt% Triblock II hydrogel in PBS at 37^{o}C. A burst release was observed in the first hour releasing 50% of the total SA^- to the environment. Then the remaining antibiotic drug was released in the next 5 hours at a reduced rate. As salicylate is a mild antibiotic drug [82], the initial quick release ensures

its antimicrobial effectiveness and, thus, serves well for the purpose of sterilizing the wound site.

One desirable property for any wound dressing hydrogel is its bactericidal or bacteriostatic activity so as to reduce the risk of bacteria colonization and wound infection [64]. For this reason, a bacteria growth inhibition assay was devised to evaluate the actual antimicrobial activity of the hydrogel using a gram negative *E.coli* K12 strain as a model species. Under the experimental conditions used in this study, the Triblock II hydrogel using salicylate as the counter ion completely inhibits bacteria growth while the bromine ion has no observable effect as compared to a negative control (Figure 4.6), indicting the bulk antimicrobial activity comes exclusively from the salicylate release.

4.3.4 Mammalian cell cytotoxicity

A major concern that comes with the use of antibiotics in biomaterials is its biocompatibility with mammalian cells. Any bioactive reagent having significant cytotoxicity to mammalian cells will be harmful to the wound healing process and thus should be avoided for such applications. We used an MTT assay to investigate the cytotoxicity of the Triblock II on the mammalian fibroblast cell line COS-7. As MTT is a colorimetric assay, it is likely that hydrogel will absorb chromophores formed in the assay, thus causing serious inaccuracy. To prevent this problem, we followed a previously reported method using leach-out products of the 20% Triblock II hydrogel (with SA^-) in phenol-red-free cell culture media and diluted to 100%, 50% and 25% solutions for test [83]. To ensure a fair comparison, the relative hydrogel dosage for 100% leachate is the same as used in bacteria growth inhibition assay. Results (Figure 4.8)

show that no observable cytotoxicity for hydrogel leachate at all three concentrations tested in the experiment.

4.3.5 Initial attachment of mammalian fibroblast onto hydrogel surface

Reepithelialization and tissue regeneration is another essential aspect of wound care. Besides the capacity to load a bioactive anion, PCBAA-1-C2 is also designed to impart a net positive charge to the dressing. A cationic hydrogel is expected to favor the adsorption of negatively charged fibronectin [84], which in turn promotes fibroblast cell adhesion [73], and the latter is shown to be crucial for the wound healing process and tissue regeneration [67, 68, 85]. To verify this hypothesis, we performed a short term cell attachment experiment on Triblock II hydrogel surface, regular polystyrene surface (PS) and tissue-culture polystyrene surfaces (TCPS). Because PS surfaces (not plasmon-treated) are generally considered unfavorable to cell adhesion, they are used as controls in these experiments [86, 87]. To prevent background interference, hydrogel solution is added onto the untreated PS surface and allowed to solidify prior to cell adhesion. In order to circumvent the problem of melting of the hydrogel at room temperature, the supernatant was collected from each well while still in the 37^{o}C incubator and the unattached cells in the supernatant were counted as an indication for cell surface affinity (i.e. the high number of unattached cell corresponds to a low surface affinity). Figure 4.7 shows that the cell adhesion property of the hydrogel surface under the aforementioned experimental condition is comparable to that of the TCPS surface, and both are much higher than the regular polystyrene, indicating that it indeed favors the surface adhesion of fibroblast cells at the initial stage. It should be pointed out that this cationic ester can

be hydrolyzed into its zwitterionic form, resulting in a tissue friendly and nonsticky material to ensure biocompatibility and easy removal [73, 46].

4.4 Conclusions

In this work, we report the synthesis and characterization of an ABA triblock copolymer containing PNIPAM and PCBAA-1-C2 SA moieties. The RAFT polymerization process is proven to have good control over both MW and structure of the polymer. The flanking PNIPAM blocks give the hydrogel its *in situ* gelation capability. Meanwhile, the salicylate counterion released from the hydrogel scaffold is shown to completely inhibit bacteria *E.coli* K12 growth within 12 hours, while, at the same dosage, does not observably affect the metabolism of mammalian COS-7 cells. The attachment of mammalian cells was also experimentally proven to be favored on the cationic hydrogel surface at early stage of tissue regeneration. This work demonstrates that it is possible to design a multifunctional hydrogel via a simple triblock copolymer to fulfill various requirements of a complex wound healing process.

4.5 Acknowledgements

This work is supported by the Defense Threat Reduction Agency (HDTRA1-10-1-0074) and the Office of Naval Research (N000140910137).

4.6 Chapter Figures

(a)

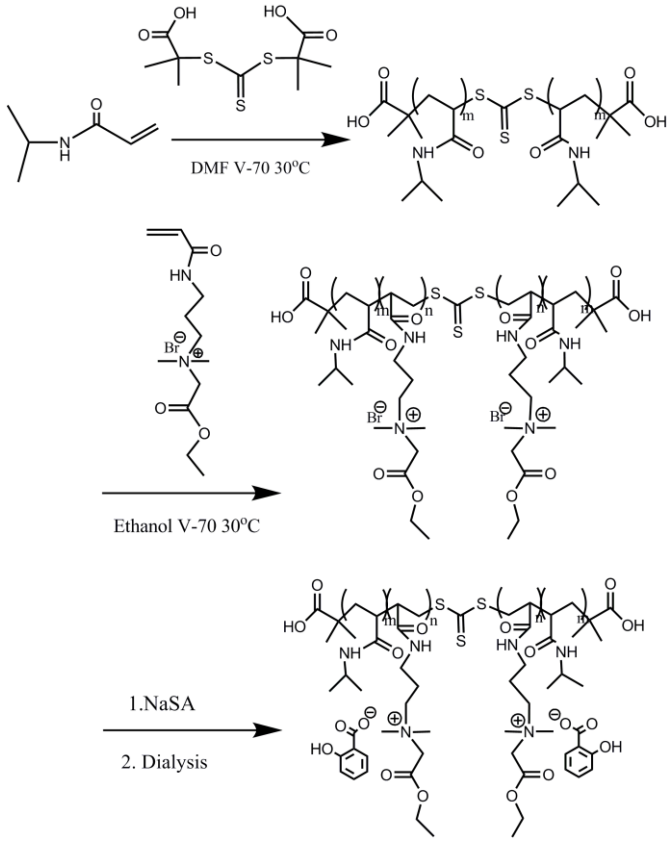

(b)

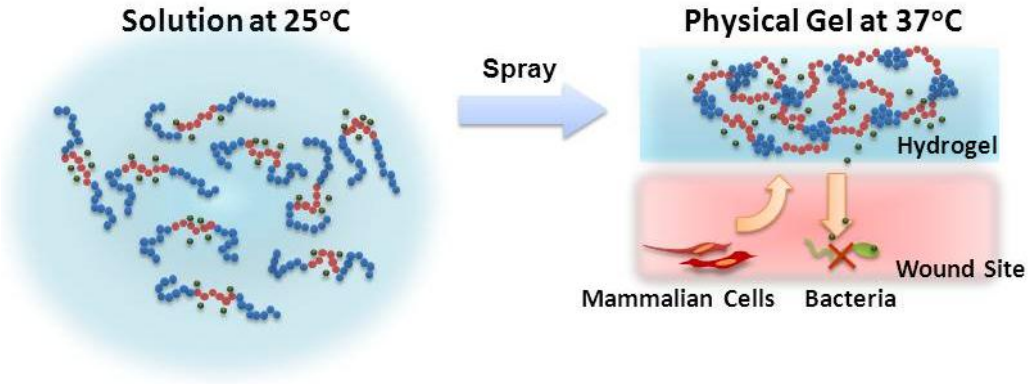

Scheme 4.1 **(a)** Synthesis route of thermo-responsive wound dressing copolymers. **(b)** Schematic illustration of the *in situ* formation of antimicrobial wound dressing hydrogel at the wound site.

Table 4.1 Polymer DP and PDI

Polymer	Designed Polymer Structure	Exp. Determined Polymer Structure	PDI
pNIPAM I	$(NIPAM)_{200}$	$(NIPAM)_{218}$	1.06
pNIPAM II	$(NIPAM)_{400}$	$(NIPAM)_{454}$	1.06
Triblock I	$(NIPAM)_{100}(CBAA\text{-}1\text{-}C2)_{200}(NIPAM)_{100}$	$(NIPAM)_{109}(CBAA\text{-}1\text{-}C2)_{214}(NIPAM)_{109}$	[a]
Triblock II	$(NIPAM)_{200}(CBAA\text{-}1\text{-}C2)_{100}(NIPAM)_{200}$	$(NIPAM)_{227}(CBAA\text{-}1\text{-}C2)_{121}(NIPAM)_{227}$	[a]

[a] Aggregation in DMF

Table 4.2 Gelation property of polymers at 37^{o}C with different concentrations

Polymer	5%(w/v)	10%(w/v)	20%(w/v)
Triblock I [a]	No Gel Formed	No Gel Formed	No Gel Formed
Triblock II	No Gel Formed	Gelation	Gelation
PNIPAM [b]	Precipitation	Precipitation	Precipitation

[a] No hydrogel formed even heated to 60^{o}C.
[b] Precipitation occurs within one hour.

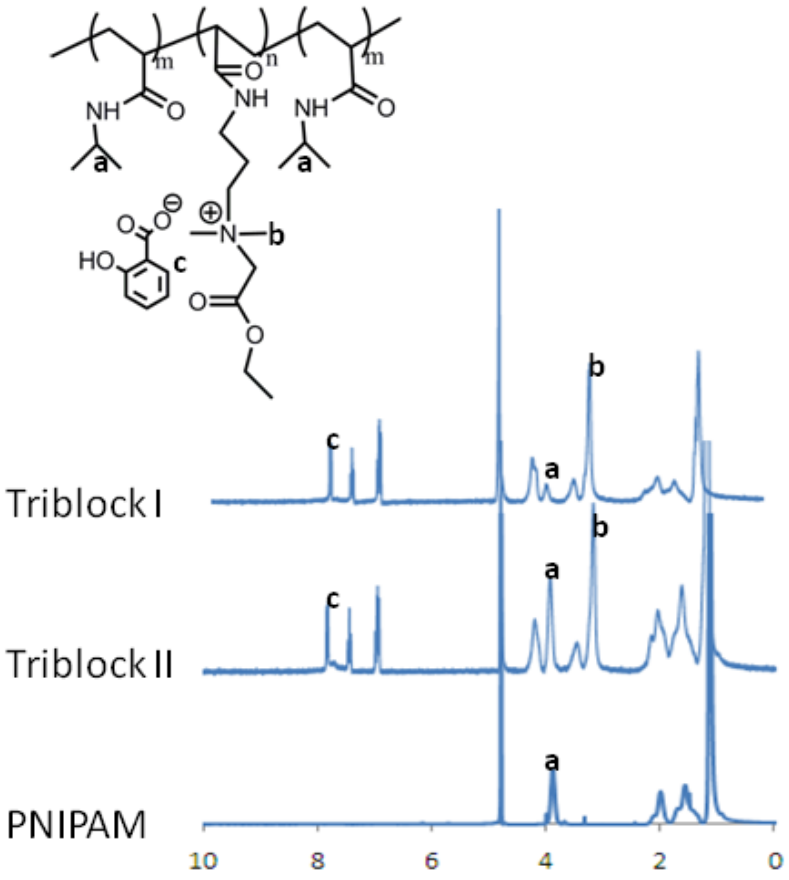

Figure 4.1 (^{1}H- NMR spectra of three polymers: Triblock I, Triblock II and PNIPAM in D_2O.)

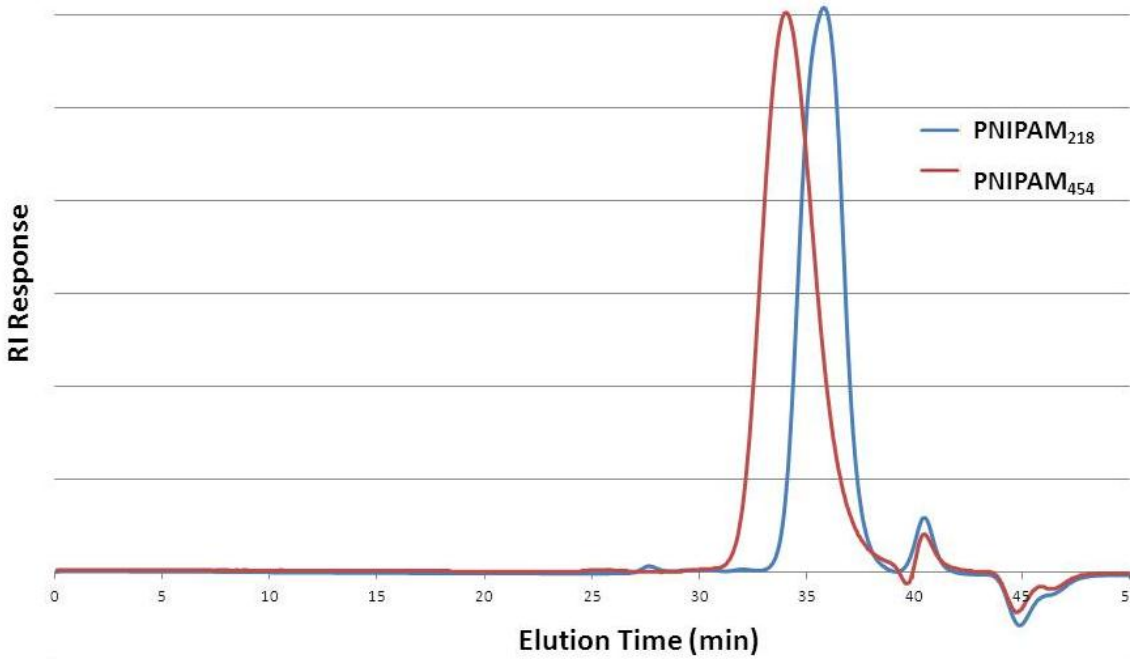

Figure 4.2 GPC trace of $PNIPAM_{218}$ and $PNIPAM_{454}$ in DMF running at 0.5ml/min and 60^{o}C. PDI for both polymers are below 1.1.

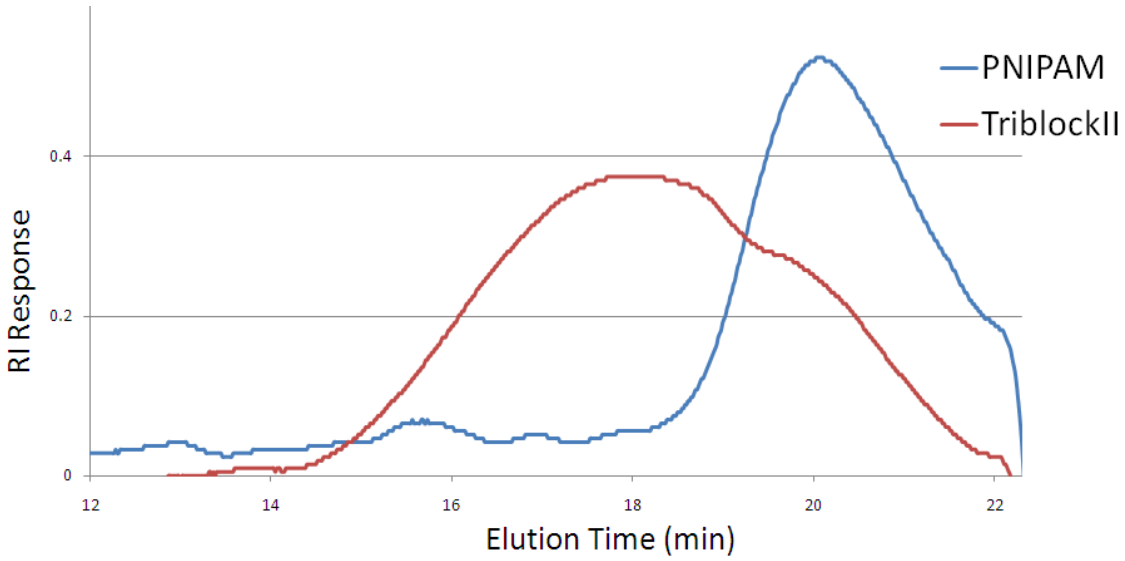

Figure 4.3 GPC trace of PNIPAM and Triblock II in water with 0.5M $NaNO_3$ running at 0.5ml/min and 25^{o}C.The reduced elution time of TriblockII as compared to PNIPAM first block homopolymer suggests an increase of polymer molecular weight and a successfully extension.

(a)

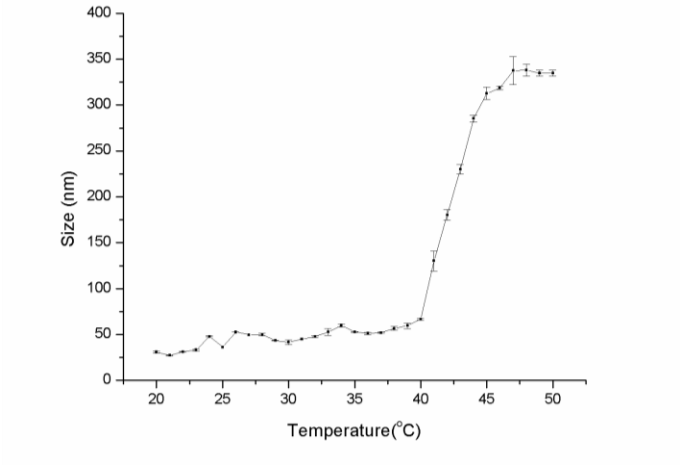
Size (nm)
Temperature(°C)

(b)

(c)

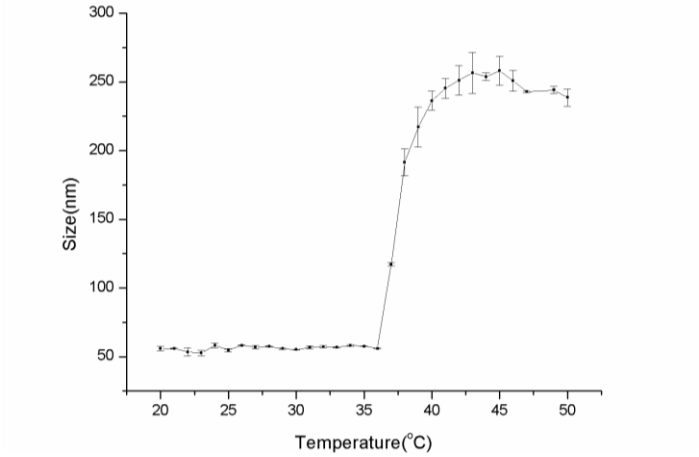
Size(nm)
Temperature(°C)

(d)

(e)

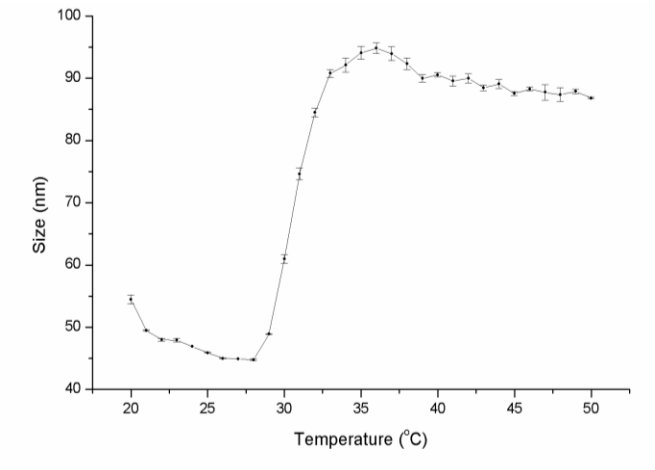
Size (nm)
Temperature (°C)

(f)

Figure 4.4 Hydrodynamic radius change of 0.1wt% (a) Triblock I, (c) Triblock II and (e) PNIPAM in water as temperature ramps from 20^{o}C to 50^{o}C together with representative pictures of three polymer solutions: (b) 20 wt% Triblock I (d) 20wt% Triblock II and (f) 5 wt% PNIPAM in a gelation test at 37^{o}C.

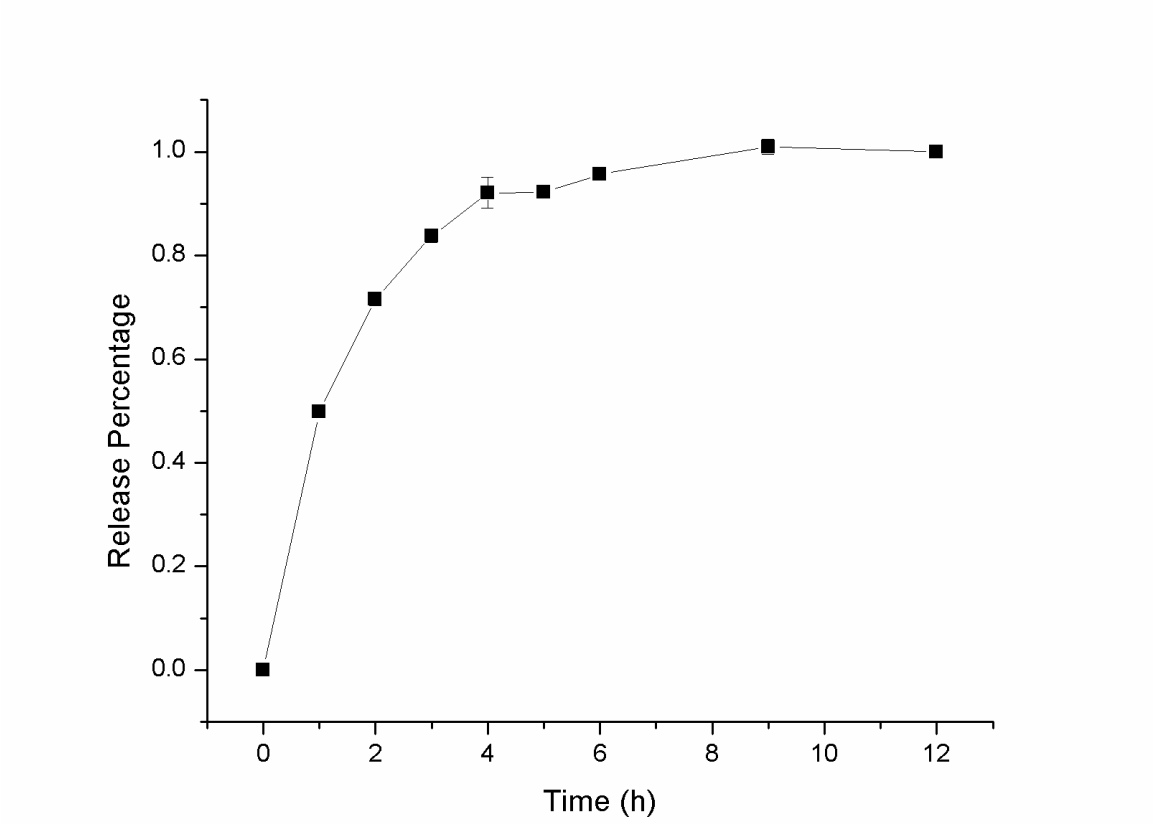

Figure 4.5 Release profile of Salicylate from the 20wt% Triblock II hydrogel disc in PBS at 37^{o}C as determined from reverse phase HPLC.

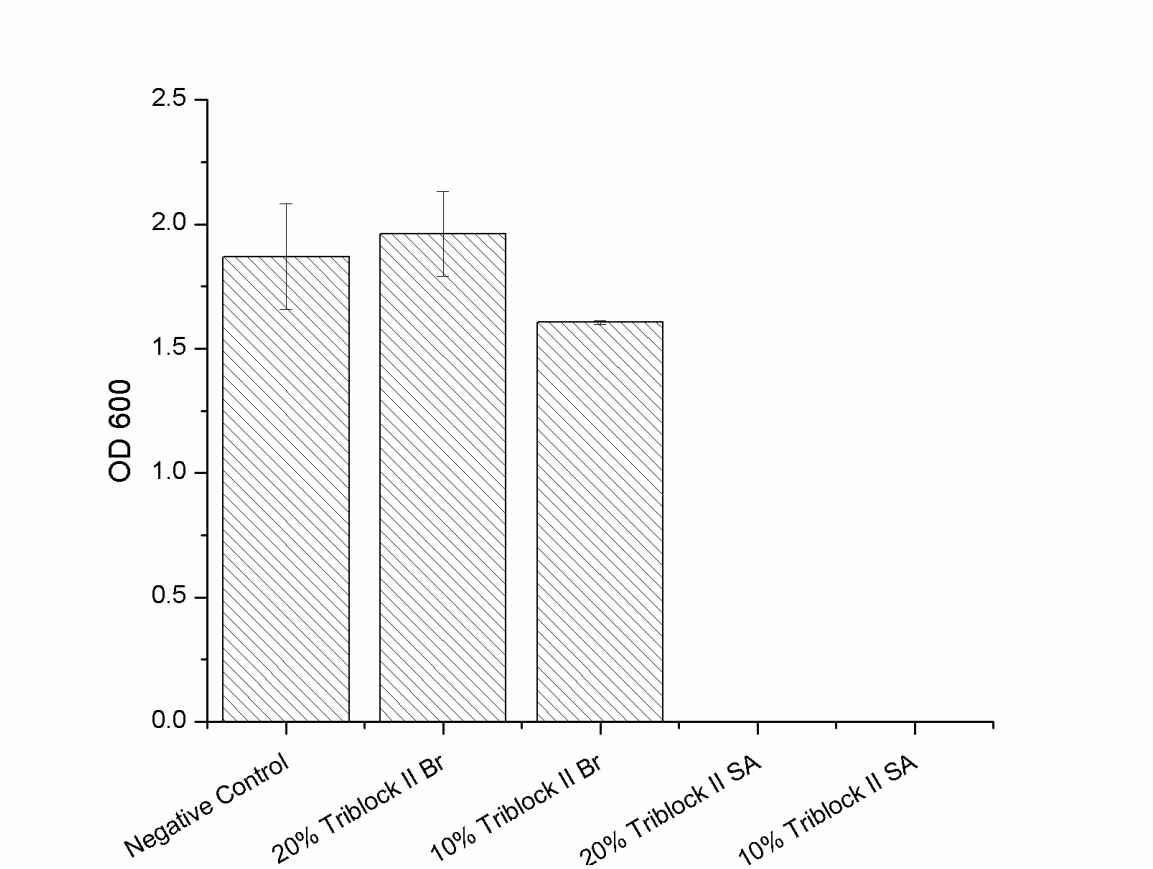

Figure 4.6 OD 600 of *E.coli* K12 inoculated LB liquid media after 12 h coincubation with various hydrogels. The final concentration of salicylate in the bacterial suspension incubated with 10% Triblock II SA is calculated to be approximately 160ug/ml.

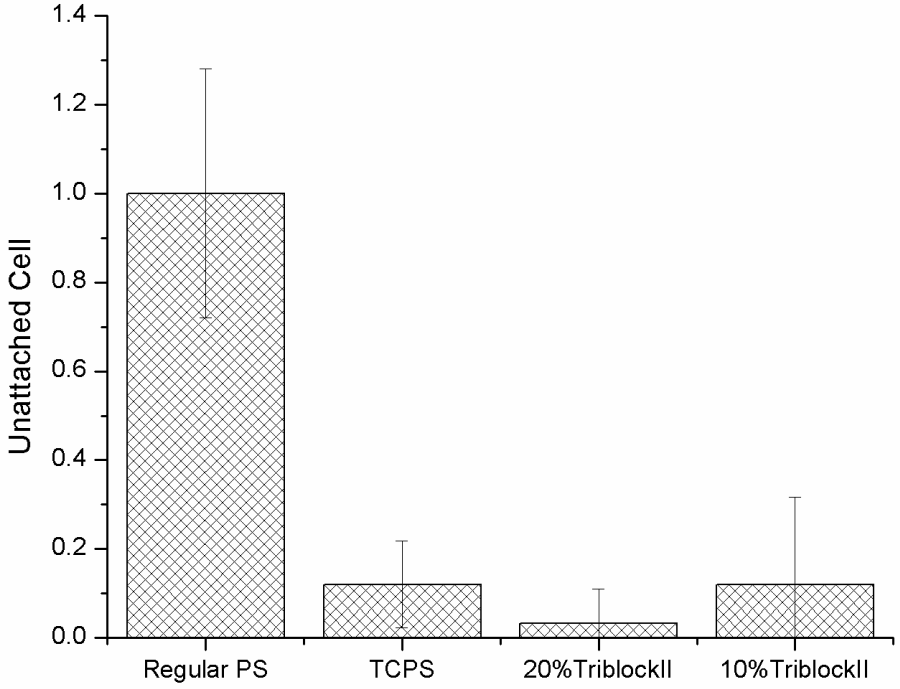

Figure 4.7 Normalized number of COS-7 cells remaining in the cell culture supernatant after 2-hour cell incubation on various surfaces.

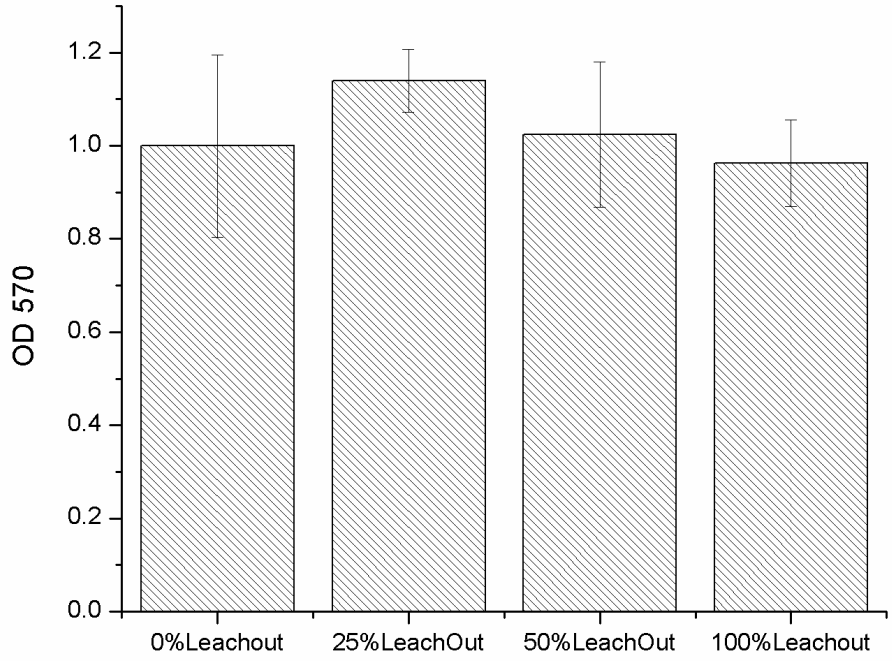

Figure 4.8 Cytotoxicity of Triblock II (SA) hydrogel leach-out on COS-7 cell as determined by MTT assay. Even at 100% leach-out, which is the same dosage used in the bacteria growth inhibition assay, no significant detrimental effect on mammalian cell metabolism is observed.

Chapter 5. Divalent Cation-mediated Polysaccharide Interactions with Zwitterionic Surfaces

One popular postulation in the design of a nonfouling surface is that a surface capable of resisting nonspecific protein adsorption should also resist bacterial adhesion and subsequent biofilm formation. Such a hypothesis, though valid in certain cases, oversimplifies complex biological systems, since they contain not only proteins but also other biomacromolecules, such as polysaccharides. This work aims to re-examine this postulation by testing the biofouling of polysaccharides onto protein-resisting zwitterionic surfaces in the presence of a multivalent cation. Our results show that Mg^{2+} plays an important role in mediating alginate adsorption onto zwitterionic surfaces through ion-bridged interactions from surface plasmon resonance (SPR) experiments. Three zwitterionic polymers tested in this work have clearly different responses to changes in Mg^{2+} concentration, indicating that such ion-bridged adsorption is strongly dependent on cation-zwitterionic polymer binding affinities and is dictated by the specific chemical structure of the polymer betaine side chain. This work underlines the necessity to go beyond current nonfouling criteria at the protein level and to take into account polysaccharides when it comes to complex environments.

5.1 Introduction

It has been postulated that bacteria adhesion occurs through the surface adsorption of proteins [9, 88]. This popular assumption has motivated many studies to use protein-

resisting surfaces, particularly polyethylene glycol (PEG) based polymers, to fend off bacteria attachment with considerable success [89-91]. However, up to now, long-term bacteria resistance in complex environmental conditions remains a major challenge for surface engineering, and it directly hampers industrial and clinical applications of nonfouling materials [92]. Further improvement over coating performance calls for a more comprehensive understanding of bacteria surface fouling at the molecular level.

Despite its general acceptance, the direct correlation between nonspecific protein adsorption and bacteria adhesion can be an oversimplification in a genuine biological environment, in which non-proteinaceous biomacromolecules, especially bacteria extracellular polysaccharides (EPS), are also major components. For example, *Pseudomonas aeruginosa*, a gram-negative bacterium causing clinical infections, has been known to produce a copious amount of EPS, surrounding the bacteria cell and diffusing into the media [15]. An adsorbed protein layer may not be a requirement for *Pseudomonas aeruginosa* adhesion. The important roles of EPS during surface conditioning, bacteria adhesion, and biofilm formation have also been widely reported for many other bacteria species [93-95]. The biological importance of polysaccharide as well as its structural difference from proteins thus poses new questions and challenges regarding the design and fabrication of nonfouling surfaces to achieve long-term bacteria resistance.

In this work, we study the adsorption of alginate, a carboxylate-group-rich polysaccharide, onto zwitterionic surfaces for two objectives: First, to test whether a protein-resisting coating alone is sufficient to resist polysaccharide adsorption; second, to probe the potential role of multivalent cations in the process of polysaccharide surface

fouling, as many bacteria-derived EPS bear acidic moieties and can bind cations in an aqueous environment [96, 97]. Zwitterionic polymers used in this study are known to effectively resist nonspecific adsorption from single-protein solutions and undiluted human blood plasma/serum [98]. A typical zwitterionic unit contains a quaternary amine cationic moiety and a negatively charged moiety in the form of carboxylate or sulfonate. Despite extensive studies so far, relatively little is known about zwitterionic polymer nonfouling properties at the polysaccharide level, especially the biofouling implications of interactions between various negatively charged head groups and divalent cations. Three zwitterionic polymer surfaces: poly(N-(3-sulfopropyl)-N-(methacryloxyethyl)-N,N-dimethylammonium betaine) (PSBMA), poly(2-carboxy-N,N-dimethyl-N-(2'-methacryloyloxyethyl) ethanaminium inner salt) (PCBMA-2) and poly(1-carboxy-N,N-dimethyl-N-(3'-acrylamidopropyl) methanaminium inner salt) (PCBAA-1) were herein prepared and tested because of their distinctive chemistries (Scheme 5.1). Significant surface adsorption of alginate was observed on PSBMA and PCBMA-2 coated surfaces which have been shown to effectively resist non-specific protein adsorption from undiluted human plasma. In addition, Mg^{2+} was found to mediate alginate adsorption in a concentration-dependent and surface-specific manner using SPR (Scheme 5.2). This divalent cation-facilitated binding was explained using quantum chemical calculations and specific ion pair interaction theory. Alginate studied in this work is a major component of many bacterial EPS and biofilm matrices. Its high surface binding in the presence of divalent cations highlights the importance to expand the current protein-resisting criteria in the design and characterization of bacteria nonfouling surfaces [99, 100].

5.2 Materials and Methods

5.2.1 Chemicals

[2-(Methacryloyloxy)ethyl]-dimethyl-(3-sulfopropyl)-ammonium hydroxide (SBMA 97%), 2,2'-Bipyridyl (BPY 99%), copper (II) bromide ($CuBr_2$ 99%), copper (I) bromide (CuBr), bromoisobutyryl bromide (BIBB 98%), 11-mercapto-1-undecanol (2, 97%), and 0.15M phosphate-buffered saline (PBS , 138 mM NaCl, 2.7 mM KCl, pH7.4) were purchased from Sigma-Aldrich (Milwaukee, WI, USA). Dextran (100,000 KDa MW), low molecular weight alginate (12-80 KDa MW), and high molecular weight alginate (80-120 KDa MW) were also purchased from Sigma-Aldrich. N,N-dimethylaminopropyl acrylamide was purchased from TCI America (Portland, OR, USA).Magnesium chloride hexahydrate ($MgCl_2$ 6H2O) was purchased from Fischer Scientific (Fair Lawn, NJ, USA). Ethanol was purchased from Decon Laboratories (King of Prussia, PA). Tetrahydrofuran (THF) was purchased from Mallinckrodt Chemicals (Phillipsburg, NJ). Pooled human blood plasma was purchased from BioChemed Services (Winchester, VA). Water used in experiments was purified using a Millipore water purification system with a resistivity of 18.2 Ω·cm.

CBMA-2 monomer was prepared following a previously published method [49].

CBAA-1 monomer was synthesized via a two-step reaction. First, N,N-dimethylaminopropyl acrylamide was reacted with ethyl bromoacetate in acetonitrile at 60^{o}C for 12 h. Upon reaction completion, the acetonitrile in the reaction solution was removed using a rotary evaporator, and the product, 3-acrylamido-N-(2-ethoxy-2-oxoethyl)-N,N-dimethylpropan-1-aminium bromide, was precipitated out with diethyl

ether at a quantitative yield. After extensive acetone washing, the product of the first step reaction was then hydrolyzed in aqueous solution using Amberlite anion exchange resin (OH^- form) to get CBAA-1 monomer. 1H NMR (D2O 300M Hz): 6.26 (m, 2H), 5.82 (m, H), 3.90 (s, 2H), 3.62 (m, 2H), 3.41 (t, 2H), 3.25 (s, 6H), 2.04 (m, 2H).

5.2.2 Preparation of self-assembled monolayers

Glass chips were first coated with an adhesion-promoting chromium layer (thickness 2 nm) and a surface plasmon active gold layer (48 nm) by electron beam evaporation under vacuum. Before self-assembled monolayer (SAM) preparation, the gold-coated glass substrate was rinsed with ethanol and water in sequence, dried with filtered air, then further cleaned in an UV ozone cleaner (Jelight, model 42) for 20 min.

The cleaned chip was immediately soaked in a 0.1mM ethanol solution of ATRP initiator for 24 h to form a SAM on the gold surface [31]. The chip was subsequently rinsed with THF, then ethanol, and dried with a stream of filtered air just prior to surface-initiated polymerization.

5.2.3 Surface-initiated atom transfer radical polymerization

Surface initiated ATRP was carried out on SAM coated gold substrates following a method similar to one previously reported [31]. Briefly, CuBr, $CuBr_2$, BPY, and gold chips with immobilized initiators were placed in a sealed reaction tube and deoxygenated via vacuum and nitrogen purging. SBMA, CBMA-2, or CBAA-1 monomer was deoxygenated in a separate sealed tube, and then dissolved in a deoxygenated solution of methanol and pure water in a 10:1 volume ratio. The monomer solution was transferred to the reaction tube using a syringe under nitrogen protection. In a shaker at 120 RPM

and 25℃, PSBMA was allowed to react for 1h; PCBMA-2 and PCBAA-1 for 3h. After polymerization, chips were removed, rinsed with pure water and PBS, and stored overnight in PBS. Chips were rinsed with Milli-Q water and dried with filtered air just prior to any experiments. Dry film thickness was measured by ellipsometer (J.A. Woollam, Alpha-SE), and chips with thicknesses of 25-32nm were used for SPR measurement.

5.2.4 Measurements of polysaccharide adsorption

For SPR, $MgCl_2$ was dissolved in PBS at 1.0mM, 3.0mM, 5.0mM, and 20.0mM concentrations. Dextran and alginate solutions were prepared at 1.0 mg/mL in PBS with or without additional Mg^{2+}.

This study used a custom-built surface plasmon resonance (SPR) sensor from the Institute of Photonics and Electronics, Academy Sciences (Prague, Czech Republic). A prepared chip was attached to the base of the prism and optical contact was established using refractive index matching fluid (Cargille). A quadruple channel flow cell with four independent parallel flow channels was used to contain liquid samples during experiments. A peristaltic pump (Ismatec) was utilized to deliver liquid samples to the four channels of the flow cell. A stable baseline was first established with PBS running buffer, then polysaccharide solution was delivered to the surface at a flow rate of 0.050 ml/min for 30 minutes, and PBS flowed again for 10 minutes before determining final wavelength shifts. A surface-sensitive SPR detector was used to monitor surface interactions in real time, and wavelength shift was used as an indication of changes on the surface.

5.2.5 Quantum chemical calculations

The electron density profiles were obtained from single-point energy calculations for both C1 and C2 with optimized structures. Calculations were carried out using the Gaussian 2009 at the B3LYP/6-311++G(d,p) level [101]. At the first step, molecular modeling with a classical UFF force field was carried out in the aim to generate the input of geometric structure for quantum calculations [102]. For C1, we rotated the N-C-C-O dihedral and six different structures with relatively low energies were selected. For C2, we rotated the N-C-C-C dihedral and selected five different structures. All of the selected structures were then optimized in an implicit water solvent at the B3LYP/6-311++G(d,p) level. For each molecule, the structure with the lowest potential energy was chosen for further single-point energy calculations.

5.3 Results and Discussion

5.3.1 Mg^{2+} mediated alginate binding on PSBMA, PCBMA-2 and PCBAA-1

PSBMA, PCBMA-2 and PCBAA-1 coated gold chips were prepared via surface initiated ATRP, and then tested for alginate adsorption under varying Mg^{2+} concentrations using SPR. Because macromolecular surface fouling can be affected by film thickness, to ensure a fair comparison, all three films used in this study were optimized to have approximately 30nm thicknesses. This particular thickness was selected as a good balance between the polymer brush nonfouling property and SPR biosensor sensitivity [103]. Under testing conditions, all surfaces used have $<5ng/cm^2$ (or <0.3nm SPR wavelength shift) adsorbed proteins from undiluted blood plasma, which is regarded to be ultralow fouling as reported previously [98, 104].

Mg^{2+} was selected as the cation of interest for two reasons. First, it is abundant in most biological environments. Typical human blood Mg^{2+} concentration, for instance, is reported to be about 1mM [105]. Secondly, compared to Ca^{2+}, Mg^{2+} has a weaker association with alginate and does not cause macroscopic gelation of the polysaccharide in solution [106]. The second factor makes it possible to differentiate the changes between interfacial and bulk properties.

Figure 5.1 shows high molecular weight alginate (80~120KDa) adsorption onto zwitterionic polymer-coated surfaces as Mg^{2+} increases from 0 to 20mM. When compared to human plasma fouling data collected on the same surface, this result strongly indicates that a protein-resisting surface does not necessarily guarantee polysaccharide nonfouling (Figure 5.2). One striking finding in the Mg^{2+} concentration dependence study is the 14-fold increase in alginate adsorption on the PCBMA-2 surface, whereas the PSBMA surface, despite its relative high alginate adsorption in un-supplemented PBS, is largely unaffected by the Mg^{2+} concentration change. This difference is believed to be caused by strong interactions between Mg^{2+} and the carboxylate groups on PCBMA-2, thus effectively forming a divalent cation bridge between the free alginate and the surface bound zwitterionic polymer. Such magnesium ion bridged interactions are indeed discovered in many biological systems, including the stabilization of protein and DNA structures [107]. The anionic form of sulfonate, on the other hand, is a less ideal ligand: the well-dispersed electron density on the head group through resonance stabilization makes sulfonate anion a much weaker Lewis base, with a reported pKa of trialkylammonio alkyl sulfonate at about 1[108]. As a result, it is unable to have significant interactions with Mg^{2+}. In addition, the divalent cation-dependent

surface fouling of PCBMA-2 was only observed at the polysaccharide level, but not at the protein level, as no statistically significant difference in protein adsorption was observed by either adding 5mM Mg^{2+} to human plasma or pretreating the PCBMA-2 surface with 1M $MgCl_2$ before SPR (data not shown).

Recently, Collins proposed a concise law of "matching hydration free energy" which gave convincing explanations to many experimentally observed phenomena related to specific ion pair interactions, including the ranking of the Hofmeister series [109]. The Collins' law states that oppositely charged ions with similar absolute free energy of hydration have a high tendency to form inner sphere ion pairs. As hydration free energy is a monotonic function of ion surface charge density, it further indicates that small multivalent cations (e.g. Mg^{2+}, Ca^{2+}) would interact favorably with anions with similarly high surface charge densities [110]. Electrostatic attraction is generally considered to be the main contributor in this type of interaction [109]. Kunz, based on a computational study, reported the surface charge density of anionic head groups prevalently found in biological systems to have the following order: $RCOO^- > R_2PO_4^- > RSO_4^- > RSO_3^-$ [111, 112]. Thus, it is not at all surprising that certain natural or synthetic macromolecules bearing specific anionic moieties (especially, carboxylate) would display considerably higher association affinity towards multivalent cations compared to others. The difference in Mg^{2+} concentration response between PCBMA-2 ($RCOO^-$) and PSBMA (RSO_3^-) observed in this study correlates well with the Kunz's theoretical prediction. It is also worth pointing out that a single Mg^{2+} cation may potentially interact with multiple anionic groups on the polymer chain, further increasing its affinity.

Interestingly, reducing the carbon spacer between the quaternary amine and carboxylate group on the carboxybetaine side chain (PCBAA-1) effectively suppressed magnesium facilitated alginate binding. This is speculated to be caused by a more pronounced inductive effect from the adjacent electron-withdrawing quaternary amine moiety and will be further explained below. It is worth pointing out that the change in polymer backbone is not expected to have major effects on the polymer property of interest, as poly(2-carboxy-N,N-dimethyl-N-(3'-arylamidopropyl) ethanaminium inner salt (PCBAA-2) displayed a Mg^{2+} dependence comparable to PCBMA-2 and is drastically different from PCBAA-1 (data not shown). PCBAA-1 rather than PCBMA-1 is used in this work due to ease in organic synthesis.

5.3.2 Quantum chemical calculations on CBMA-2 and CBAA-1 head groups

In order to gain insight into their distinctive response to divalent cations, quantum chemical calculations were performed on the two zwitterionic carboxylate head groups to investigate the effect of changing quaternary amine proximity on the local electron density of the carboxylate group. Figure 5.3 shows the calculation results of the electrostatic potential of the two molecules. On the same color scale, a deeper red color corresponds to a more negative local charge of the molecule. Evidently from the calculations, reducing the carbon spacer from two to one between carboxylate and the strong electron withdrawing group drastically changes the charge distribution on the carboxylate moiety. Compared to its two carbon spacer counterpart, this lowered charge density on CBAA-1 carboxylate stabilized its anionic form, thus reduced its affinity towards multivalent cations. The significance of this structural difference between two carboxybetaine head groups is also reflected in their tendency towards protonation. The

measured pKa for carboxybetaine one carbon spacer (CB-1) and two carbon spacer (CB-2) are 1.8 and 3.3 respectively [52]. This previously reported large pKa shift corroborates well with our experimental results and theoretical calculations in this study.

5.3.3 Effect of polysaccharide molecular weight and chemical structure on Mg^{2+} mediated surface adsorption

To confirm our ionic bridging hypothesis and probe the effect of molecular weight and chemical structure on divalent cation-mediated polysaccharide surface adsorption, we further tested the PCBMA-2 surfaces with lower molecular weight alginate (LW alginate) (12~80KDa) and dextran, another biologically important polysaccharide that bears no carboxylate group. Experiments were conducted following the same SPR procedure at Mg^{2+} concentrations of 0 mg/ml, 5 mg/ml, and 20mg/ml. Figures 5.4 (a) and (b) show the representative SPR sensorgrams and statistic results of PCBMA-2 surface fouling of LW alginate and dextran, as well as the previously used high molecular weight alginate (HW alginate). Both alginate polymers adsorb onto PCBMA-2 surface in a strong Mg^{2+} concentration dependent manner, and, between the two, HW alginate appears to be more sensitive to the presence of cation, suggesting that polymer molecular weight is a relevant factor in polysaccharide biofouling. Dextran, on the other hand, does not attach onto PCBMA-2 surfaces at all Mg^{2+} concentrations tested. As a non-ionic and hydrophilic neutral polymer, dextran is expected to be nonsticky and inert to changes in the ionic environment.

5.4. Conclusions

In this work, we studied alginate adsorption onto three zwitterionic polymer surfaces (PSBMA, PCBMA-2, and PCBAA-1) at varying concentrations of Mg^{2+} using SPR. The

divalent cation-mediated surface adsorption is found to be affected by the type of the anionic moiety on zwitterionic polymers as well as its local chemical environment. The relatively high negative charge density on the PCBMA-2 carboxylate group makes it most responsive to Mg^{2+} concentration changes. More importantly, all three surfaces studied in this work were tested to withstand very challenging protein fouling conditions (undiluted human plasma) and yet showed drastically different responses to cation-facilitated alginate fouling. This finding indicates a fundamental difference between polysaccharide and protein surface adsorption. It further suggests that a nonfouling surface capable of resisting both protein and polysaccharide fouling, such as PCBAA-1, is desirable to cope with the complex nature of bacteria biofouling processes.

5.5 Acknowledgements

This work is supported by the Defense Threat Reduction Agency (HDTRA1-10-1-0074).

5.6 Chapter Figures

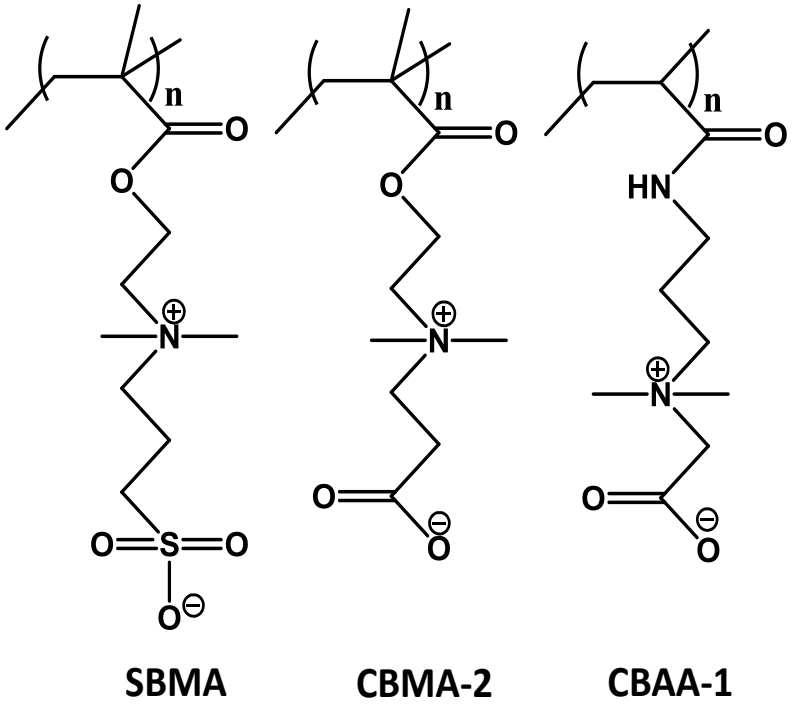

Scheme 5.1 Chemical structures of PSBMA, PCBMA-2 and PCBAA-1 polymers.

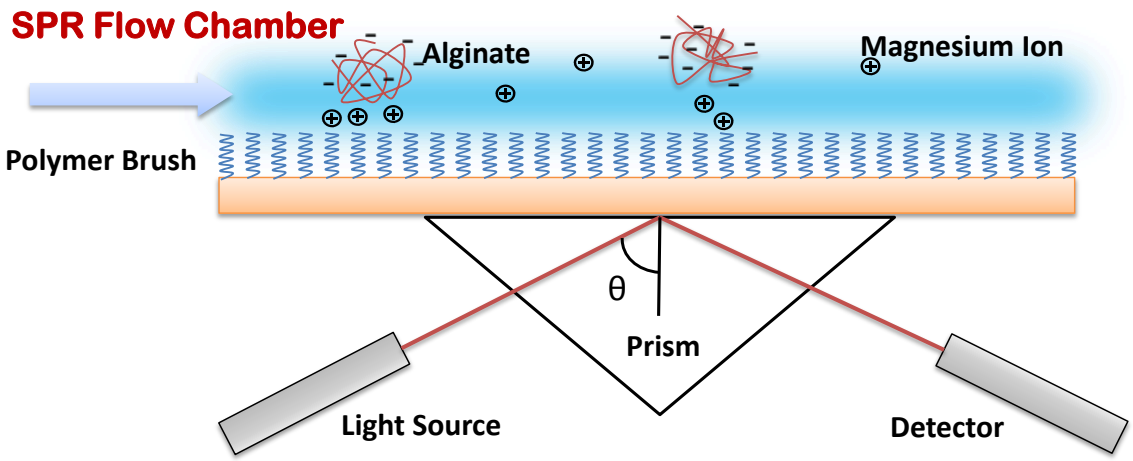

Scheme 5.2 Scheme 2: Mg^{2+} mediated alginate adsorption onto zwitterionic polymer coated surfaces monitored by SPR.

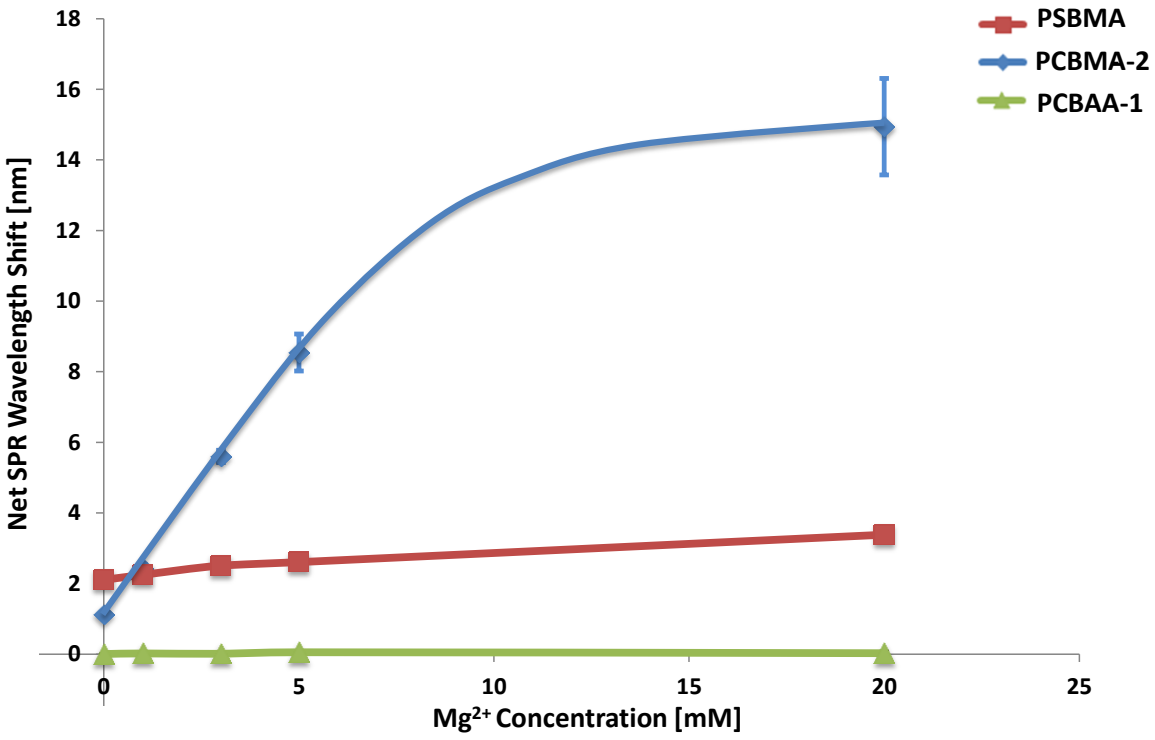

Figure 5.1. High molecular weight alginate adsorption onto PSBMA, PCBMA-2, and PCBAA-1 polymer surfaces as Mg^{2+} concentration changes from 0 to 20 mM in the PBS running buffer.

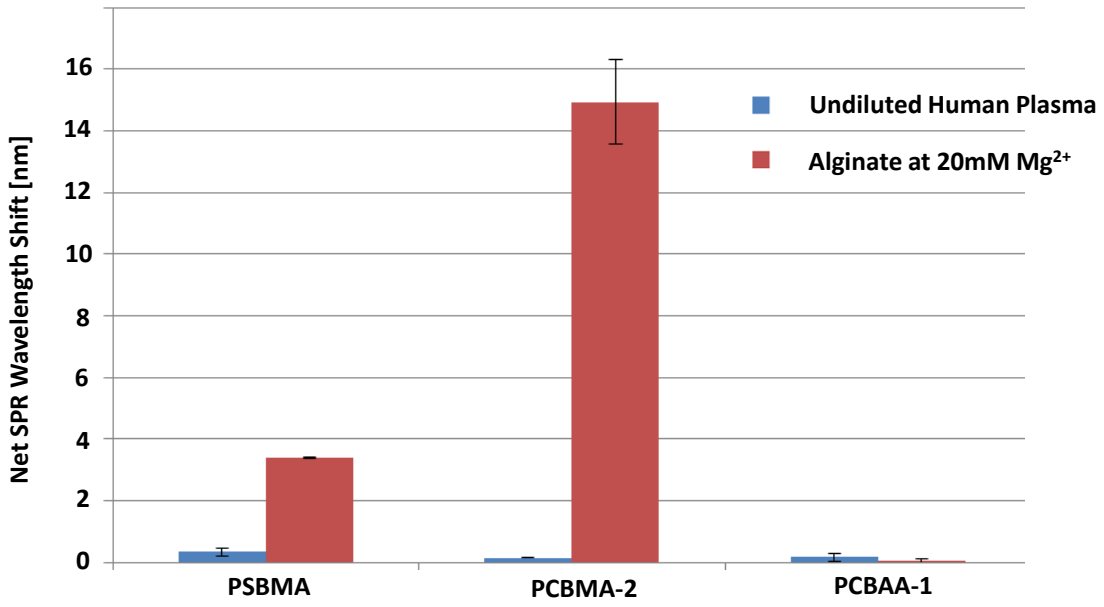

Figure 5.2 Comparison between protein fouling (undiluted human plasma) and polysaccharide adsorption at 20mM Mg^{2+} on three zwitterionic polymer coated surfaces

(a)

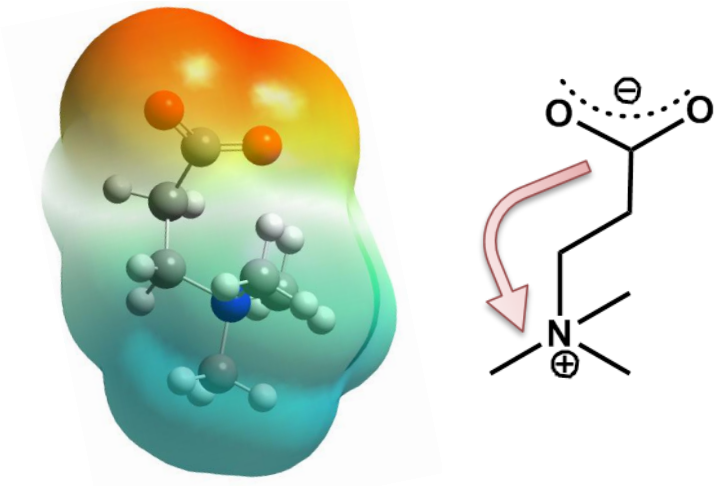

(b)

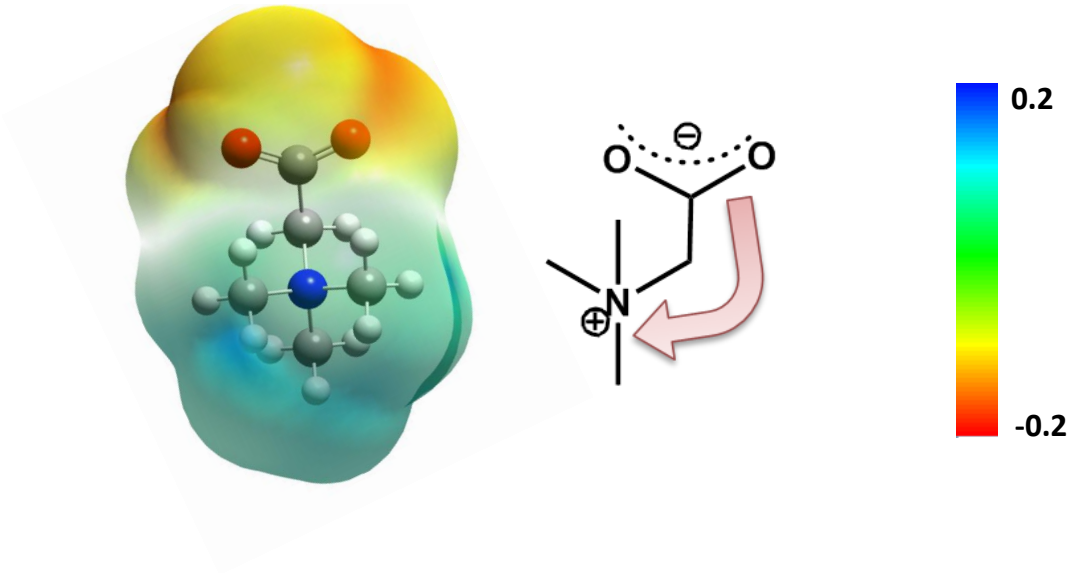

Figure 5.3 Electron density surfaces of CBMA-2 (a) and CBAA-1 (b) head groups colored according to the electrostatic potential obtained from quantum chemical calculations. A deeper red color corresponds to a higher local negative charge.

(a)

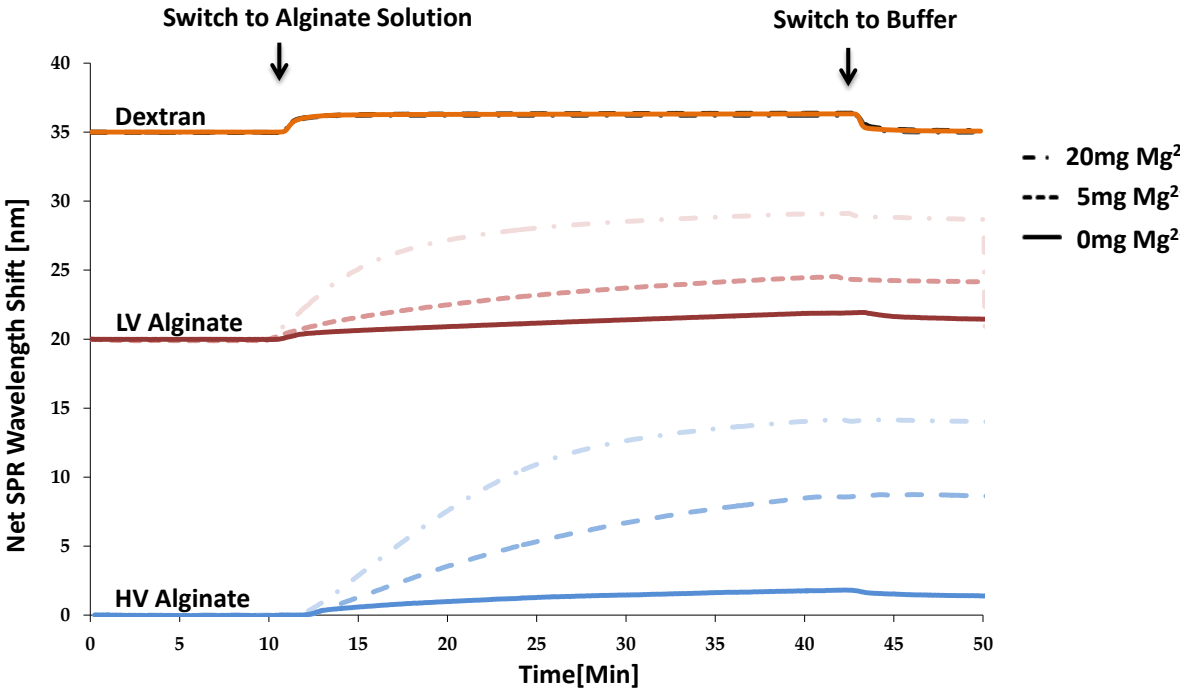
Switch to Alginate Solution
Switch to Buffer
Dextran
LV Alginate
HV Alginate
Net SPR Wavelength Shift [nm]
Time[Min]
20mg Mg2
5mg Mg2
0mg Mg2

(b)

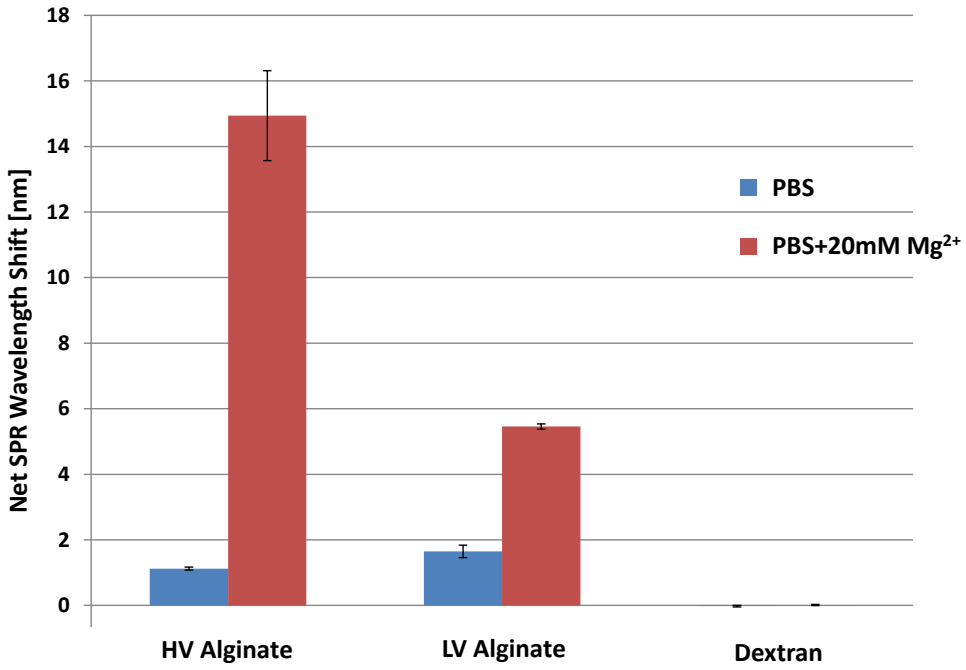
Net SPR Wavelength Shift [nm]
PBS
PBS+20mM Mg2+
HV Alginate
LV Alginate
Dextran

Figure 5.4 (a) Representative SPR sensorgrams of high molecular weight alginate, low molecular weight alginate, and dextran adsorption on PCBMA-2 surfaces with a PBS running buffer supplemented with 0mM, 5mM and 20mM Mg^{2+}. (b) Statistical results of high molecular weight alginate, low molecular weight alginate, and dextran adsorption on PCBMA-2 surfaces with a PBS running buffer supplemented with 0mM or 20mM Mg^{2+}.

Chapter 6. Chemical Insights into Dodecylamine Spore Lethal Germination

Bacterial endospores can withstand common disinfection procedures and extreme environmental adversities. This tenacity for survival, coupled with pathogenicity, makes spores a major threat for the food and medical industries as well as national security. Though unsuitable for practical usage due to their high environmental toxicity, primary ammonium surfactants, dodecylamine (DDA) in particular, are the most potent antispore molecules known. However, over half a century after the initial discovery, the mechanism of DDA spore killing remains largely elusive and antispore compounds with practical utility are still greatly needed. Herein, we propose and provide evidence that DDA bioactivity may lie in its capacity to form hydrophobically stabilized salt bridges with carboxylate anions of the spore cortex, a structure critical in maintaining a low water content in the spore core. More importantly, the proposed mechanism of action was experimentally shown to be useful in guiding the design of potential antispore agents.

6.1 Introduction

Bacterial spores are known to survive under extreme environmental adversities, including heat, UV radiation, conventional antibiotics as well as strong acidic/basic conditions [113,114]. In contrast to this tremendous tenacity, spores show unexpectedly high susceptibility to primary ammonium surfactants: at as low as 10^{-4} M, dodecylamine (DDA) was reported to trigger *Bacillus megaterium* spore germination followed by inactivation at near physiological temperature [16,115]. However, more than half a

century after its initial discovery, the molecular details of the DDA lethal germination process – its direct biological target(s) and the physiochemical nature of this interaction – remain largely unknown. This lack of fundamental understanding, together with the natural resistance of bacterial spores to conventional disinfection procedures and antibiotic compounds, makes the study of DDA-spore interaction of both scientific and practical importance.

The capability of spores to withstand harsh environmental conditions is mainly attributed to the low water content in the spore central core [113,114,116]. Besides the low permeability of the inner membrane [117], the high osmotic pressure originated from the electrostatic potential of the negatively-charged peptidoglycan matrices constituting the cortex layer has also been suggested to play a critical role in maintaining this low water content [118-120]. We hypothesize that DDA may initiate spore germination by quenching the negatively charged carboxylate groups within the spore cortex layer via salt bridge formation, a hybrid of hydrogen bonding and electrostatic interaction, thus annulling the osmoregulatory function of spore cortex, leading to core rehydration and finally the loss of viability after prolonged exposure to this cationic surfactant (Scheme. 6.1).

This proposed mechanism of action has the following merits: 1), it is consistent with the known structure [121] and suggested function [118] of spore cortex; 2), the model is compatible with the high permeability of the outer membrane [122]; 3), the proposed interaction through salt-bridge formation neatly explains the almost qualitative difference in lethal germination potency between primary-ammonium-based DDA and quaternary ammonium surfactants [123].

In this work, we present experimental evidence supporting this hypothesis through the study of DDA structural analogues and germination inhibitors, a chemical approach proven useful not only for gaining insights of the fundamental mechanism but also in unveiling the structural determinants for its bioactivity. It was discovered that dodecylguanidinium (DDG), another surfactant molecule capable of forming salt bridges with carboxylate, has a lethal germination potency comparable to DDA, and both are at least two orders of magnitude more effective than dodecyl trimethylammonium chloride (DTAC) – a quaternary-ammonium-based cationic surfactant. Furthermore, our study also indicated that the main function of DDA alkyl tail is to stabilize the salt bridge through hydrophobic interactions with the cortex matrices rather than creating multivalent binding via self-assembly. Lastly, it is demonstrated through one example that the molecular understanding acquired in this study can be useful in the design and discovery of potential antispore agents that ideally share the high bioactivity of DDA while exempt from its severe environmental toxicity [124].

6.2 Materials and Methods:

6.2.1 Chemicals

Dodecylamine (DDA), NaCl, $CaCl_2$, $NiCl_2$, $ZnSO_4$, $CuCl_2$, $FeCl_3 \bullet 6H_2O$, [2-(acryloyloxy)ethyl]trimethylammonium chloride (TMAEMA), 2-carboxyethyl acrylate (CAA), 3-[dimethyl-[2-(2-methylprop-2-enoyloxy) ethyl]azaniumyl] propane-1-sulfonate (SBMA), 2-mercaptoethanol, dodecyl trimethylammonium chloride (DTAC), 1H-pyrazole- 1- carboxamidine hydrochloride, 4,4'-azobis(4-cyanovaleric acid) (V-501), 4-cyano-4-[(dodecylsulfanylthiocarbonyl) sulfanyl]pentanoic acid (CTA), N,N'-methylenebis(acrylamide) (MBAA), 3,5-Dimethyladamantane-1-acetic acid (DMAA), 2-

hydroxy-2-methylpropiophenone and 1,12-diaminododecane, methacrylic anhydride were purchased from Sigma-Aldrich Chemical Co. (MO, USA); 2-aminoethyl methacrylate hydrochloride (AMA), 2-(dimethylamino)ethyl methacrylate (DMAEMA), 2-hydroxyethyl methacrylate glycol methacrylate (HEMA), and urea were purchased from Acros Organics (PA, USA); acrylic acid was purchased from Alfa Aesar (MA, USA); sodium dodecyl sulfate was purchased from Fisher Scientific (PA, USA); N-[(3,5-dimethyl-1-adamantyl)methyl]guanidine hydrochloride (DMAG) was purchased from Chembridge Co. (CA, USA)

Nutrient Broth No1 was purchased from Fluka Analytical (MO, USA); Bacto Agar was purchased from BD (NJ, USA); *Bacillus megaterium* spore stock solution was purchased from Mesa Laboratories, Inc. (MT, USA).

Dodecyl guanidine (DDG) was synthesized based on a previously published method [125]. In a typical reaction, 2.93 g 1H-pyrazole- 1- carboxamidine hydrochloride, 3.71 g dodecyl amine (DDA), and 2.58 g N,N-diisopropylethlamine (DIEA) was added to 10ml dimethylformamide (DMF), and the reaction was vigorously stirred for 18 h. Dry ether was then added into the reaction to precipitate out the crude product. This crude product was then further purified with a silica gel column using methanol and dichloromethane mixed solvent as the eluent. The resulting compound was characterized by 1H NMR (300 MHz, MeOD): δ3.19 p.p.m. (t, 2H), δ1.56 p.p.m. (m, 2H), δ1.32 p.p.m. (m, 2H), δ1.13 p.p.m (m, 16H), δ0.86 p.p.m. (t, 3H), and 13C NMR (300 MHz, MeOD): δ 158.59, 42.56, 33.12, 30.54, 27.78, 23.80, 14.63.

12-methacrylamidododecan-1-aminium chloride (MDA) was synthesized based on a previously published method [126]. In a typical reaction, 5 g protonated 1, 12-diaminododecane was first mixed with 8.09 g unprotonated 1,12-diaminododecane in 100 ml H_2O. The suspension was vigorously stirred for 1 h. 100 ml methanol was then added to the reaction flask, and the reaction was cooled to 0^oC on an ice bath. In a separate flask, 5.47 ml methacrylic anhydride and trace amount of hydroquinone was mixed with 15 ml methanol. After adding the solution of the second flask to the original mixture, the whole reaction was kept at 0^oC for 2 h. Following this, the system was acidified to pH 1 and left for 24 h. At the end of the 24 h reaction, solvent was removed on a rotary evaporator; the crude product was washed extensively with diethylether and then dissolved in acetic acid. The insoluble portion was filtered out on a Buchner funnel, and organic phase was subsequently dried on a rotary evaporator, resulting a white powder. The product was characterized by 1H NMR (300 MHz, DMSO): δ5.79 p.p.m. (s, 1H), δ5.41 p.p.m. (s, 1H), δ3.33 p.p.m. (t, 2H), δ3.11 p.p.m. (t, 2H), δ1.98 p.p.m. (s, 3H), δ1.77 p.p.m. (m, 2H), δ 1.56 p.p.m. (m, 2H), δ 1.34 p.p.m. (m, 16H).

6.2.2 RAFT Polymerization of AMA Monomer

AMA monomer was polymerized via reversible addition-fragmentation chain-transfer polymerization (RAFT) based on a previously published procedure that was shown to have good control over the degree of polymerization (DP) and yield a narrow polydispersity [127]. In a typical reaction, 3.33 g AMA monomer was dissolved in 12ml H_2O/dioxane 3:1 mixed solvent. The amount of chain transfer agent (CTA) was added based on the desired DP. Initiator V501 amount was kept at 1/5 of the CTA in all RAFT reactions. The solution was then deoxygenated by bubbling with dry nitrogen gas for 1h.

Following this, the reaction was heated to 70^{o}C and stirred vigorously. After 24 h, the reaction solution was characterized by 1H NMR to determine the polymerization conversion. The polymer was then purified by dialysis and finally dried via lyophilization. The degree of polymerization was calculated based on the initial monomer/CTA ratio and the conversion of the reaction.

6.2.3 Spore Lethal Germination Assay

In a typical assay of spore germination and lethality, bacterial spores were suspended in 100 mM NaCl or 150 mM PBS (Phosphate Buffer Saline) solutions containing the testing molecules for 30min under predetermined pH and temperature. After incubation, spore suspensions were, in the case of testing cationic surfactants, quenched with 1 mM SDS, diluted and spread onto Broth I agar plates (10g/L tryptone. 10g/L NaCl, 5g/L yeast extract and 1g/L glucose) for overnight culture at 37^{o}C. Broth I agar was verified in this study to completely germinate *B. megaterium* spores without the need for prior heat activation, thus ensuring that the difference in colony formation only comes from loss of viability in surfactant treatment and not from the incomplete germination during subsequent incubation. The viable spore number was determined by counting the colonies formed the following day as an indication for lethal germination potency. 100 mM NaCl was used in several experiments because PBS was found to cause precipitation with DDG; Tris buffer, another commonly used biological buffer, was not chosen because it has primary amine groups in the buffering agent, which could potentially interfere with the results.

For multivalent cation inhibition of DDA lethal germination, 0.1mM DDA in water was supplemented with various metal cations at various predetermined concentrations. *B.*

megaterium spores were subsequently added to the mixtures and incubated at 40^{o}C for 30min before dilution and eventual plating as described above.

6.2.4 Molecular Dynamic Simulations

Molecular dynamics simulations were used to evaluate binding free energies in fixed volume (NVT) simulations with explicit water and complete orienatational freedom. A single cation (primary amine, quaternary amine, or guanidinium) and carboxylate anion were placed in 30 Å cubes with TIP4P-Ew water molecules and the equivalent of 100 mM NaCl. The large box size is important to allow binding and unbinding of the two ions. The interatomic forces for the simulations were calculated using the OPLS-AA force field which is parameterized to replicate properties of small organic molecules [128]. The systems were prepared with energy minimization, annealing, and 200 ps equilibration molecular dynamics in Parrinello-Rahman NPT [129]. Production simulations were conducted in NVT with replica-exchange. 40 replicas with temperatures from 300 K to 350 K for 20ns with exchanges attempted every 100 fs giving total simulation time of 800 ns. The stochastic Bussi-Donadio-Parrinello NVT thermostat (τ=0.5 ps) was used [130]. Particle-mesh Ewald summation was used for the long range coulombic force calculations [131] and a shifted, truncated Van der Waals potential was used. A cutoff of 8 Å was used for interatomic forces. All covalent hydrogen bonds were constrained using the LINCS algorithm [132]. The GROMACS simulation engine was used for the molecular dynamics simulations [133]. The potential mean force was calculated from the radial distribution function using $A(r) = -k_b T ln[g(r)]$.

6.3 Results and Discussions

6.3.1 DDA primary ammonium head group.

Besides the primary ammonium, guanidinium is the most common cation in biological systems to form salt bridges with carboxylate anions [134]. We thus tested our hypothesis through the synthesis and characterization of DDG, a surfactant molecule with the same alkyl chain length as DDA but bearing guanidinium instead of primary ammonium as its head group. The efficacy of DDG in inducing germination and killing spores was tested with *B. megaterium* spores at 40^{o}C and pH 8 in 100 mM NaCl. After a 30-min exposure, the cationic surfactants were diluted and quenched by sodium dodecyl sulfate (SDS) to stop the interaction [135]. The spore suspensions were then immediately spread onto nutrient agar plates. The drop in viable spore count, measured by the reduction in colony number compared to the control samples, was used as an indication for lethal germination potency of surfactant molecules. The results showed that both DDA and DDG at 10^{-4} M can cause significant reduction in *B. megaterium* viability: 0% and 11% survival respectively, compared to that of the negative control (Figure 6.1a). In comparison, DTAC and SDS, two commonly used cationic and anionic surfactants, barely exhibited appreciable lethal germination activity even at 10^{-2} M under otherwise identical experimental settings.

To help bring insight to the functional differences between the three cationic surfactant molecules (DDA, DDG and DTAC), their head group binding free energies with carboxylate groups were evaluated in a fixed volume (NVT) molecular dynamic simulation with explicit water and complete orientational freedom (Figure 6.1b). The equivalent of 100 mM NaCl was also added to the simulation system to mimic the actual

experimental conditions. The potential mean force free energy calculated from radial distribution function indicates that the binding of carboxylate anion with primary ammonium or guanidinium is much more energetically favoured in comparison with the quaternary ammonium, thus corroborating our previous experimental findings.

We further reasoned that if DDA and DDG indeed interact with spore cortex carboxylate groups via salt bridging, the change in their lethal germination potency in response to environmental pH should parallel the protonation states of the participating head groups, as the coexistence of oppositely charged ionic groups is a prerequisite for salt bridge formation. This postulate was tested and the results are presented in Figure 6.1c and d. At pH 4, neither DDA nor DDG effectively induced *B.megaterium* spore lethal germination – though both surfactants were expected to bear positive charges under the acidic condition, the protonation of carboxylate groups (pKa 3.5~5) [136] within the spore cortex made the interaction unfavourable. It is also worth noting that pH 4 is significantly higher than the intrinsic pKa values of most phosphonate anions (pKa<1) [137] found in membrane phospholipids, and the loss of DDA bioactivity at this pH thus suggests that the spore inner membrane itself is not the direct target for DDA salt bridge formation. At pH 8, salt bridges can be readily established for DDA as well as DDG, as was duly reflected in their antispore activities. At pH 12, most DDA molecules are unprotonated and charge neutral as a result of their comparatively low pKa of 10.6 [136]. Meanwhile, the majority of DDG remains positively charged due to their higher pKa of 13.6 [136]. This difference in pKa corresponded to DDA and DDG's drastically different activities in initiating lethal germination at high pH.

Consistent with the effect of protonation of carboxylate groups at low pH preventing salt bridge formation, different multivalent metal cations were also observed to block lethal germination by DDA (Figure 6.1 d). By measuring the concentrations needed for various cations to effectively block the DDA lethal germination, the relative inhibition potency of these metal ions can be determined. This experimentally obtained ranking (Fe^{3+} > Cu^{2+} > Zn^{2+}> Ni^{2+} >Ca^{2+} >Na^{+}) matches exactly the relative affinity of these metal ions to a carboxylate-based anionic polymer matrix, thus suggesting an inhibition through competitive binding [138]. Another piece of noteworthy information supportive of cortex being the direct target of DDA is the observed higher inhibition potency of Zn^{2+} over Ni^{2+}: as previously reported, in the case of monomeric, polydentate ligand binding, Ni^{2+} is almost always more favoured than Zn^{2+}, while Zn^{2+} binds more strongly to an anionic polymer matrix due to its less strained tetrahedral stereochemical configuration [139].

6.3.2 DDA alkyl tail.

In addition to the cationic head groups, the hydrophobic alkyl tail also played an important role in DDA bioactivity: for primary ammonium surfactants from octylamine (C8) to tetradecylamine (C14), the extension of every two carbon atoms in the alkyl tail lowers the minimal antispore effective concentration approximately 10-fold [115]. We reason that there are two plausible explanations for this observation: first, the increase in hydrophobicity favours the adsorption of DDA on to cortex polymeric matrices and stabilizes the salt bridges subsequently formed [140,141]. The magnitude of typical hydrophobic interactions was calculated to be around 30 cal/(mol*$Å^2$), corresponding to a 3.5-fold increase in binding constant for a single methyl group [142], which numerically matches the change in the bioactivity of primary ammonium surfactants with increasing

tail length. Second, the long alkyl chain may also facilitate multivalent interactions via self-assembled micelle structures [143]. Multivalency here refers to the simultaneous interaction of multiple binding sites between two entities, and is often used to elevate the binding affinity in a competitive biological environment [144]. However, the fact that minimal antispore effective concentration of DDA is one order of magnitude lower than its reported critical micelle concentration (CMC) argues against the second explanation [145].

To further understand and confirm the role of DDA alkyl chain in the chemical germination process, we tested the lethal germination properties of various primary ammonium monomers and polymers, as they offered an easy way to orthogonally manipulate the molecular hydrophobicity and valency. As a starting point, six types of hydrophilic monomers bearing primary ammonium, quaternary ammonium, tertiary ammonium, sulfobetaine zwitterion, carboxylate, and hydroxyl groups were incubated with *B. megaterium* spores at 5% w/v and 80^{o}C in PBS for 30 min. Among the six monomers, only the one having primary ammonium group, 2-aminoethyl methacrylate hydrochloride (AMA), gave a statistically significant reduction in spore viability, albeit with much decreased potency compared to DAA as evidenced by the elevated incubation temperature and high concentration of AMA needed (equivalent to 300 mM) (Figure 6.2 a, b). The results of this experiment suggested that the biological activity of primary ammonium group in DDA is functionally enhanced by but structurally separable from its alkyl tail. Based on this, we reason that if simple hydrophobic interactions are responsible for the increased efficacy, a boost in bioactivity should be observed by switching to a hydrophobic but non-micelle-forming (critical packing parameter >1) primary

ammonium monomer. If, on the other hand, multivalency plays a role in the process, a difference should be expected between a primary ammonium monomer and its corresponding polymers. To this end, we synthesized the hydrophobic primary ammonium monomer 12-methacrylamidododecan-1-aminium chloride (MDA) as well as poly(2-aminoethyl methacrylate hydrochloride) (PAMA) with varying degree of polymerization (DP) (Figure 6.2 c, e) [126,127]. Their effects on spore viability were similarly tested in PBS at 80^{o}C for 30 min. 1% w/v of monomers was used when comparing AMA and MDA, and 5% w/v when AMA and PAMA were compared. Our results show that the bioactivity of the molecule correlates strongly with monomer hydrophobicity, but is largely independent of the degree of polymerization (Figure 6.2 d, f). This indicates that the chief role of the alkyl chain in DDA is to promote hydrophobic interaction and not to facilitate multivalent binding.

6.3.3 Structural determinants for antispore compounds

Taken together, the two essential structural features determining the potency of DDA-like molecules in inducing spore lethal germination are: 1) cationic head groups capable of forming salt bridges with carboxylate groups; 2) hydrophobic moieties, not necessarily unbranched alkyl chains that enhance surface adsorption and stabilize salt bridge interactions. Once spore germination is triggered, the germinated spore can then be killed by further exposure to the cationic compound initially used to induce germination (e.g. DDA or DDG) with or without the additional assistance of heating. To examine this assertion, we acquired a molecule with no previously reported bioactivity, N-[(3,5-dimethyl-1-adamantyl)methyl]guanidine hydrochloride (DMAG), from a chemical screening library. DMAG was chosen as it meets the aforementioned criteria of a salt-

bridge-forming guanidinium portion and a hydrophobic dimethyladamantyl group, while bearing minimal structural resemblance to the original DDA molecule. At 1 mM, DMAG was found to reduce the surviving *B.megaterium* spore count by 57% upon a 30 min incubation at 50^{o}C and pH 10, and completely eliminated viable spores when the temperature was increased to 60^{o}C (Figure 6.3). A slightly basic condition was used as it was shown in previous experiments to favour guanidinium-based DDG lethal germination. In comparison, 10-fold higher concentration of guanidinium, 3,5-dimethyladamantane-1-acetic acid (DMAA) or a mixture of both showed no activity towards spores at 80oC at the same pH. The weaker bioactivity of DMAG compared to DDA and DDG is presumably a result of its relatively lower hydrophobicity (The calculated octanol-water partition coefficient is 1.6 for DMAG and 3.1 for DDA) [146].

The direct biological target of DDA has been the subject of significant speculation over the years. Past studies eliminated the spore coats and core from the list of possible targets, as the removal of the spore coats does not affect DDA bioactivity [147] and the accessibility of the core is blocked by the inner membrane permeation barrier [148]. Of the several remaining possibilities – mainly, the interactions between DDA and specific inner membrane proteins, the nonspecific interactions with inner membrane, or the nonspecific inter-actions with spore cortex – the chemical evidence presented in this study certainly favours the last possibility. The SpoVA proteins that are most likely constituents of an inner membrane Ca-DPA ion channel have been suggested to be involved in the DDA germination process [159], but several types evidence indicate that this channel likely plays a downstream biological function instead of interacting with DDA directly, since: 1) besides exposure to DDA, other experimental conditions,

including the degradation of spore cortex by lysozyme [149], also activate this ion channel, making it a converging point of different biological inputs; 2) many DDA structural derivatives and primary ammonium polymers studied in this work can similarly decrease spore chemical/heat resistance to various degrees, displaying the nature of nonspecific interactions.

The spore core dehydration mechanism has been associated with the outer cortex layer ever since J. Lewis pointed out that a low permeability of inner membrane cannot really account for the unusually low water content within the spore core [150]. A later calculation further suggested that the osmotic pressure created in the cortex by carboxylate groups and their counter ions can easily exceed 30 atm [118], a condition almost certainly contributory to core dehydration. This potential biological function thus makes the spore cortex a viable target for chemically triggering core rehydration, as likely in the case of DDA lethal germination. It is interesting to note that while low pH and multivalent cations have also been known to affect the charge density on anionic polymer matrices, they themselves do not effectively trigger *ab initio* lethal germination at near physiological temperature as does DDA (though the reduction in spore resistance under acidic conditions or in the presence of mutltivalent cations is nevertheless well-documented [118,151]). This difference in bioactivity may stem from the difference in affinity of binding to carboxylate groups as well as the extent to which matrix osmotic pressure is altered after binding.

6.4 Conclusions

Through the study of various structural analogues and specific inhibitors, we have gained new chemical insights into DDA-spore interactions, suggesting that DDA head group interaction with spore cortex carboxylate via salt bridge formation and the hydrophobic stabilization from the alkyl tail are central to the exceptional antispore activity of DDA. We also demonstrated that this understanding enables one to make predictions of such bioactivities. The molecular understanding of DDA lethal germination acquired through this work will be useful in guiding the design and screening of potential antispore molecules that ideally possess high efficacy but without the potent environmental toxicity that has so far limited broader applications of DDA [124].

6.5 Acknowledgements

We thank Dr. Y. Li, Dr. Q. Shao and M.A. Giarmarco for helpful discussions.

This work was supported by a grant from the Defence Threat Reduction Agency (HDTRA1-10-1-0074) and the National Science Foundation (CBET-1264477).

6.6 Chapter Figures

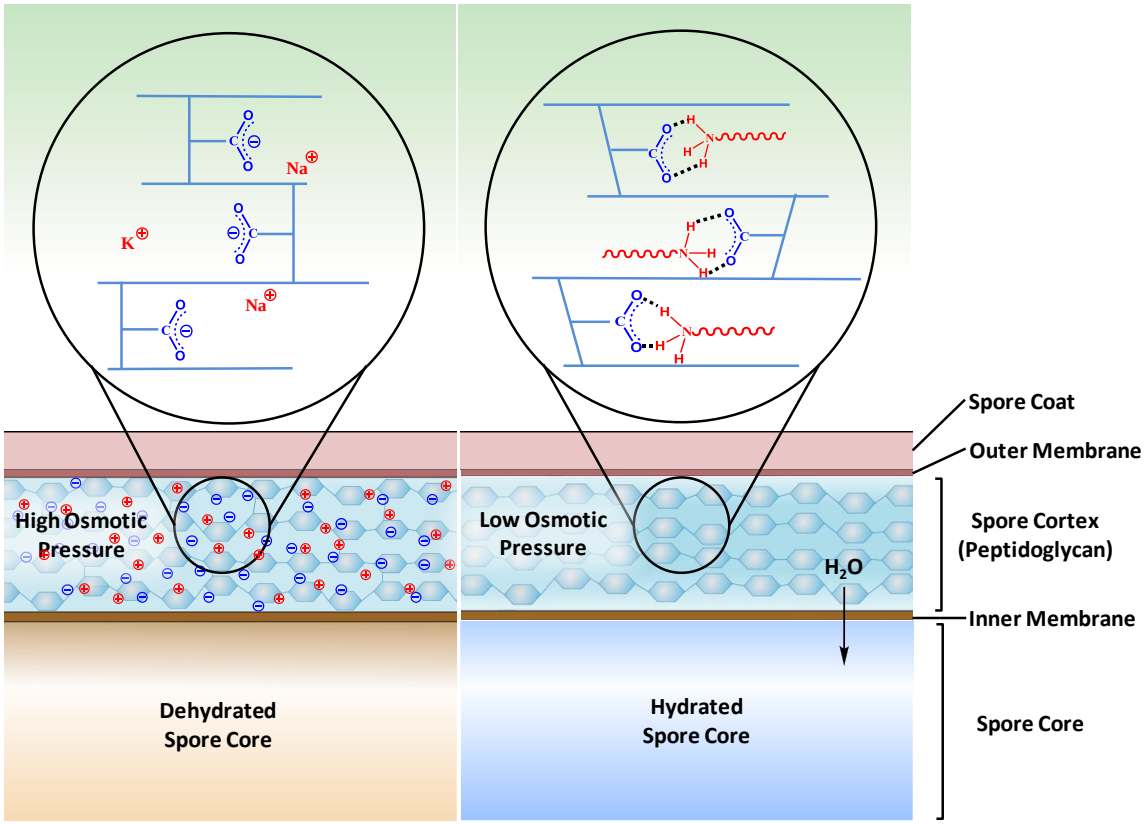

Scheme 6.1. Proposed model of interactions between DDA and spores: prior to DDA exposure, the high osmotic pressure within the spore cortex helps maintain the core low water content; after DDA exposure, the primary ammonium head groups of DDA form hydrophobically stabilized salt bridges with carboxylate groups within the spore cortex, and this neutralization of the peptidoglycan layer nullifies the osmo-regulatory function of the cortex layer, causing the core to take up significant amounts of water.

Functional Substitution

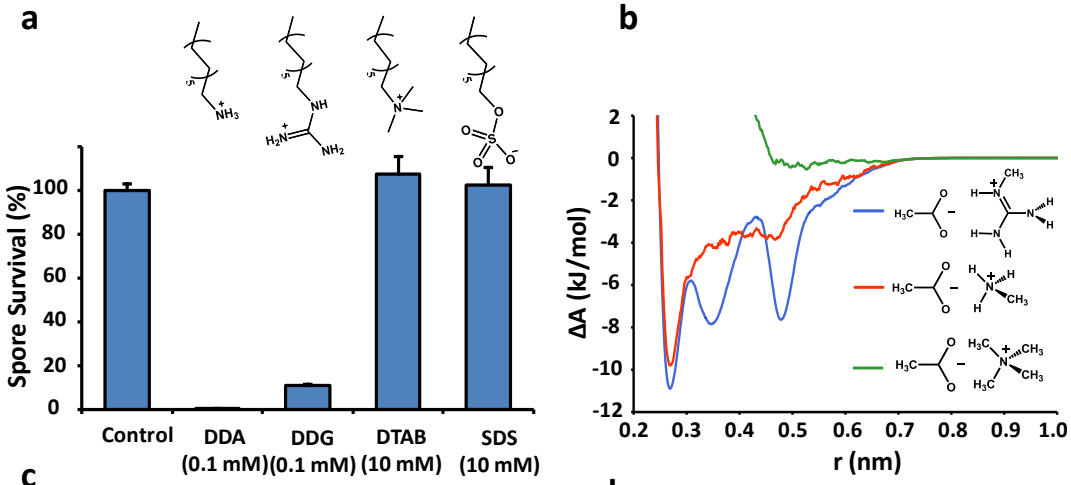

c

pH Dependence

	pH 4	pH 8	pH 12
DDA (Survival %)	88±7	0	88±5
DDG (Survival %)	84±3	11±2	0

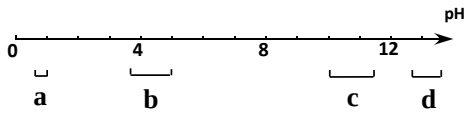

a. Phosphonate
b. Carboxylate
c. Primary Ammonium
d. Guanidinium

d

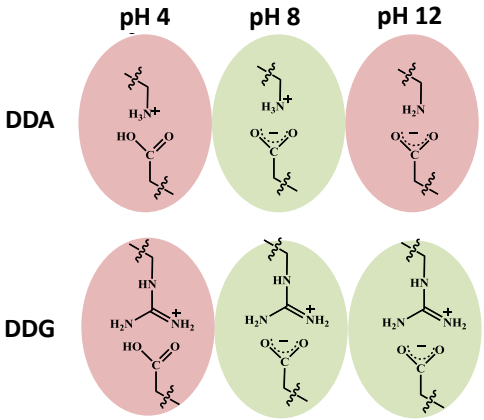

e

Specific Inhibition

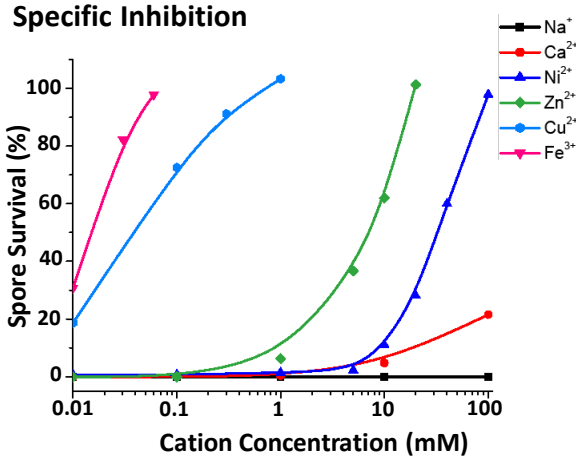

Figure 6.1 Primary ammonium head groups in DDA lethal germination. **a,** Survival percentage of *B. megaterium* spores after exposure to DDA or DDG at 0.1 mM and DTAB or SDS at 10 mM for 30 min at 40^{o}C and pH 8. **b,** The potential mean force free energy between carboxylate anion binding with primary ammonium, guanidinium or quaternary ammonium cations. The three local energy minima in guanidinium-carboxylate interaction reflect multiple strong binding conformations. **c,** Compiled results of DDA and DDG lethal germination efficacy under different pH conditions. All experiments were performed at 40^{o}C and 0.1 mM surfactant concentration for 30 min. The legend at the bottom indicates the pKa range of common anions (phosphonate, carboxylate) and cations (primary ammonium, guanidinum) in biological molecules for comparison. **d,** Schematic illustrations of DDA and DDG forming salt bridges with carboxylate groups in response to the environmental pH. **e,** Multivalent cation inhibition of DDA lethal germination of *B. megaterium* spores as evaluated by supplementing 0.1 mM DDA with various metal cations at 40^{o}C.

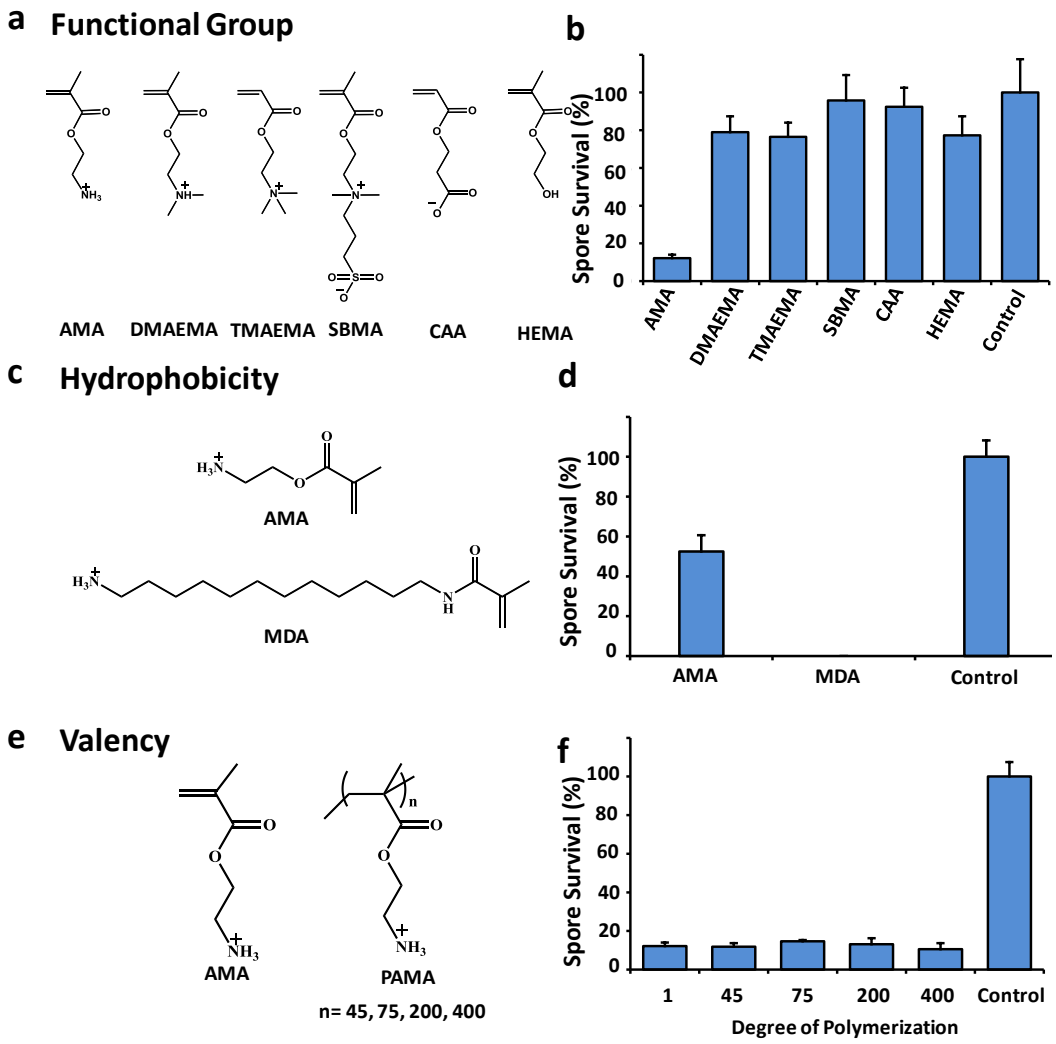

Figure 6.2. The role of DDA alkyl tail in spore germination studied using primary ammonium monomers and polymers. **a,** The chemical structures of seven hydrophilic monomers. **b,** The loss of *B. megaterium* spore viability after exposure to various hydrophilic monomers (5% w/v) at 80^{o}C for 30 min in PBS. **c,** The chemical structures of two primary ammonium monomers: hydrophilic AMA and hydrophobic MDA. **d,** The loss of *B. megaterium* spore viability after exposure to AMA and MDA (1% w/v) at 80^{o}C for 30 min. **e,** The chemical structures of AMA monomer and PAMA polymers of different degrees of

polymerization. **f,** The loss of *B. megaterium* spore viability after exposure to AMA monomer and PAMA polymers (5% w/v) at 80^{o}C for 30 min.

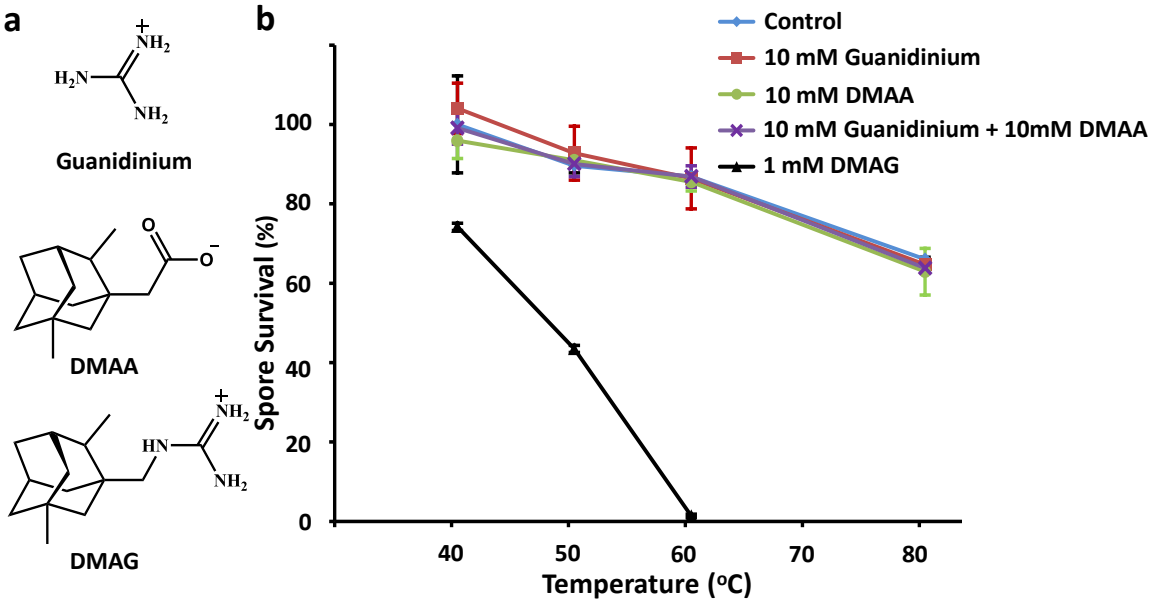

Figure 6.3 The loss of spore viability after exposure to DMAG. a, The chemical structures of guanidinium, DMAA and DMAG. Guanidinium and DMAA, each possessing the cationic and hydrophobic portions of DMAG, were included as controls in this experiment. b, The loss of *B. megaterium* spore viability after a 30-min exposure to guanidinium, DMAA, guanidinium/DMAA, or DMAG at different temperatures at pH 10. Note that the concentration of DMAG was 10 times lower than that of guanidinium, DMAA or guanidinium/DMAA.

Chapter 7. A Green-Chemistry-Oriented Sporicidal Cocktail

Bacterial endospores survive traditional disinfection methods and are a common cause for foodborne illness and nosocomial infections. The existing chemical antispore methods invariably require the use of strong oxidizing agents (ethylene oxide, hydrogen peroxide or peracetic acid), which are environmentally detrimental as well as economically unfavourable. Here we report the first green chemistry oriented antispore strategy — a tri-component system of low pH, anionic surfactants and ethanol — that kills spores under relatively mild conditions by sequentially targeting spore resistance and viability. The biological efficacy of the approach was demonstrated with three different spore species both in liquid suspension and on surface. The mechanism underlying this sporicidal activity was also herein explored and discussed. Furthermore, the chemical simplicity of this system, allows it to be easily duplicated using common household products.

7.1 Introduction

Sporulation is the ultimate defense mechanism of many types of bacteria, including the clinically important *Bacillus cereus* and *Bacillus anthracis* species. As a result of the dehydrated and therefore metabolically dormant state of spore cores, traditional disinfection procedures, such as UV radiation, detergents, alcohols and quaternary ammonium compounds, have little effect on spore viability[113,152]. The standard spore sterilants recommended by US Centers for Disease Control and Prevention (CDC) require the use of strong oxidizing agents[153] – ethylene oxide, hydrogen peroxide or

peracetic acid – that are inevitably corrosive and toxic. A safer and more easily implementable antispore agent is therefore in great need.

During our recent study, we discovered that the surfactant sodium dodecyl sulfate (SDS) under acidic conditions can uniquely and effectively breach the spore chemical resistance at near-physiological temperature, making spores vulnerable to further chemical incursions. The general availability and the low toxicity of the chemicals required, particularly in comparison to the existing sporicidal agents, spurred our interest for further research. In this report, we systematically explore and study the efficacy, spectrum, as well as mechanism of this surprisingly simple solution to a long-standing bioengineering challenge, demonstrating its practicality as a cost-effective and environmentally-friendly improvement to conventional spore sterilization procedures.

7.2 Materials and Methods

7.2.1 Chemicals

Na2HPO4, citric acid, phenol, urea, sodium chloride, calcium chloride, iron (III) chloride, aluminum chloride, tetrazolium chloride (TTC), sodium dodecyl sulfate (SDS), dodecyltrimethylammonium chloride (DTAC), ethylenediaminetetraacetic acid (EDTA), sodium hexyl sulfate (SHS) were purchased from Sigma-Aldrich Chemical Co. (MO, USA). Hand soap (Softsoap® Energizing Pomegranate & Mango) was acquired from Colgate Co. (NY, USA). Lemon juice (Tantillo®) was purchase from T&M Imports (NY, USA). 100 proof vodka (Monarch®) was purchased from Hood River Distillers (OR, USA). Antispore “cocktail” (per milliliter) contains 200ul vodka, 700ul lemon juice and 100ul hand soap.

Nutrient Broth No1 was purchased from Fluka Analytical (MO, USA); Bacto Agar was purchased from BD (NJ, USA); *Bacillus megaterium* and *Bacillus cereus* spore stock suspensions were purchased from Mesa Laboratories, Inc. (MT, USA). Bacillus atrophaeus spore suspension was purchased from STERIS Co. (OH, USA).

7.2.2 Evaluating chemical antispore potency in solution

B. megaterium endospores were acquired through commercial sources. After exposure to various chemicals at 40^{o}C for 30min, spore suspensions were immediately washed, diluted and spread onto Broth No1 agar plates. The colony numbers were determined in the following day after overnight incubation at 37^{o}C. Broth No1 Agar (10g/L tryptone. 10g/L NaCl, 5g/L yeast extract and 1g/L glucose) was verified to completely germinate B. megaterium spores without the need for prior heat activation, thus ensuring the difference in colony number observed comes from loss of viability during chemical exposure and not from incomplete germination in subsequent incubation.

7.2.3 Evaluating chemical antispore potency on surface

All spore suspensions were acquired from commercial sources. The spore suspensions were diluted in sterilized MilliQ water and subsequently sprayed onto UV-cleaned glass slides, after which the slides were air-dried at ambient temperature for 1h to ensure spore surface attachment. The dried slides were then half-submerged into various testing solutions prewarmed to 40^{o}C for 30 min. After the 30-min incubation, slides were gently rinsed with sterilized phosphate buffer to clean off of various testing solutions. The slides were individually placed into clean petri dishes then overlaid with molten Broth No1 agar supplemented with 50 ppm TTC at 45^{o}C. The plates were later incubated at 37^{o}C (*B.*

megaterium and *B. atrophaeus*) or 30^{o}C (*B. cereus*) overnight before counting the colony number.

7.2.4 Phase contrast microscopy

Dormant, nutrient germinated *B. megaterium* spores as well as spores exposed to 10mM SDS in pH 2 solution were observed directly under a standard phase contrast microscope. The nutrient germination was carried out under a previously reported condition[154]: spores were first heat activated at 60^{o}C for 15min, followed by incubation at 30^{o}C with 10mM D-glucose in PBS for 60min to ensure complete germination.

7.3 Results and Discussions

As a starting point, we examine the combined effect of SDS and low pH on *Bacillus megaterium* spore viability with or without additional chemical assistance. From a standard colony formation assay, it was observed that supplementing McIlvaine's buffer (citric acid/Na_2HPO_4) at pH 2 with 10mM SDS decreased the viable spore count to below 50% after 30 min at 40^{o}C (Figure 7.1 a). Though not particularly potent as a sporicide by itself, the SDS/low-pH treatment evidently breached the spore chemical resistance, as creating a more biologically challenging milieu with additional 10% ethanol caused the surviving spore number to plummet below 6%. Confirming this observed synergy, separately or in other combinations of SDS, low pH and ethanol showed no impact on spore viability (Figure 7.1 a). The addition of ethanol is to facilitate the killing of defense-compromised spores that would otherwise be immune to these organic compounds. As such, 10% ethanol can be readily replaced by other common antiseptics, e.g. 1% phenol solution in combination with SDS under acidic condition saw the complete annihilation of viable *B. megaterium* spores. As a reference, a previous study

indicated that to impair spore viability with acid alone required the use of HCl above 500mM [155], fifty times more acidic than the condition used in this work. The complete lack of antispore activity of its individual components demonstrated in this experiment as well as the high specificity of the chemicals needed in this antispore combination (see below) suggests a concerted action of defence-weakening (SDS/low-pH) followed by inactivation (ethanol or phenol), rather than merely imposing a universally destructive environment that indiscriminately exterminates all life forms within. This mechanistic aspect shall be further explored in a later part of this report.

A major motivation behind our study of the SDS/low-pH antispore effect is that it offers a considerably cheaper and milder procedure than the currently prevailing spore sterilization protocols. To emphasize this point, we effectively recreated the same chemical mixture (SDS/low-pH/ethanol) used in our previous experiments with a combination of common household products: hand soap (typically containing 0.1~0.4% anionic surfactants), lemon juice (pH naturally at 2), and 100 proof vodka. While, as expected, these components individually display no antispore activity, the combined "cocktail" eliminates over 95% viable spores after an incubation time of 30 min at 40oC (Figure 7.1 b).

We further test the utility of this approach by mimicking the common clinical scenarios in which substrate surfaces are to be sterilized and rid of all viable spores. To this end, spore suspensions of *B. megaterium*, *Bacillus atrophaeus* (*B. anthracis* simulant) and *B. cereus* (a common culprit for food poisoning) were sprayed onto glass surfaces. After air-drying for 1 h to allow for spore surface attachment, the glass slides were half-submerged into a solution containing 10mM SDS and 10% ethanol at pH 2. Following 30 min

incubation at 40^{o}C, the slides were removed from the solution mixture, gently rinsed with sterilized phosphate buffer and the surviving surface-bound spores were quantified in a colony formation assay (Figure 7.1 c). The SDS/ethanol mixture at pH 2 lead to a complete elimination of viable spores from all three bacterial species, while no sporicidal effect was observed in samples exposed to 10mM SDS solution or 100% ethanol separately, evincing its high efficacy and broad spectrum (Figure 7.1 d-f).

After demonstrating the effectiveness and practicality of this antispore cocktail, we aimed to probe into its mechanism of action. The ability of bacterial spores to withstand environmental adversity is resulted from the dehydrated state of the spore core[114]. Consistent with this consensus, the core section of dormant *B. megaterium* spores after exposure to pH 2, 10mM SDS solution at 40^{o}C for 30min showed an increase in water content under phase contrast microscope (significant darkening in the central region of the spore), thus providing an morphological account of the previously observed loss of spore chemical resistance (Figure 7.2 a).

On a molecular level, though the details for maintaining spore core dehydration are not completely clear, it is generally accepted that both the high pressure from spore cortex[150] and the low permeability of inner membrane towards small molecules (including water and H^{+})[148] are critical in maintaining this dehydrated state. It has been further suggested that the role of the cortex layer in core dehydration partly lies in the high osmotic pressure created by the anionic carboxylate groups on the cortex peptidoglycan matrices ions[118]. Under acidic conditions (which protonate the carboxylate anions, hence lowering the matrix osmotic pressure), the loss of spore chemical resistance reported in this work (Figure 7.2 b) and the previously noted

reduction in heat resistance[151] are both consistent with this cortex osmoregulatory model. Furthermore, the low pH used in the antispore cocktail can be in part functionally substituted by multivalent metal cations (Figure 7.2 c), which are known to bind strongly to the anionic polymer matrices, including the spore cortex layer, through chelation. Taken together, the most plausible explanation for the role of low pH in this antispore combination therefore lies in its ability to quench the negatively-charged peptidoglycan matrix, thus dampening the cortex high osmotic pressure critical for core dehydration.

Meanwhile, SDS is hypothesized to weaken the inner membrane as a permeation barrier based on the surfactant's well-known function in cell biology. It is worth noting that this speculated membrane interaction is specific for anionic surfactants, including SDS (Figure 7.2 d) and, to a much lesser degree, sodium hexyl sulfate (SHS) (Figure 7.2 e). In contrast, a representative cationic surfactant (dodecyltrimethyl-ammonium chloride, DTAC), strong protein denaturing agent (urea), or metal chelating agent (ethylenediaminetetraacetic acid, EDTA) displays no antispore effects when similarly mixed with 10% ethanol under pH 2 (Figure 7.2 e). The overall proposed mechanism is summarized in Fig. 7.3. Under this scheme, the low pH condition and SDS interact with spore cortex and inner membrane respectively, leading to partial rehydration of spore core and an increase in spore susceptibility to organic compounds including ethanol.

7.4 Conclusion

The first green-chemistry-oriented sporicidal strategy via spore sensitization (low pH and anionic surfactants) followed by elimination (ethanol, phenol or other regular bactericidal agents) was presented in this study. A strong synergy was observed between low pH conditions and SDS, and their respective interactions with spore cortex and inner

membrane were hypothesized to be the structural basis for this synergy in bioactivity. This observation also suggests that the high osmotic pressure from spore cortex may play a role in maintaining the crystalline-like inner membrane structure as a permeability barrier. A future and more systematic study on the combined usage of carboxylate binding molecules (e.g. ammonium or metal cations) and membrane destabilizing agents may be proven fruitful in discovering novel sporicidal recipes with even higher potency and less environmental damage.

7.5 Chapter Figures

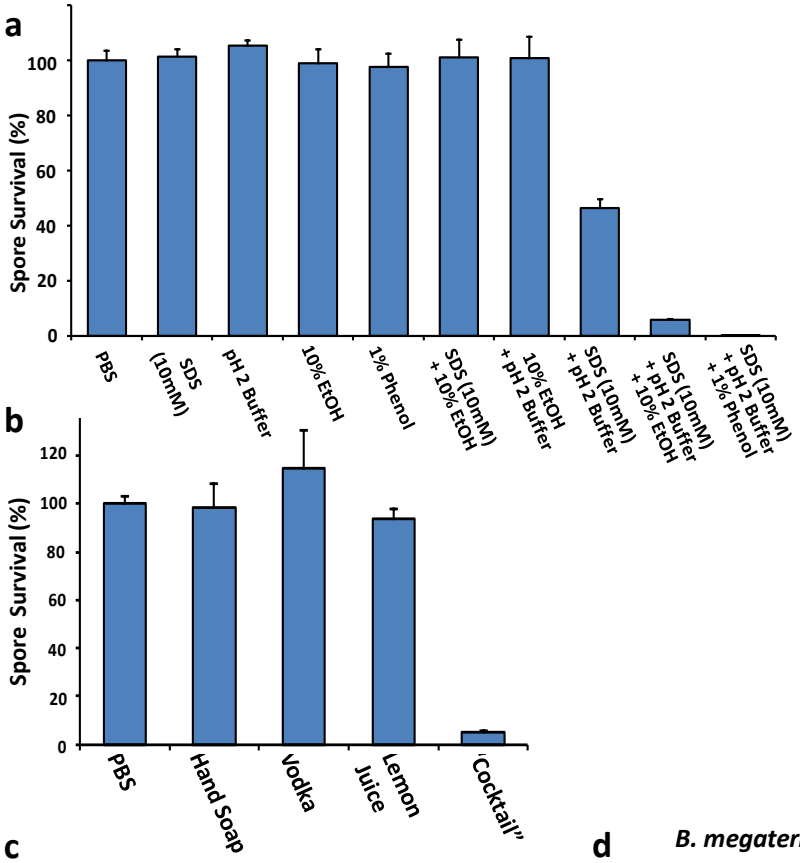

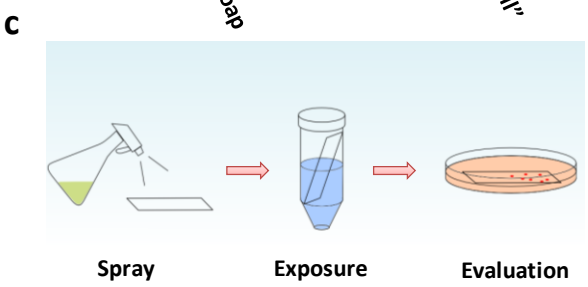

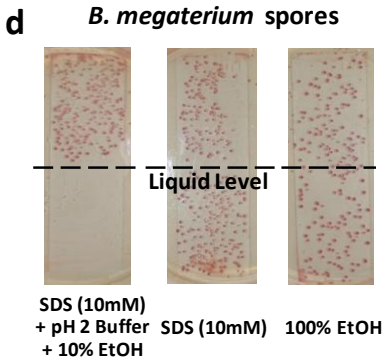

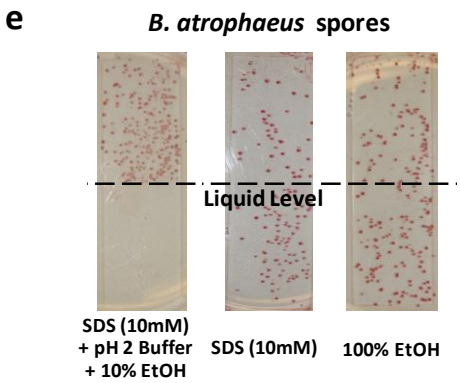

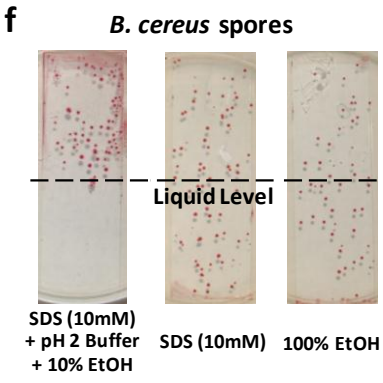

Figure 7.1 a) *B. megaterium* spore survival percentage after exposure to various chemical conditions at 40^{o}C for 30 min. Spores suspended in phosphate buffer saline (PBS) were included as control. **b**) *B. megaterium* spore survival percentage after exposure to common household products at 40^{o}C for 30 min. **c)** Scheme for testing surface sterilizing potency of SDS/low-pH plus 10% ethanol against spores from three bacterial species. Note that the upper halves of the slides were not submerged under the antispore solution and were used as references for comparison. **d-f)** The surface antispore effects of SDS/low-pH plus 10% ethanol against *B. megaterium*, *B. atrophaeus* and *B. cereus* spores. The incubation conditions were 40^{o}C 30 min for all experiments. 50 ppm tetrazolium chloride (TTC) was added into the overlaying Lysogeny broth to aid visualization.

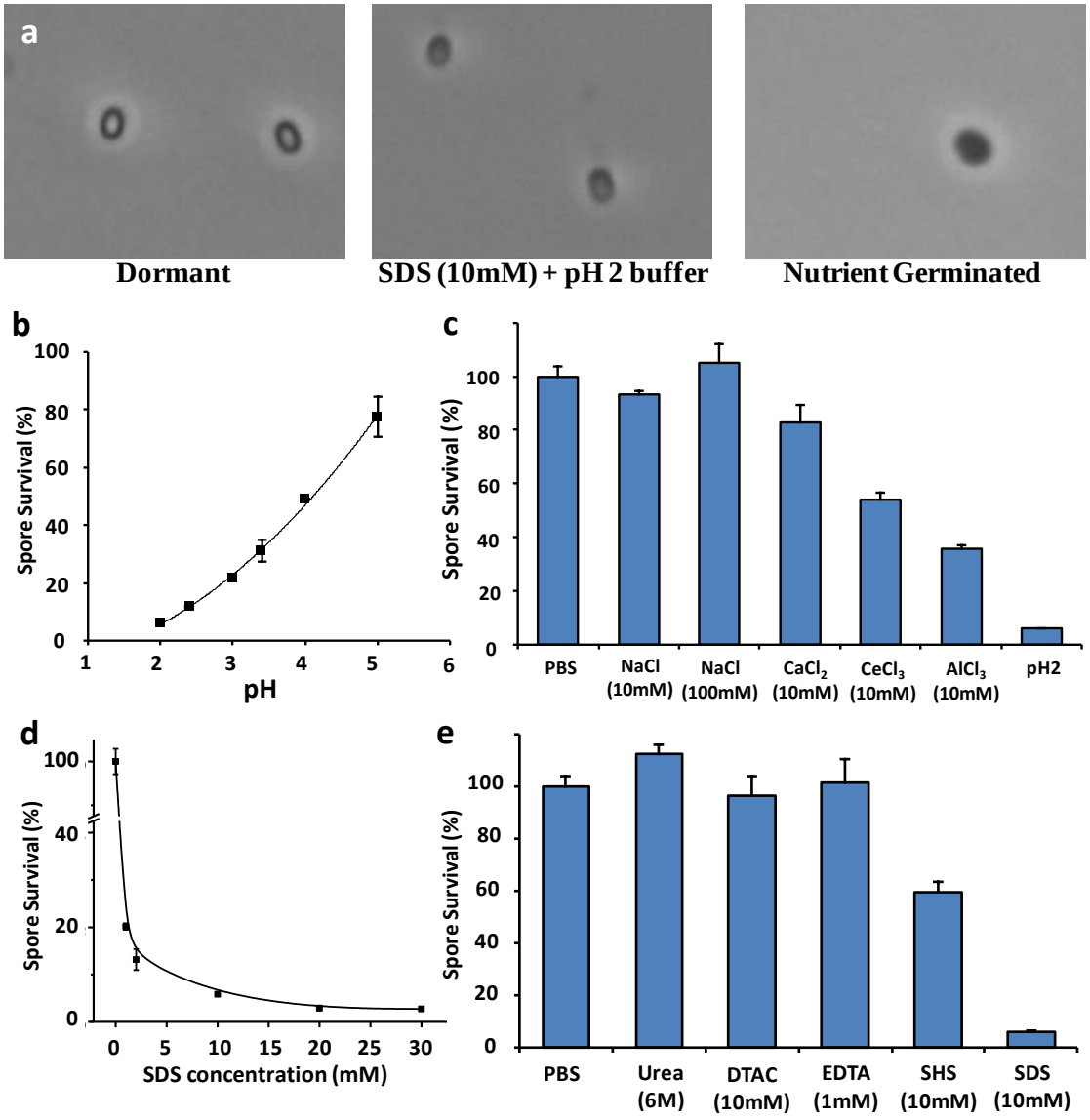

Figure7.2 a) Representative phase contrast microscopy photos of dormant and nutrient-germinated *B. megaterium* spores as well as spores exposed to pH 2 10mM SDS solution at 40^{o}C for 30min. Darker colour at the spore core region is indicative of a higher water content. **b)** *B. megaterium* spore survival percentage after exposure to 10mM SDS solution with 10% ethanol under different pH. **c)** *B. megaterium* spore survival percentage after exposure to 10mM SDS solution with 10% ethanol at neutral pH but

supplemented with various metal cations. 10mM SDS solution with 10% ethanol at pH 2 was included as a control experiment. The actual concentrations of Ca^{2+}, Ce^{3+} and Al^{3+} are expected to be lower than the 10mM originally prepared, as the solutions turned partially turbid upon mixing due to the ion pair formation between multivalent cations and SDS. **d)** *B. megaterium* spore survival percentage after exposure to pH 2 buffer with 10% ethanol at various SDS concentrations. **e)** *B. megaterium* spore survival percentage after exposure to pH 2 buffer with 10% ethanol supplemented with anionic surfactant SDS and SHS, cationic surfactant DTAC, metal chelating agent EDTA and protein denaturing agent urea. All incubation conditions from **b-e** were identical at 40^{o}C and 30 min.

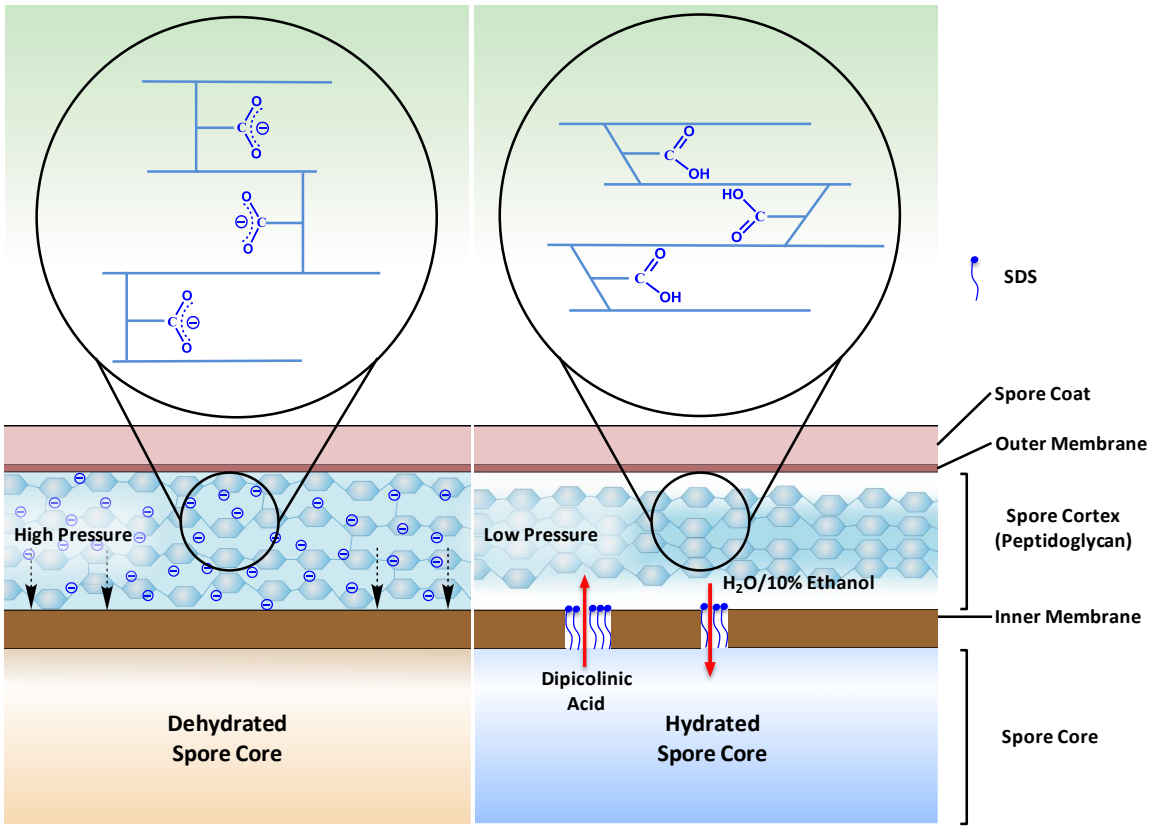

Figure7.3 The proposed antispore mechanism of low pH and SDS, in which reduced cortex osmotic pressure due to carboxylate protonation and inner membrane instability triggered by SDS work in synergy, leading to the diminishment of spore chemical resistance and the eventual inactivation by ethanol.

Chapter 8 Reducing *Pseudomonas aeruginosa* Biofilm Formation with Osmoprotectant Analogues as Anti-virulence Metabolites

The extensive usage of antibiotics for clinical and agricultural purposes in the past fifty years has resulted in a global spread of antibiotic-resistant bacterial strains. This rapid reduction in antimicrobial potency is directly caused by the strong evolutionary selection pressure of classical antibiotics. One promising alternative strategy to avoid this increasing antibiotic resistance is the development of anti-virulence compounds, which seeks to alleviate the aforementioned selection pressure by specifically mitigating pathogenic phenotypes, e.g., toxin secretion or biofilm formation, but without directly limiting bacterial proliferation. In this work, we identify through molecular design followed by small-scale chemical screening bacterial that osmoprotectant analogues can be used as potential anti-virulence metabolites against biofilm formation. Among the 19 compounds tested, ethylcholine, a biosynthetic precursor of ethyl glycine betaine and previously reported to induce glycine betaine catabolism, was found to effectively inhibit biofilm establishment without adversely affecting normal bacterial growth. The potential complementary usage of this molecule with traditional antibiotic compounds and its other impacts on bacterial physiology were also herein explored and discussed.

8.1 Introduction

Bacterial biofilm formation on human body tissue or implantable devices has been known to lead to immune-evasion and chronical infection of many bacterial species [21,156,157]. While traditional antibiotics are no doubt effective in various clinical applications,

several obstacles exist when applying them in preventing and eradicating biofilm formation. Some of these difficulties include the lack of efficacy in killing biofilm-embedded bacterial cells[158,159]; the induction of nascent biofilm formation at a sublethal antibiotic dosage[160] and, above all, the quick development as well as spread of the antibiotic-resistant mutants within the bacterial population[161,162]. In fact, the past several decades saw the rapid emergence of antibiotic-resistant strains far outpacing the discovery and development of antibiotic compounds, leading to a global concern over the diminishment of existing tools in fighting bacterial infection and the worrying possibility of returning to a pre-antibiotics age.

One promising strategy to avoid the problem of bacteria quickly developing a defense mechanism against the chemical therapeutic agents is to shift the drug targets away from the pathogenic bacteria viability, but instead aim at reducing specific virulent phenotypes. Currently many such anti-virulence compounds are under development with their biological targets ranging from bacterial toxin production to biofilm formation [163,164]. As the successful applications of these anti-virulence compounds do not rely on the elimination or growth inhibition of drug-sensitive bacterial cells, the evolutionary pressure for bacteria under treatment is thus considerably weaker in comparison to the bacterial population exposed to traditional antibiotics, resulting a much reduced rate in the emergence and spread of resistant strains[165].

While past efforts to develop anti-virulence drugs against biofilm establishment have largely revolved around the search for quorum sensing inhibitors [163,164], more recent microbiological studies based on mutant library screening and physiological analysis have significantly expanded the list of potential anti-virulence targets by identifying other

genetic pathways essential for biofilm formation but not for bacterial proliferation. These genetic determinants for biofilm establishment include pH homeostasis[166], arginine metabolism[166], iron uptake[167] as well as osmotic adaptation[166,168]. More specifically for osmotic adaptation, as bacteria transit from a free-living planktonic state to a matrix-dwelling biofilm phenotype, bacterial cells experience a major increase in extracellular osmotic pressure[168,169]. To prevent the quick loss of cellular water, bacteria in response accumulate osmoprotectant molecules, perhaps most famously glycine betaine, via active transport and partial or *de novo* synthesis to balance this cross-membrane difference in ionic strength [170]. In the particular case of *Pseudomonas aeruginosa*, a bacterial species notorious for causing biofilm-related clinical infections, the intracellular increase of glycine betaine concentration can be achieved via either direct molecular import or a partial synthesis from its choline precursor [171].

Compared with other genetic determinants for biofilm formation, interfering intercellular osmoprotectant pool as a potential anti-biofilm route offers the following advantages: first, various chemical analogues of natural osmoprectants are structurally simple, thus reducing the technical burden of creating the chemical screening library; second, these structural mimics generally show low or no toxicity (see below), making it harder for bacteria to develop resistance; and third, certain glycine betaine and choline transmembrane transporters in *P.aeruginosa* showed a relatively low substrate specificity, making it plausible to design small molecular analogues to actually enter into the cells and alter relevant enzyme activity via competitive binding or other potential mechanisms[172]. The central goal of this work is through the integration of molecular design and small-scale chemical screening to examine the feasibility of reducing biofilm

formation with osmoprotectant analogues as potential anti-virulence metabolites. To this end, the bioactivity of 17 osmoprotectant analogues together with the indigenous choline and glycine betaine were tested against *P.aeruginosa* biofilm formation. The impacts of these compounds on other aspects of bacterial physiology including growth curve and susceptibility against conventional antibiotic compounds were also herein explored.

8.2 Materials and Methods

8.2.1 Chemicals:

Six new choline analog structures were synthesized in this study. In a typical reaction, 1 molecular equivalent of tertiary ammine alcohol was mixed with 1.2 molecular equivalent of alkylation agent iodoalkane in acetonitrile. The reaction was then stirred vigorously under nitrogen protection at 60oC for 24h. After reaction, the solvent was removed in a rotary evaporator (BÜCHI, Switzerland). The product was subsequently precipitated and washed with anhydrous diethylether in excess. The resulting white powder was characterized using 1H nuclear magnetic resonance (NMR) in D2O to give the correct structure. All other chemicals tested were purchased from Sigma-Aldrich and used without further purification.

8.2.2 Bacterial strains and culture conditions:

P.aeruginosa PAO1 wild type strain was purchased from ATCC. Various *P.aeruginosa* mutant strains as well as MPAO1 (the wild type strain used to construct the mutant library) were purchased from University of Washington Manoil Lab[173].

All bacteria were cultured in Lysogeny Broth (LB) media at 37oC with or without the addition of specified compounds.

8.2.3 Growth curve measurement and biofilm quantification:

Bacteria growth curve was measured by first diluting a *P.aeruginosa* overnight culture to an Optical Density at wavelength 600nm (O.D.600) to 0.05. The second culture was subsequently incubated at 37^{o}C. At every predetermined time point, bacterial culture was thoroughly mixed and new O.D.600 value measured as an indication for bacterial growth.

24h biofilm formation was quantified using standard crystal violet staining. In a typical measurement, *P.aeruginosa* overnight culture was diluted in LB media with or without the addition of testing chemicals to a final O.D.600 = 0.05. 500ul of the second culture was subsequently added into a 48-well plate and incubated at 37^{o}C for 24h to allow biofilm formation. After 24h, the bacteria-containing media was removed and each well washed gently with sterilized PBS three times before adding 1ml 0.1% w/v crystal violet solution into each well. The staining was carried out at room temperature for 20min. After 20min, the staining solution was removed and each well washed gently with sterilized PBS three times, before finally adding 95% ethyl alcohol to dissolve the crystal violet stain absorbed into the biofilm matrix. The O.D.540 reading of the resulting alcohol solution was used as an indication for *P.aeruginosa* biofilm formation.

8.2.4 Antibiotic susceptibility test

P.aeruginosa overnight culture was diluted in LB media with or without the addition of testing chemicals to a final O.D.600 = 0.05. After 24h incubation at 37^{o}C, various antibiotics were added into the bacterial culture to its predetermined concentration (20ug/ml tobramycin, 10ug/ml gentamicin or 60ug/ml nalidixic acid) for an additional 6h. After exposure, the bacterial cells were washed via three cycles of centrifugation and resuspension in sterilized PBS. The final bacteria suspension was diluted and plated on

LB agar plates. The subsequent reduction in colony number formed is used an indication for bacteria antibiotic susceptibility.

8.3 **Results and Discussion**

8.3.1 Anti-biofilm effects of osmoprotectant analogues

A total of 19 chemicals, including the indigenous choline (compound 1) and glycine betaine (compound 11) were tested for their effects on *P.aeruginosa* PAO1 24h biofilm formation in LB media using a standard crystal violet staining (Fig. 8.1). Among these 19 chemicals, compound 2-10 were structural mimics of choline, whereas compound 12-19 were zwitterions and shared similarities with glycine betaine to various degrees. In particular, compound 17 (trigonelline) and 18 (taurine) are natural products: trigonelline is commonly found in coffee and has previously been suggested to affect in bacteria surface adhesion[174]; meanwhile, taurine exist widely in animal tissues and is a major component of bile[175].

At the relatively high 10mM concentration used in the initial screening, 6 of the 19 testing chemicals lead to a more than 40% reduction in 24 h biofilm formation (Fig. 8.2). The most significant differences were observed for compound 4 (ethylcholine) and compound 17 (trigonelline), 32% and 28% of the biofilm biomass respectively in comparison to the negative control as determined from standard crystal violet staining. However, unlike ethylcholine, which did not alter bacterial growth curve, trigonelline slowed *P.aeruginosa* proliferation significantly as manifested by a prolonged initial lag phase (Fig. 8.3). As one goal of this study is to identify potential osmoprotectant analogues that specifically reduce bacteria biofilm phenotype without inhibiting cell growth, we hence limit our focus on ethylcholine for the rest of the study. Iodoalkanes

were used in the synthesis of various choline analogues, resulting an iodide anion associated with every molecule of cationic chonline analogue synthesized. To rule out the possible anion interference on experimental results, LB media supplemented with 10mM potassium iodide were also tested and confirmed to have no appreciable effects on bacterial growth and biofilm formation.

This capability to inhibit *P.aeruginosa* PAO1 biofilm phenotype was largely retained at lower concentrations of 5mM and 1mM for ethylcholine (33% at 5mM and 45% at 1mM in comparison to the wild type biofilm formation), evincing the biological potency of this molecule (Fig. 8.4). An essentially indistinguishable ethylcholine dosage response was also observed for another *P.aeruginosa* PAO1 strain (labeled MPAO1), which was used in a previous construction of a near-saturation *P.aeruginosa* transposon insertion mutant library and utilized in a later part of this study (see below)[173]. This extra caution in testing wild type strains from different sources is necessary, as significant genome differences due to decades of separate culture between PAO1 (deposited in ATCC) and MPAO1 has been previously reported[176].

8.3.2 Ethylcholine and bacterial antibiotic susceptibility

A chief motivation behind our efforts to search for anti-bioflm osmoprotectant analogues was to identify and demonstrate a potential new route of mitigating this key bacterial virulent phenotype without necessarily incurring a strong selection pressure for its resistance. Ethylcholine was so far proven a viable candidate for this purpose due to its anti-biofilm activity and minimal cytotoxicity, i.e. not affecting bacterial growth curve. To get a more complete understanding of the evolutionary footprint of ethylchoine on bacteria physiology, and more particularly its effect on bacterial survivability under stress,

we tested the *P.aeruginosa* PAO1 antibiotic susceptibility to three commonly used antibiotics with or without the presence of 10mM ethylcholine (Fig. 8.5). Our results showed that in all three cases – tobramycin (20ug/ml), gentamicin (10ug/ml) and nalidixic acid (60ug/ml), the coexistence of ethylcholine in the culturing environment does not change the survival percentage of *P.aeruginosa* PAO1 under antibiotic treatment. This observation suggests the relative evolutionary neutrality of ethylcholine for bacteria under different growth conditions, and, more alluringly, the potential of using osmoprotectant analogues to combat bacterial infection in combination with traditional antibiotic compounds while not significantly accelerating the development for resistance.

8.3.3 Metabolic fate of ethylcholine and its genetic-level impact

In a recent study aiming to characterize *P.aeruginosa* GbdR regulon, Hampel and coworkers reported that ethylcholine can be used as a noncatabolizable chemical probe to strongly induce glycine betaine catabolic pathway transcription in a GbdR-controlled fashion [177]. Evidence was also presented in the same work that ethylcholine is transported into *P.aeruginosa* cells as a choline analogue and oxidized by BetAB to its zwitteroinic form ─ ethyl glycine betaine ─ before exerting its biological function. (Fig. 8.6a) [177]. Interestingly, supplementing *gbdR* knockout mutant, which has previously been reported to have a defective biofilm phenotype [166], with 1mM ethylcholine in the growth medium actually saw a near 5-fold increase in the subsequent biofilm formation (Fig. 6b). As ethylcholine suppressed biofilm phenotype in wild type MPAO1 strain, this unexpected reverse effect on a *gbdR* mutant biofilm formation makes it tempting to speculate that the reduction of biofilm formation by ethylcholine in wild type strain at 1mM may in part involves a hyperactivation of glycine betain catabolism due to the

primary or secondary metabolic effects of ethylcholine. This physiological shift following exposure to ethylcholine might then be partially offset by a genetic knockout (*gbdR*, in this case) controlling this catabolic pathway. Indeed a similar restoration of biofilm formation capability was also observed in *dgcA* and *anr* mutant strains, both mutants are closely related to glycine betaine catabolism and display defects in biofilm formation [177,178]. In contrast, adding 1mM ethylcholine into the growth media of a *P.aeruginosa* surface attachment deficient (*sad*) mutant, which has a defective biofilm phenotype due to unregulated cellular motility[179], resulted in a further decrease in its biofilm formation.

8.4 Conclusions

Many anti-virulence compounds are currently under development in response to the rapid emergence of antibiotic-resistant bacterial strains. This work pointed to bacterial osmotic adaptation as a novel target for antibiofilm molecule design and showed the potential to limit biofilm formation through interfering glycine betaine catabolism. While the current study successfully demonstrates the effectiveness of ethylcholine in reducing the establishment and initiation of biofilm formation, one interesting aspect to be studied in future research is to investigate the physiological impacts of these osmoprotectant analogues on bacterial cells embedded within mature biofilms. These follow-up studies would be of great clinical relevance, particularly in biofilm-related chronic infections, as cells embedded deeply within biofilms are constantly subjected to a high osmotic pressure caused by biofilm polymer matrices, and they are particularly recalcitrant to traditional antibiotic treatment.

8.5 Chapter Figures

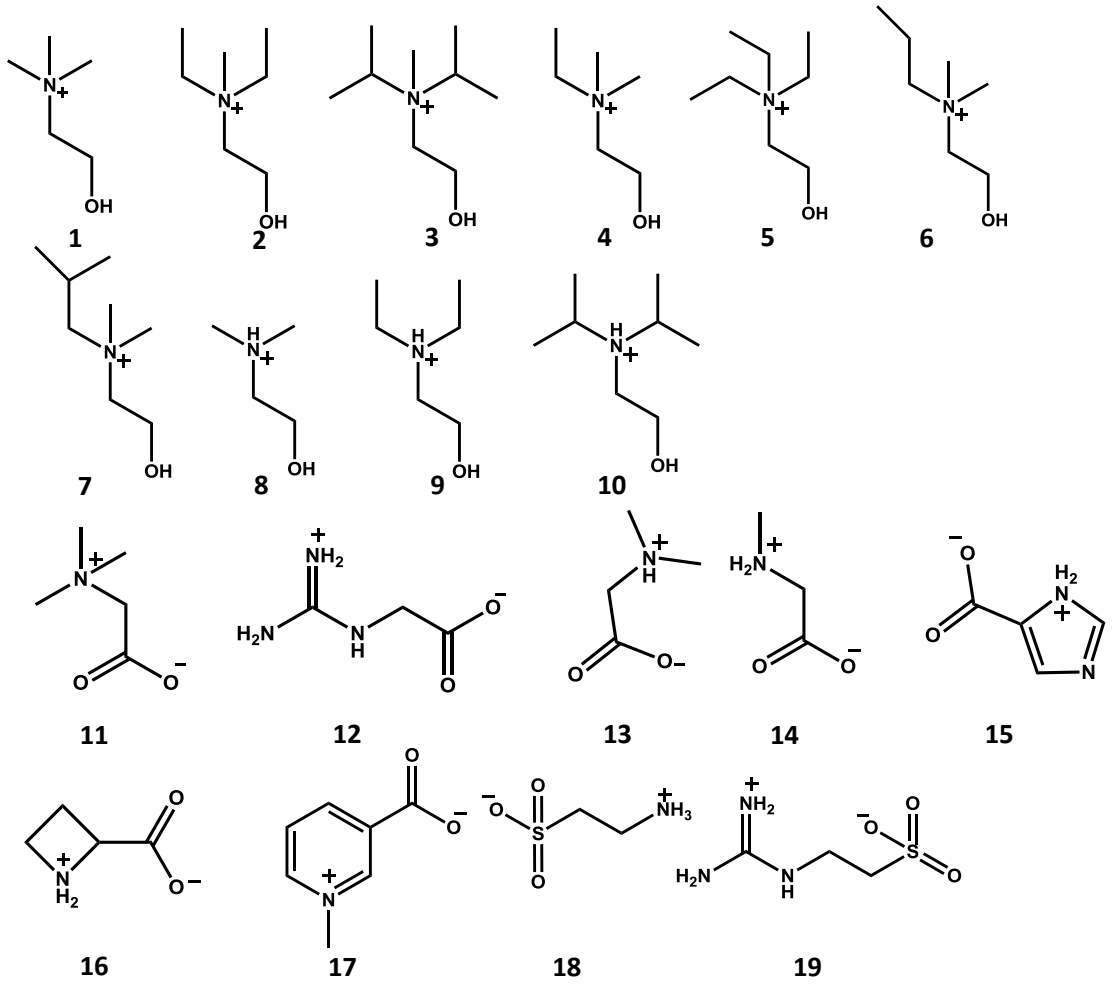

Figure 8.1: Chemical structures of osmoprotectant analogues together with glycine betaine and choline tested in this study.

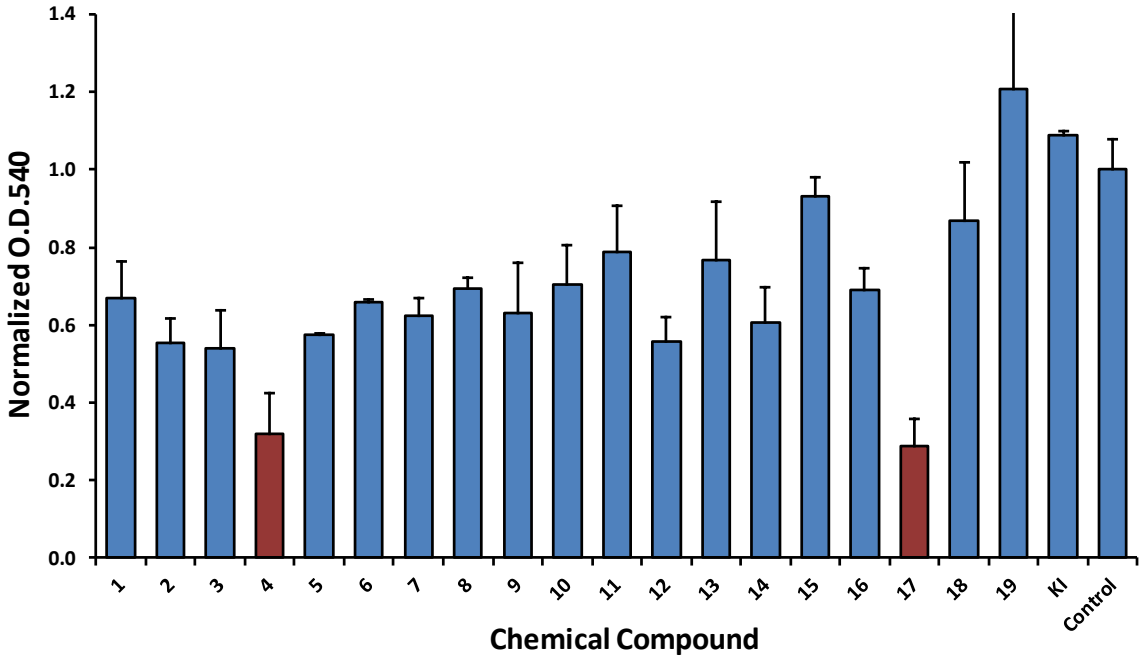

Figure 8.2 24 h biofilm formation of *P.aeruginosa* PAO1 supplemented with various chemical compounds at 10mM in LB media. All O.D.540 readings from standard crystal violet staining were normalized to the result of the negative control.

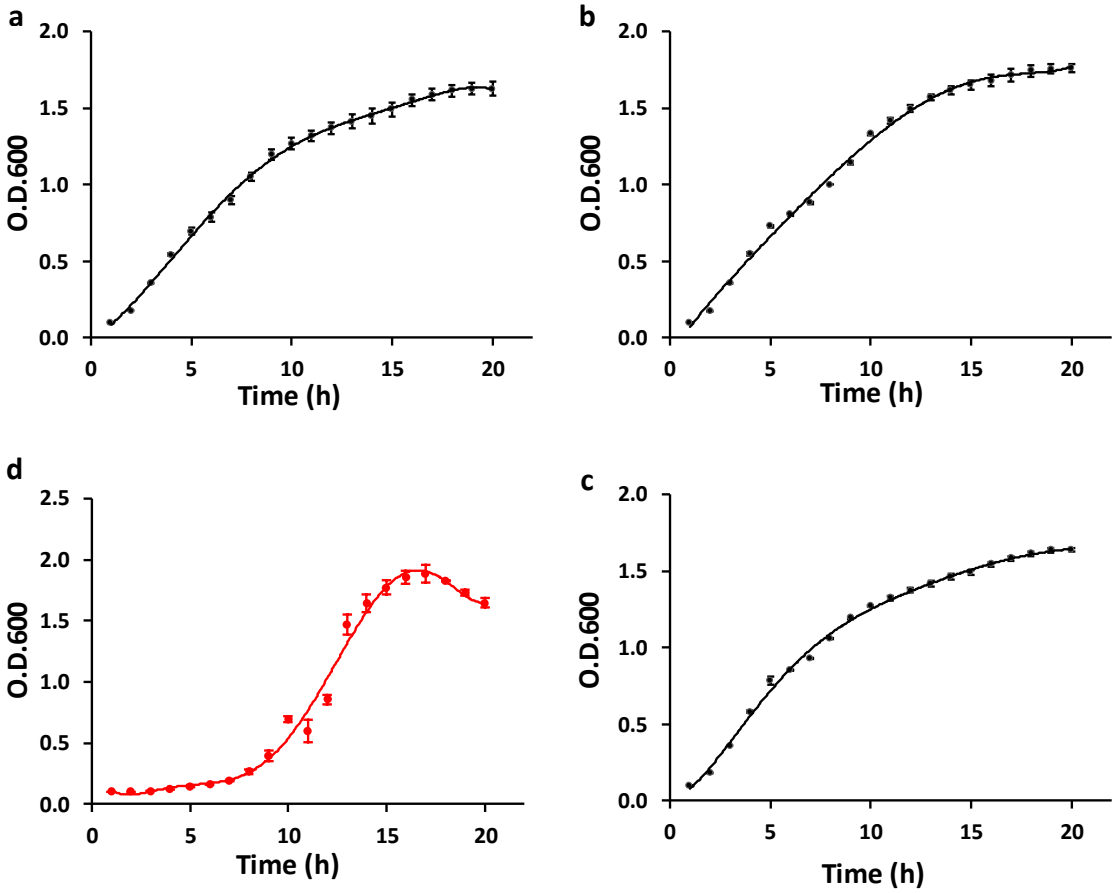

Figure 8.3 Growth curves of *P.aeruginosa* PAO1 in LB media (a); LB media supplemented with 10mM compound 4 ethylcholine (b); LB media supplemented with 10mM compound 17 trigonelline (c) and LB media supplemented with 10mM potassium iodide (d).

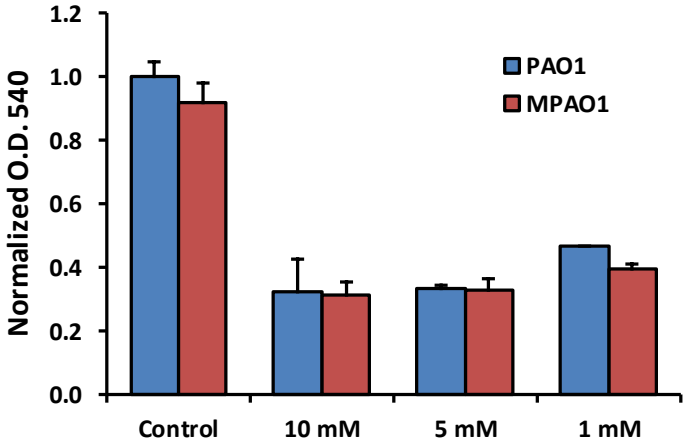

Figure 8.4 24 h biofilm formation of *P.aeruginosa* PAO1 and *P.aeruginosa* MPAO1 at 10mM, 5mM and 1mM ethylcholine concentration. All O.D.540 readings from standard crystal violet staining were normalized to the result of the PAO1 negative control.

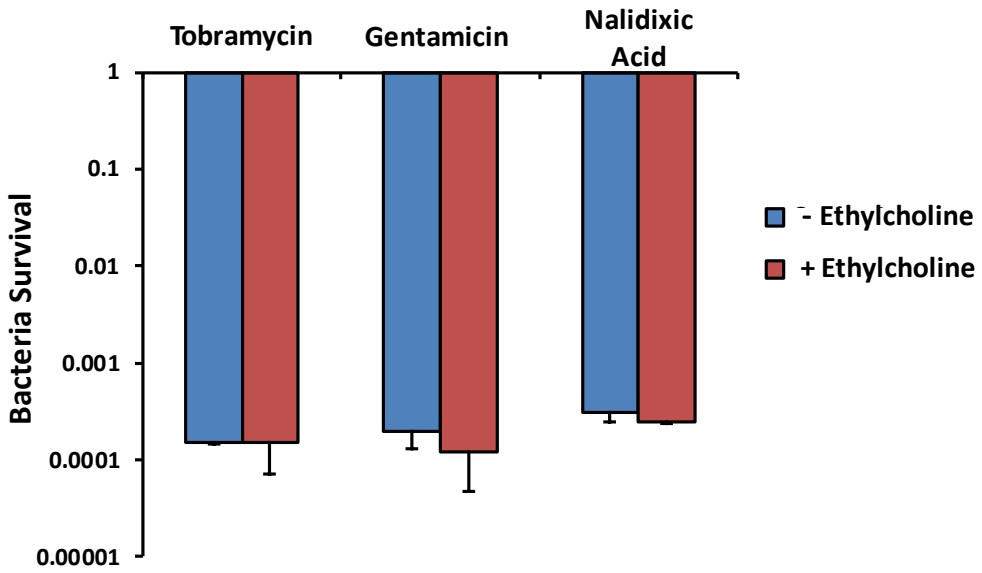

Figure 8.5 *P.aeruginosa* PAO1 survival after exposure to tobramycin (20ug/ml), gentamicin (10ug/ml) or nalidixic acid (60ug/ml) with or without additional ethylcholine at 10mM.

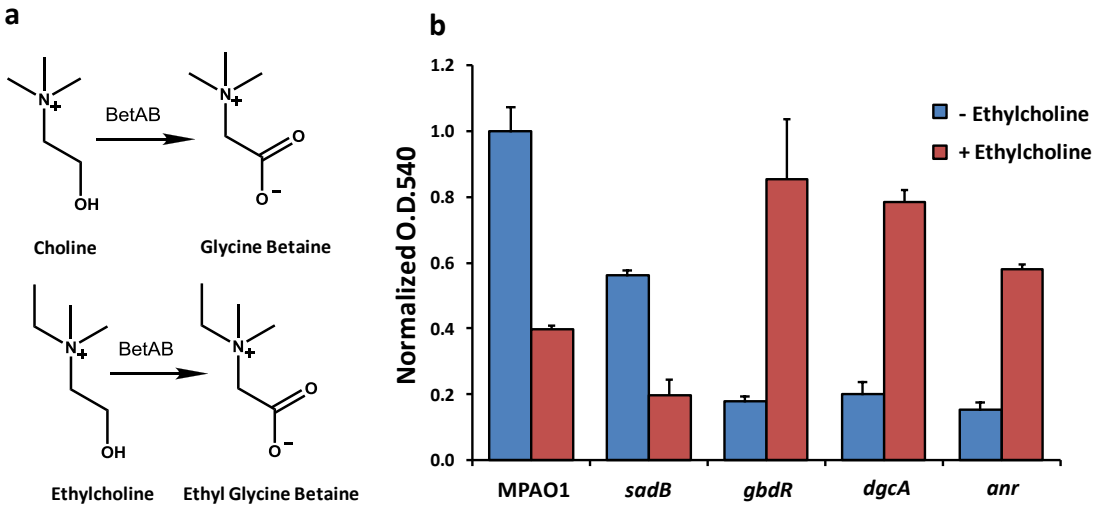

Figure 8.6: (a) Conversion of choline and ethylcholine into their respective zwitterionic forms in *P.aeruginosa* by BetAB. (b) 24 h biofilm formation of *P.aeruginosa* MPAO1 and various isogenic mutants with or without additional 1mM ethylcholine in the growth media. All O.D.540 readings from standard crystal violet staining were normalized to the result of the MPAO1 negative control.

Chapter 9. Conclusions

This thesis explores and investigates molecular engineering approaches against bacterial fouling, spore resistance as well as biofilm formation. Through the application of organic synthesis, polymer chemistry and microbiology, new scientific understandings and practical engineering solutions were obtained in this process.

The first part of the thesis (chapter 2~5) demonstrates the versatility of zwitterionic polymers as a molecular design platform. Chapter 2 shows an effective way to maximize the pH-responsive fouling and nonfouling behavior of zwitterionic polymer surfaces through total charge separation. Using the pH difference between zwitterionic polymer carboxylate pKa and the isoelectric point of bacterial cells (and potentially other biomacromolecules), it is possible to manipulate the interfacial behavior of cells and biomacromolecules using environmental pH as a cue. This pH responsive material property was shown through one example for biodetection, but same principle may also be applied for bioseperation processes. Chapter 3 offers one strategy to use zwitterionic polymers as a drug release platform. One defining difference between the reported functional zwitterionic hydrogels and other hydrogel-based drug release approaches lies in its capability to blend the strong charge of bioactive agents into a zwitterionic nonfouling material background. In addition to the high drug loading, this strategy may also find its application in the delivery of many short-circulation drugs. Chapter 4 demonstrates the feasibility to integrate zwitterionic moiety with other biologically functional segments. Though, in order to achieve optimal functionality, engineering

optimization will be needed, the presented case highlights the possibility to use zwitterionic-based materials for complicated and multi-staged biological processes. Lastly chapter 5 challenges the long-standing material design principle of equating bacterial fouling with non-specific protein adsorption by showing that different zwitterionic surfaces with very similar protein nonfouling property can have drastically different response to environmental cations and bacterial polysaccharide fouling. This discovery suggests the necessity to go beyond protein-level when designing and evaluating bacterial nonfouling materials.

The second part of thesis (chapter 6 and 7) explores the possible strategies to overcome the strong resistance of bacterial endospores. Through a chemical biology approach, chapter 6 provides evidence for spore cortex as a likely target for dodecylamine unusual sporecidal activity. The structural determinants for dodecylamine bioactivity were also elucidated in the study. This knowledge opens doors for future combinatorial-chemistry-assisted structure-activity relationship (SAR) study, and can eventually lead to the discovery of antispore compounds with high activity while avoiding the severe environmental toxicity of dodecylamine. Chapter 7 reports the strong synergy between low pH and anionic surfactants in breaching spore chemical resistance. Due to general availability and low toxicity of the chemicals, this engineering approach can be readily used for applications in various clinical scenarios as well as food industry.

The third and last part of this thesis (chapter 8) points to bacterial osmotic adaptation as a new target to design antivirulence drugs against P.aeruginsa biofilm formation through molecular design and a small-scaled chemical screening. Such antivirulence metabolites take forms of structural analogues to osmotic protectants or its direct synthetic precursor

(in this particular case, glycine betaine and choline). Compared to other existing antibiofilm approaches, these analogues have the advantages of being chemically simple (reduce the burden of creating a screening library) and generally low cytotoxicity (lower evolutionary selection pressure for bacterial resistance). However, to find a molecule that can interfere with biofilm establishment at a clinically-relevant potency, future structural optimization will still be needed. Also the effectiveness of this approach against biofilms of gram-positive bacterial species should also be tested experimentally.

Acknowledgements

I would love to thank all my friends and colleagues that have helped me in the past five and a half years. This includes too many names to be exhausted here. My particular gratitude goes to Dr. Hong Xue, Dr. Yuting Li, Dr. Jean Rene Ella, Dr. Qing Shao and Dr. Akihiro Ueda, whom I've had the honor of working with and whom I've learned so much from. I am indebted to Dr.Jiang for giving me the opportunity to work in a brand new field and granting me his trust to explore. I would also love to thank Dr. Lily Church, Dr. Dan Doug and Rebecca Foreman for helping me through the toughest times.

And, my mother, father and Jing, I dedicate this work to you.

Curriculum Vitae

Luo Mi was born and raised in Shanghai, China. Upon receiving his bachelor degree (2007) in biology from Shanghai Fudan Univeristy, he joined Texas A&M University microbiology PhD program. He spent one year studying bacterial physiology and molecular microbiology before moving to University of Washington and shifting his research focus on biomaterial and bioengineering.

Publications:

1. L. Mi & S. Jiang, Integrated antimicrobial and nonfouling zwitterionic polymers, Angew Chem Int Ed DOI: 10.1002/anie.201304060 (Journal IF: 13.7)

2. L. Mi, H. Xue, Y. Li & S. Jiang, A Thermoresponsive antimicrobial wound dressing hydrogel based on a cationic betaine ester, Advanced Functional Materials,21,4028 (2011).(Journal IF: 9.8)

3. L. Mi, M. Bernards, Q. Yu, G. Cheng & S. Jiang, Tunable and highly effective mixed charge polymer brushes to repel or release microorganisms and biomolecules, Biomaterials, 31, 2919 (2010).(Journal IF: 7.6)

4. L. Mi and S. Jiang, Synchronizing nonfouling and antimicrobial properties in a zwitterionic hydrogel, Biomaterials, 33, 8928 (2012). (Journal IF: 7.6)

5. L. Mi, M. Giarmarco, Q. Shao & S. Jiang, Divalent cation-mediated polysaccharide interactions with zwitterionic surfaces, Biomaterials, 33, 2001 (2012). (Journal IF: 7.6)

6. L. Mi, A. White, YQ. Li, P. Setlow & S. Jiang, Chemical insights into dodecylamine spore lethal germination. (Chemical Science under review)

7. L. Mi, G. Licina & S.Jiang, Concoction of an antispore cocktail (Submitted)

8. L. Mi, G. Licina & S.Jiang, Reducing *Pseudomonas aeruginosa* biofilm formation with osmoprotectant analogues (To be submitted)

9. C. J. Huang, L. Mi, and S. Jiang, Interactions of alginate-producing and-deficient *Pseudomonas aeruginosa* with zwitterionic polymers, Biomaterials, 33, 3626 (2012).

10. Z. Cao, L. Mi, J. Mendiola, J.-R. Ella-Menye, L. Zhang, H. Xue, & S. Jiang, Reversibly switching the function of a surface between attacking and defending against bacteria, Angew. Chem. Int. Ed. 50, 1 (2012)

11. G. Cheng, L. Mi, Z. Cao, H. Xue, Q. Yu, L. Carr & S. Jiang, Functionalizable and ultra-stable zwitterionic nanogels, Langmuir, 26, 6883 (2010).

12. L. Zhang, J. Xu, L. Mi, H. Gong, S. Jiang & Q. Yu, Multifunctional magnetic–plasmonic nanoparticles for fast concentration and sensitive detection of bacteria using SERS, Biosensors and Bioelectronics, 31, 130 (2012).

13. Q. Shao, L. Mi, , X. Han, Y. Li, T. Bai, S. Liu & S.Jiang Similarity in cationic and anionic charge strengths determines zwitterionic associations and stimuli responses (Submitted to JACS)

References

[1] Mah T-FC, O'Toole GA. Mechanisms of biofilm resistance to antimicrobial agents. Trends in Microbiology 2001;9(1):34-39.
[2] An YH, Friedman RJ. Concise review of mechanisms of bacterial adhesion to biomaterial surfaces. Journal of Biomedical Materials Research 1998;43(3):338-348.
[3] Ratner BD, Bryant SJ. Biomaterials: Where we have been and where we are going. Annual Review of Biomedical Engineering 2004;6(1):41-75.
[4] Kenawy E-R, Worley SD, Broughton R. The chemistry and applications of antimicrobial polymers: a state-of-the-art review. Biomacromolecules 2007;8(5):1359-1384.
[5] Zhang Z, Vaisocherova H, Cheng G, Yang W, Xue H, Jiang SY. Nonfouling behavior of polycarboxybetaine-grafted surfaces: structural and environmental effects. Biomacromolecules 2008;9(10):2686-2692.
[6] Amitai G, Murata H, Andersen JD, Koepsel RR, Russell AJ. Decontamination of chemical and biological warfare agents with a single multi-functional material. Biomaterials 2010;31(15):4417-4425.
[7] Wang Y, Jones EM, Tang Y, Ji E, Lopez GP, Chi EY, et al. Effect of polymer chain length on membrane perturbation activity of cationic phenylene ethynylene oligomers and polymers. Langmuir 2012;27(17):10770-10775.
[8] Haldar J, An D, Alvarez de Cienfuegos L, Chen J, Klibanov AM. Polymeric coatings that inactivate both influenza virus and pathogenic bacteria. Proc Natl Acad Sci 2006;103(47):17667-17671.
[9] Ostuni E, Chapman RG, Liang MN, Meluleni G, Pier G, Ingber DE, et al. Self-assembled monolayers that resist the adsorption of proteins and the adhesion of bacterial and mammalian cells. Langmuir 2001;17(20):6336-6343.
[10] Jiang S, Cao Z. Ultralow-fouling, functionalizable, and hydrolyzable zwitterionic materials and their derivatives for biological applications. Adv Mater 2010;22(9):920-932.
[11] Cheng G, Li GZ, Xue H, Chen SF, Bryers JD, Jiang SY. Zwitterionic carboxybetaine polymer surfaces and their resistance to long-term biofilm formation. Biomaterials 2009;30(28):5234-5240.
[12] Winter GD. Formation of the scab and the rate of epithelization of superficial wounds in the skin of the young domestic pig. Nature, 1962. 193(4812): p. 293-294.
[13] Hutchinson JJ, Occlusive dressings: A microbiologic and clinical review. Am J Infect Control, 1990. 18: p. 12.
[14] Banerjee I, Pangule RC, Kane RS. Antifouling coatings: recent developments in the design of surfaces that prevent fouling by proteins, bacteria, and marine organisms. Adv Mater 2011;23(6):690-718.
[15] Robinson JA, Trulear MG, Characklis WG. Cellular reporoduction and extracellular polymer formation by *Pseudomonas aeruginosa* in continuous culture. Biotechnol Bioeng 1984;26(12):1409-1417.

[16] Rode LJ, Foster JW. Germination of bacterial spores by long-chain alkyl amines. Nature 1960;188(4756):1132-1134.
[17] Quirynen M, Vansteenberghe D. Bacterial-colonization of the internal part of 2-stage implants - an *in vivo* Study. Clinical Oral Implants Research 1993;4(3):158-161.
[18] Persson LG, Lekholm U, Leonhardt A, Dahlen G, Lindhe J. Bacterial colonization on internal surfaces of Branemark System(R) implant components. Clinical Oral Implants Research 1996;7(2):90-95.
[19] Murphy TF, Sethi S. Bacterial-infection in chronic obstructive pulmonary-disease. American Review of Respiratory Disease 1992;146(4):1067-1083.
[20] Crump JA, Griffin PM, Angulo FJ. Bacterial contamination of animal feed and its relationship to human foodborne illness. Clinical Infectious Diseases 2002;35(7):859-865.
[21] Costerton JW, Stewart PS, Greenberg EP. Bacterial biofilms: A common cause of persistent infections. Science 1999;284(5418):1318-1322.
[22] Harden VP, Harris JO. The isoelectric point of bacterial cells. Journal of Bacteriology 1953;65(2):198-202.
[23] Rose SF, Okere S, Hanlon GW, Lloyd AW, Lewis AL. Bacterial adhesion to phosphorylcholine-based polymers with varying cationic charge and the effect of heparin pre-adsorption. Journal of Materials Science-Materials in Medicine 2005;16(11):1003-1015.
[24] Ostuni E, Chapman RG, Holmlin RE, Takayama S, Whitesides GM. A survey of structure-property relationships of surfaces that resist the adsorption of protein. Langmuir 2001;17(18):5605-5620.
[25] Chen SF, Zheng J, Li LY, Jiang SY. Strong resistance of phosphorylcholine self-assembled monolayers to protein adsorption: Insights into nonfouling properties of zwitterionic materials. J Am Chem Soc 2005;127(41):14473-14478.
[26] Cheng G, Zhang Z, Chen SF, Bryers JD, Jiang SY. Inhibition of bacterial adhesion and biofilm formation on zwitterionic surfaces. Biomaterials 2007;28(29):4192-4199.
[27] S. Chen, S. Jiang. An new avenue to nonfouling materials. Advanced Materials 2008;20(2):335-338.
[28] Chen S, Yu F, Yu Q, He Y, Jiang S. Strong resistance of a thin crystalline layer of balanced charged groups to protein adsorption. Langmuir 2006;22(19):8186-8191.
[29] Bernards MT, Cheng G, Zhang Z, Chen SF, Jiang SY. Nonfouling polymer brushes via surface-initiated, two-component atom transfer radical polymerization. Macromolecules 2008;41(12):4216-4219.
[30] Jones DM, Brown AA, Huck WTS. Surface-initiated polymerizations in aqueous media: effect of initiator density. Langmuir 2002;18(4):1265-1269.
[31] Zhang Z, Chen SF, Chang Y, Jiang SY. Surface grafted sulfobetaine polymers via atom transfer radical polymerization as superlow fouling coatings. Journal of Physical Chemistry B 2006;110(22):10799-10804.

[32] Gomez-Suarez C, Busscher HJ, van der Mei HC. Analysis of bacterial detachment from substratum surfaces by the passage of air-liquid interfaces. Applied and Environmental Microbiology 2001;67(6):2531-2537.
[33] Cao L, Sukavaneshvar S, Ratner BD, Horbett TA. Glow discharge plasma treatment of polyethylene tubing with tetraglyme results in ultralow fibrinogen adsorption and greatly reduced platelet adhesion. Journal of Biomedical Materials Research Part A 2006;79A(4):788-803.
[34] Schweiss R, Welzel PB, Werner C, Knoll W. Dissociation of surface functional groups and preferential adsorption of ions on self-assembled monolayers assessed by streaming potential and streaming current measurements. Langmuir 2001;17(14):4304-4311.
[35] Ruzicka F, Horka M, Hola V, Votava M. Capillary isoelectric focusing - useful tool for detection of the biofilm formation in *Staphylococcus epidermidis*. Journal of Microbiological Methods 2007;68(3):530-535.
[36] Kugler R, Bouloussa O, Rondelez F. Evidence of a charge-density threshold for optimum efficiency of biocidal cationic surfaces. Microbiology-Sgm 2005;151:1341-1348.
[37] Nejadnik MR, van der Mei HC, Busscher HJ, Norde W. Determination of the shear force at the balance between bacterial attachment and detachment in weak-adherence systems, using a flow displacement chamber. Applied and Environmental Microbiology 2008;74(3):916-919.
[38] Boks NP, Norde W, van der Meil HC, Busscher HJ. Forces involved in bacterial adhesion to hydrophilic and hydrophobic surfaces. Microbiology-Sgm 2008;154:3122-3133.
[39] Pasche S, Voros J, Griesser HJ, Spencer ND, Textor M. Effects of ionic strength and surface charge on protein adsorption at PEGylated surfaces. Journal of Physical Chemistry B 2005;109(37):17545-17552.
[40] Sirghi L, Nakagiri N, Sugimura H, Takai O. Analysis of atomic force curve data for mapping of surface properties in water. Japanese Journal of Applied Physics Part 1-Regular Papers Short Notes & Review Papers 2001;40(3A):1420-1424.
[41] Gristina A. Biomaterial-centered infection: microbial adhesion versus tissue integration. Science 1987;237(4822):1588-1595.
[42] Costerton JW, Montanaro L, Arciola CR. Biofilm in implant infections: its production and regulation. Int J Artif Organs 2005;28(11):1062-1068.
[43] Ratner BD, Hoffman AS, Schoen FJ, Lemons JE. Biomaterials science, an introduction to materials in medicine, 2nd ed. Amsterdam, Elsevier, 2004.
[44] Wach J-Y, Bonazzi S, Gademann K. Antimicrobial surfaces through natural product hybrids. Angew Chem Int Ed 2008;47(37):7123-7126.

[45] Cao Z, Mi L, Mendiola J, Ella-Menye J-R, Zhang L, Xue H, et al. Reversibly switching the function of a surface between attacking and defending against bacteria. Angew Chem Int Ed 2012;124(11):2656-2659.
[46] Cheng G, Xue H, Zhang Z, Chen S, Jiang S. A switchable biocompatible polymer surface with self-sterilizing and nonfouling capabilities. Angew Chem Int Ed 2008;47(46):8831-8834.
[47] Cheng G, Xue H, Li G, Jiang S. Integrated antimicrobial and nonfouling hydrogels to inhibit the growth of planktonic bacterial cells and keep the surface clean. Langmuir 2010;26(13):10425-10428.
[48] Bryers JD, Jarvis RA, Lebo J, Prudencio A, Kyriakides TR, Uhrich K. Biodegradation of poly(anhydride-esters) into non-steroidal anti-inflammatory drugs and their effect on *Pseudomonas aeruginosa* biofilms in vitro and on the foreign-body response in vivo. Biomaterials 2006;27(29):5039-5048.
[49] Zhang Z, Chao T, Chen S, Jiang S. Superlow fouling sulfobetaine and carboxybetaine polymers on glass slides. Langmuir 2006;22(24):10072-10077.
[50] Loll PJ, Garavito RM, Carrell CJ, Carrell HL. 2-bromoacetoxybenzoic acid, a brominated aspirin analog. Acta Crystallogr C 1996;52(2):375-377.
[51] Wright SW, Hageman DL, Wright AS, McClure LD. Convenient preparations of t-butyl esters and ethers from t-butanol. Tetrahedron Lett 1997;38(42):7345-7348.
[52] Weers JG, Rathman JF, Axe FU, Crichlow CA, Foland LD, Scheuing DR, et al. Effect of the intramolecular charge separation distance on the solution properties of betaines and sulfobetaines. Langmuir 1991;7(5):854-867.
[53] Hoare TR, Kohane DS. Hydrogels in drug delivery: progress and challenges. Polymer 2008;49(8):1993-2007.
[54] Lin C-C, Anseth K. PEG hydrogels for the controlled release of biomolecules in regenerative medicine. Pharm Res 2009;26(3):631-643.
[55] Sundaram HS, Cho Y, Dimitriou MD, Weinman CJ, Finlay JA, Cone G, et al. Fluorine-free mixed amphiphilic polymers based on PDMS and PEG side chains for fouling release applications. Biofouling 2011;27(6):589-602.
[56] Carr LR, Xue H, Jiang S. Functionalizable and nonfouling zwitterionic carboxybetaine hydrogels with a carboxybetaine dimethacrylate crosslinker. Biomaterials 2011;32(4):961-968.
[57] Wheeler JC, Woods JA, Cox MJ, Cantrell RW, Watkins FH, Edlich RF. Evolution of hydrogel polymers as contact lenses, surface coatings, dressings, and drug delivery systems. J Long Term Eff Med Implants, 1996. 6(3-4):207-217.
[58] Winter GD. Formation of the scab and the rate of epithelization of superficial wounds in the skin of the young domestic pig. Nature, 1962. 193(4812):293-294.
[59] Svensjo T, Pomahac B, Yao F, Slama J, Eriksson E. Accelerated healing of full-thickness skin wounds in a wet environment. Plast Reconstr Surg, 2000. 106(3):602-612.

[60] Balakrishnan B, Mohanty M, Umashankar PR, Jayakrishnan A. Evaluation of an in situ forming hydrogel wound dressing based on oxidized alginate and gelatin. Biomaterials, 2005. 26(32): 6335-6342.
[61] Ishihara M, Nakanishi K, Ono K, Kikuchi M, Saito Y, Yura H, Matsui T, Hattori H, Uenoyama M, Kurita A. Photocrosslinkable chitosan as a dressing for wound occlusion and accelerator in healing process. Biomaterials, 2002. 23(3): 833-840.
[62] Lu GZ, Ling K, Zhao P, Xu ZH, Deng C, Zheng H, Huang J, Chen JH. A novel in situ-formed hydrogel wound dressing by the photocross-linking of a chitosan derivative. Wound Repair Regen, 2010. 18(1): 70-79
[63] Escobar-Chávez J. Applications of thermo-reversible pluronic F-127 gels in pharmaceutical formulations. J Pharm Pharm Sci, 2006. 9(3): 20.
[64] Hutchinson JJ, Occlusive dressings: A microbiologic and clinical review. Am J Infect Control, 1990. 18: 12.
[65] Poon VKM, Burd A. In vitro cytotoxity of silver: implication for clinical wound care. Burns, 2004. 30(2): 140-147.
[66] Ong S-Y, Wu J, Moochhala SM, Tan MH, Lu J. Development of a chitosan-based wound dressing with improved hemostatic and antimicrobial properties. Biomaterials, 2008. 29(32): 4323-4332.
[67] Tettamanti G, Grimaldi A, Rinaldi L, Arnaboldi F, Congui T, Valvassori R, de Eguileor M. The multifunctional role of fibroblasts during wound healing in Hirudo medicinalis (Annelida, Hirudinea). Biology of the Cell, 2004. 96(6): 443-455.
[68] Ross R. The fibroblast and wound repair. Biol Rev, 1968. 43(1): 51-91.
[69] Schneider GB, English A, Abraham M, Zaharias R, Stanford C, Keller J. The effect of hydrogel charge density on cell attachment. Biomaterials, 2004. 25(15): 3023-3028.
[70] Fischer D, Li Y, Ahlemeyer B, Krieglstein J, Kissel T. *In vitro* cytotoxicity testing of polycations: influence of polymer structure on cell viability and hemolysis. Biomaterials 2003;24(7):1121-1131.
[71] Fujishige S, Kubota K, Ando I Phase transition of aqueous solutions of poly(N-isopropylacrylamide) and poly(N-isopropylmethacrylamide). J Phys Chem, 1989. 93(8): 3311-3313.
[72] Kirkland SE, Hensarling RM, McConaughy SD, Guo Y, Jarrett WL, McCormick CL. Thermoreversible hydrogels from RAFT-synthesized BAB triblock copolymers: steps toward biomimetic matrices for tissue regeneration. Biomacromolecules, 2007. 9(2): 481-486.
[73] Carlsson R, Engvall E, Freeman A, Ruoslahti E. Laminin and fibronectin in cell adhesion: enhanced adhesion of cells from regenerating liver to laminin. Proc Natl Acad Sci U S A, 1981. 78(4): 2403-2406.
[74] Zhang Z, Cheng G, Carr LR, Visocherova H, Chen S, Jiang S. The hydrolysis of cationic polycarboxybetaine esters to zwitterionic polycarboxybetaines with controlled properties. Biomaterials, 2008. 29(36): 4719-4725.

[75] Feil H. Bae YH, Feijen J, Kim SW. Effect of comonomer hydrophilicity and ionization on the lower critical solution temperature of N-isopropylacrylamide copolymers. Macromolecules, 1993. 26(10): 2496-2500.
[76] Lai, J.T., D. Filla, and R. Shea, functional polymers from novel carboxyl-terminated trithiocarbonates as highly efficient RAFT agents. Macromolecules, 2002. 35(18): 6754-6756.
[77] Convertine AJ, Ayres N, Scales CW, Lowe AB McCormick CL. Facile, controlled, room-temperature RAFT polymerization of N-isopropylacrylamide. Biomacromolecules, 2004. 5(4): 1177-1180.
[78] Makarand RRB, Risbud V. Polyacrylamide-chitosan hydrogels: in vitro biocompatibility and sustained antibiotic release studies. Drug Deliv, 2000. 7(2): 69-75
[79] Fotakis G, Timbrell JA. In vitro cytotoxicity assays: comparison of LDH, neutral red, MTT and protein assay in hepatoma cell lines following exposure to cadmium chloride. Toxicol Lett, 2006. 160(2): 171-177.
[80] Raspaud E, Lairez D, Adam M, Carton JP. Triblock copolymers in a selective solvent. 1. aggregation process in dilute solution. Macromolecules, 1994. 27(11): 2956-2964.
[81] Ten Brinke G, Hadziioannou G. Topological constraints and their influence on the properties of synthetic macromolecular systems. 2. Micelle formation of triblock copolymers. Macromolecules, 1987. 20(3): 486-489.
[82] Schaller A, Guo M, Gisanrin O, Yang Y. *Escherichia coli* genes involved in resistance to pyrazinoic acid, the active component of the tuberculosis drug pyrazinamide. FEMS Microbiol Lett, 2002. 211(2): 265-270.
[83] Makarand RRB, Risbud V. Polyacrylamide-chitosan hydrogels: in vitro biocompatibility and sustained antibiotic release studies. Drug Deliv, 2000. 7(2): 69-75.
[84] Heath MD, Henderson B, Perkin S. Ion-Specific Effects on the Interaction between Fibronectin and Negatively Charged Mica Surfaces. Langmuir, 2010. 26(8): 5304-5308.
[85] Carlson MA, Longaker MT. The fibroblast-populated collagen matrix as a model of wound healing: a review of the evidence. Wound Repair Regen, 2004. 12(2): 134-147.
[86] Steele JG, Dalton BA, Johnson G, Underwood PA. Polystyrene chemistry affects vitronectin activity: An explanation for cell attachment to tissue culture polystyrene but not to unmodified polystyrene. J Biomed Mater Res, 1993. 27(7): 927-940.
[87] Steele JG, McFarland C, Dalton BA, Johnson G, Evans MD, Howlett CR, Underwood PA. Attachment of human bone cells to tissue culture polystyrene and to unmodified polystyrene: the effect of surface chemistry upon initial cell attachment. J Biomater Sci Polym Ed, 1994. 5: 245-257.
[88] Banerjee I, Pangule RC, Kane RS. Antifouling coatings: recent developments in the design of surfaces that prevent fouling by proteins, bacteria, and marine organisms. Adv Mater 2011;23(6):690-718.

[89] Park KD, Kim YS, Han DK, Kim YH, Lee EHB, Suh H, et al. Bacterial adhesion on PEG modified polyurethane surfaces. Biomaterials 1998;19(7-9):851-859.
[90] Saldarriaga Fernandez IC, van der Mei HC, Lochhead MJ, Grainger DW, Busscher HJ. The inhibition of the adhesion of clinically isolated bacterial strains on multi-component cross-linked poly(ethylene glycol)-based polymer coatings. Biomaterials 2007;28(28):4105-4112.
[91] Kingshott P, Wei J, Bagge-Ravn D, Gadegaard N, Gram L. Covalent attachment of poly(ethylene glycol) to surfaces, critical for reducing bacterial adhesion. Langmuir 2003;19(17):6912-6921.
[92] Krishnan S, Weinman CJ, Ober CK. Advances in polymers for anti-biofouling surfaces. J Mater Chem 2008;18(29):3405-3413.
[93] Ian WS. Microbial polysaccharides from Gram-negative bacteria. Int Dairy J 2001;11(9):663-674.
[94] Allison DG, Sutherland IW. The role of exopolysaccharides in adhesion of freshwater bacteria. J Gen Microbiol 1987;133(5):1319-1327.
[95] Vuong C, Kocianova S, Voyich JM, Yao Y, Fischer ER, DeLeo FR, et al. A crucial role for exopolysaccharide modification in bacterial biofilm formation, immune evasion, and virulence. J Biol Chem 2004;279(52):54881-54886.
[96] Strathmann M, Wingender J, Flemming H-C. Application of fluorescently labelled lectins for the visualization and biochemical characterization of polysaccharides in biofilms of *Pseudomonas aeruginosa*. J Microbiol Methods 2002;50(3):237-248.
[97] Sutherland IW. Biosynthesis and composition of gram-negative bacterial extracellular and wall polysaccharides. Annu Rev Microbiol 1985;39(1):243-270.
[98] Yang W, Xue H, Li W, Zhang J, Jiang S. Pursuing zero protein adsorption of poly(carboxybetaine) from undiluted blood serum and plasma. Langmuir 2009;25(19):11911-11916.
[99] Boyd A, Chakrabarty AM. *Pseudomonas aeruginosa* biofilms: role of the alginate exopolysaccharide. Ind Microbiol Biotechnol 1995;15(3):162-168.
[100] Fett WF, Osman SF, Dunn MF. Characterization of exopolysaccharides produced by plant-associated fluorescent pseudomonads. Appl Environ Microbiol 1989;55(3):579-583.
[101] Frisch MJ, Trucks GW, Schlegel HB, Scuseria GE, Robb MA, Cheeseman JR, et al. Gaussian, Inc., Wallingford CT, Gaussian 09, Revision A.1, 2009.
[102] Rappe AK, Casewit CJ, Colwell KS, Goddard WA, Skiff WM. UFF, a full periodic table force field for molecular mechanics and molecular dynamics simulations. J Am Chem Soc 1992;114(25):10024-10035.
[103] Yang W, Chen S, Cheng G, Vaisocherova H, Xue H, Li W, et al. Film thickness dependence of protein adsorption from blood serum and plasma onto poly(sulfobetaine)-grafted surfaces. Langmuir 2008;24(17):9211-9214.

[104] Kwak D, Wu Y, Horbett TA. Fibrinogen and von Willebrand's factor adsorption are both required for platelet adhesion from sheared suspensions to polyethylene preadsorbed with blood plasma. J Biomed Mater Res A 2005;74A(1):69-83.
[105] Huskens J, Main M, Malloy CR, Sherry AD. The determination of magnesium in human blood plasma by 31P magnetic resonance spectroscopy using a macrocyclic reporter ligand. Biochim Biophys Acta - General Subjects 1997;1336(3):434-444.
[106] Lattner D, Flemming H-C, Mayer C. 13C-NMR study of the interaction of bacterial alginate with bivalent cations. Int J Biol Macromol 2003;33(1-3):81-88.
[107] Lyons JW, Kotin L. The effect of magnesium ion on the secondary structure of deoxyribonucleic acid. J Am Chem Soc 1965;87(8):1781-1785.
[108] Reichmuth DS, Kirby BJ. Effects of ammonioalkyl sulfonate internal salts on electrokinetic micropump performance and reversed-phase high-performance liquid chromatographic separations. J Chromatogr A 2003;1013(1-2):93-101.
[109] Collins KD. Ions from the Hofmeister series and osmolytes: effects on proteins in solution and in the crystallization process. Methods 2004;34(3):300-311.
[110] Collins KD. Ion hydration: Implications for cellular function, polyelectrolytes, and protein crystallization. Biophys Chem 2006;119(3):271-281.
[111] Vlachy N, Jagoda-Cwiklik B, Vacha R, Touraud D, Jungwirth P, Kunz W. Hofmeister series and specific interactions of charged headgroups with aqueous ions. Adv Colloid Interface Sci 2009;146(1-2):42-47.
[112] Kunz W. Specific ion effects in colloidal and biological systems. Curr Opin Colloid Interface Sci 2010;15(1-2):34-39.
[113] Setlow P. Spores of *Bacillus subtilis*: their resistance to and killing by radiation, heat and chemicals J. Appl. Microbiol. 2006; 101(3):514-525.
[114] Gould GW. History of science--spores. J. Appl. Microbiol. 2006;101(3):507-513.
[115] Rode LJ, Foster JW. Germination of bacterial spores with alkyl primary amines. J. Bacteriol. 1961; 81(5):768-779.
[116] Beaman TC, Gerhardt P, Heat resistance of bacterial spores correlated with protoplast dehydration, mineralization, and thermal adaptation. Appl. Environ. Microbiol. 1986;52(6):1242-1246.
[117] Stewart GSAB, Eaton MW, Johnstone K, Barrett MD, Ellar DJ. An investigation of membrane fluidity changes during sporulation and germination of *Bacillus megaterium* K.M. measured by electron spin and nuclear magnetic resonance spectroscopy. Biochim. Biophys. Acta. 1985;600(2):270-290.
[118] Gould GW, Dring GJ. Heat resistance of bacterial endospores and concept of an expanded osmoregulatory cortex. Nature 1975;258(5534):402-405.
[119] Bhothipaksa K, Busta FF. Osmotically induced increase in thermal resistance of heat-sensitive, dipicolinic acid-less spores of Bacillus cereus Ht-8. Appl. Environ. Microbiol. 1978;35(4):800-808.

[120] Curran HR, Influence of osmotic pressure upon spore germination. J. Bacteriol. 1931;21(3):197-209.
[121] Atrih A, Foster SJ. The role of peptidoglycan structure and structural dynamics during endospore dormancy and germination. Antonie van Leeuwenhoek 1999;75(4): 299-307.
[122] Gerhardt P, Black SH. Permeability of bacterial spores II. J. Bacteriol. 1961;82(2):750-760.
[123] Rode LJ, Foster JW. The action of surfactants on bacterial spores. Arch. Microbiol. 1960:36(1):67-94.
[124] Material safety data sheet: http://fscimage.fishersci.com/msds/11741.htm 2007.
[125] Bernatowicz MS, Wu Y, Matsueda GR. 1H-Pyrazole-1-carboxamidine hydrochloride an attractive reagent for guanylation of amines and its application to peptide synthesis. J. Org. Chem. 1992;57(8):2497-2502.
[126] Deng Z, et al. Facile synthesis of controlled-structure primary amine-based methacrylamide polymers via the reversible addition-fragmentation chain transfer process J. Polym. Sci. A Polym. Chem. 2008;46(15):4984-4996.
[127] He L, Read ES, Armes SP, Adams DJ. Direct synthesis of controlled-structure primary amine-based methacrylic polymers by living radical polymerization. Macromolecules 2007;40(13):4429-4438.
[128] Damm W, Frontera A, Tirado-Rives J, Jorgensen WL. OPLS all-atom force field for carbohydrates. J. Comput. Chem. 1997;18(16):1955-1970.
[129] Parrinello M, Rahman A. Polymorphic transitions in single crystals: A new molecular dynamics method. J. Appl. Phys. 1981;52(12):7182–7190.
[130] Bussi G, Donadio D, Parrinello M, Canonical sampling through velocity rescaling. J. Chem. Phys. 2007;126(1):014101–014108.
[131] Essmann U, et al. A smooth particle mesh Ewald method. J. Chem. Phys. 1995:103(19):8577–8593.
[132] Hess B, Bekker H, Berendsen HJC, Fraaije JGEM. LINCS: A linear constraint solver for molecular simulations. J. Comput. Chem. 1997;18(12):1463–1472.
[133] D. Van Der Spoel, et al. GROMACS: fast, flexible, and free. J. Comput. Chem. 2005;26(16):1701–1718.
[134] Springs B, Haake P. Equilibrium constants for association of guanidinium and ammonium ions with oxyanions: The effect of changing basicity of the oxyanion. Bioorg. Chem. 1977;6(2):181-190.
[135] Lawrence CA. Mechanism of action and neutralizing agents for surface-active materials upon microorganisms. Ann. N. Y. Acad. Sci. 1950;53(1):66-75.
[136] Perrin DD, Dissociation constants of organic bases in aqueous solution (Butterworths, London, 1965; Supplement, 1972).

[137] Moncelli MR, Becucci L, Guidelli R. The intrinsic pKa values for phosphatidylcholine, phosphatidylethanolamine, and phosphatidylserine in monolayers deposited on mercury electrodes. Biophys. J. 1994;66(6):1969-1980.
[138] Gustafson RL, Lirio JA. Interaction of cross-linked polymethacrylic acid with polyvalent metal ions. J. Phys. Chem. 1965;69(9):2849-2856.
[139] Gustafson RL, Lirio JA. Binding of divalent metal ions by crosslinked polyacrylic acid. J. Phys. Chem. 1968;72(5):1502-1505.
[140] Meot-Ner M. The ionic hydrogen bond. Chem. Rev. 2005;105(1):213-284.
[141] Fersht AR, et al. Hydrogen bonding and biological specificity analysed by protein engineering. Nature. 1985;314(6008):235-238.
[142] Bissantz C, Kuhn B, Stahl M. A medicinal chemist's guide to molecular interactions. J. Med. Chem. 2010;53(16):5061-5084.
[143] Mammen M, Choi S-K, Whitesides GM. Polyvalent interactions in biological systems: implications for design and use of multivalent ligands and inhibitors. Angew. Chem. Int. Ed. Engl. 1998;37(20):2754-2794.
[144] Barnard A, Smith DK. Self-assembled multivalency: dynamic ligand arrays for high-affinity binding. Angew. Chem. Int. Ed. Engl. 2012;51(27):6572-6581.
[145] Herzfeld SH, Corrin ML, Harkins WD. The effect of alcohols and of alcohols and salts on the critical micelle concentration of dodecylammonium chloride. J. Phys. Colloid. Chem. 1950;54(2):271-283.
[146] Ghose AK, Crippen GM. Atomic physicochemical parameters for three-dimensional-structure-directed quantitative structure-activity relationships. 2. Modeling dispersive and hydrophobic interactions. J. Chem. Inf. Model. 1987;27(1):21-35.
[147] Setlow B, Cowan AE, Setlow P. Germination of spores of *Bacillus subtilis* with dodecylamine. J. Appl. Microbiol. 2003;95(3):637-648.
[148] Swerdlow BM, Setlow B, Setlow P. Levels of H^+ and other monovalent cations in dormant and germinating spores of *Bacillus megaterium*. J. Bacteriol. 1981;148(1):20-29.
[149] Vepachedu VR, Setlow P. Role of SpoVA proteins in release of dipicolinic acid during germination of *Bacillus subtilis* spores triggered by dodecylamine or lysozyme. J. Bacteriol. 2007;189(5):1565-1572.
[150] Lewis JC, Snell NS, Burr HK. Water permeability of bacterial spores and the concept of a contractile cortex. Science 1960;132(3426):544-545.
[151] Alderton G, Snell N. Bacterial spores: chemical sensitization to heat. Science 1969; 163(3872):1212-1213.
[152] McKenney PT, Driks AP, Eichenberger P. The *Bacillus subtilis* endospore: assembly and functions of the multilayered coat. Nat. Rev. Micro. 2013;11(1):33-44.
[153] United States Centers for Disease Control and Prevention (CDC). Guideline for Disinfection and Sterilization in Healthcare Facilities 2008, 108-111.
[154] Hyatt MT, Levinson HS. Interaction of heat, glucose, L-alanine, and potassium nitrate in spore germination of *Bacillus megaterium*. J. Bacteriol. 1961, 81(2), 204-211.

[155] Setlow B, Loshon CA, Genest PC, Cowan AE, Setlow C, Setlow P. Mechanisms of killing spores of *Bacillus subtilis* by acid, alkali and ethanol. J. Appl. Microbiol. 2002;92(2):362-375.
[156] Costerton JW. Cystic fibrosis pathogenesis and the role of biofilms in persistent infection. Trends in Microbiology, 2001;9(2):50-52.
[157] Singh PK, et al., Quorum-sensing signals indicate that cystic fibrosis lungs are infected with bacterial biofilms. Nature, 2000;407(6805):762-764.
[158] Davies D. Understanding biofilm resistance to antibacterial agents. Nat. Rev. Drug Discov, 2003;2(2):114-122.
[159] Brooun A, Liu S, and Lewis K, A dose-response study of antibiotic resistance in *Pseudomonas aeruginosa* biofilms. Antimicrob. Agents Chemother. 2000;44(3):640-646.
[160] Hoffman LR, et al., Aminoglycoside antibiotics induce bacterial biofilm formation. Nature 2005;436(7054):1171-1175.
[161] Neu HC. The crisis in antibiotic resistance. Science 1992;257(5073):1064-1073.
[162] Martinez JL, Baquero F. Mutation frequencies and antibiotic resistance. Antimicrob. Agents Chemother. 2000;44(7):1771-1777.
[163] Rasko DA, Sperandio V. Anti-virulence strategies to combat bacteria-mediated disease. Nat. Rev. Drug Discov. 2010;9(2):117-128.
[164] Mellbye B, Schuster M. The sociomicrobiology of antivirulence drug resistance: a proof of concept. mBio. 2011;2(5).
[165] Allen RC, et al., Targeting virulence: can we make evolution-proof drugs? Nat. Rev. Micro. 2014;12(4):300-308.
[166] Musken M, et al., Genetic determinants of *Pseudomonas aeruginosa* biofilm establishment. Microbiology. 2010;156(2):431-441. (a comprehensive list of critical genes for biofilm formation, including genes involved in glycine betaine catabolism pathway, can be found in supplementary material Table S1)
[167] Banin E, Vasil ML, Greenberg EP. Iron and *Pseudomonas aeruginosa* biofilm formation. PNAS 2005;102(31):11076-11081.
[168] Prigent-Combaret C, et al., Abiotic surface sensing and biofilm-dependent regulation of gene expression in *Escherichia coli*. J. Bacteriol. 1999;181(19):5993-6002.
[169] Seminara A, et al., Osmotic spreading of *Bacillus subtilis* biofilms driven by an extracellular matrix. PNAS 2011;109(4):1116-1121.
[170] Csonka LN. Physiological and genetic responses of bacteria to osmotic stress. Microbiol. Rev. 1989;53(1):121-147.
[171] Wargo MJ. Homeostasis and catabolism of choline and glycine betaine: lessons from *Pseudomonas aeruginosa*. Appl. Environ. Microbiol. 2013;79(7):2112-2120.
[172] Fitzsimmons LF, et al., Small-molecule inhibition of choline catabolism in *Pseudomonas aeruginosa* and other aerobic choline-catabolizing bacteria. Appl. Environ. Microbiol. 2011;77(13):4383-4389.

[173] Jacobs MA. et al., Comprehensive transposon mutant library of *Pseudomonas aeruginosa*. PNAS 2003;100(24):14339-14344.
[174] Daglia M, et al., Antiadhesive effect of green and roasted coffee on *Streptococcus mutans'* adhesive properties on saliva-coated hydroxyapatite beads. J. Agric. Food Chem., 2002;50(5):1225-1229.
[175] Hayes KC. A review on the biological function of taurine. Nutr. Rev. 1976. 34(6):161-165.
[176] Klockgether J, et al., Genome diversity of *Pseudomonas aeruginosa* PAO1 laboratory strains. J. Bacteriol. 2010;192(4):1113-1121.
[177] Hampel KJ, et al., Characterization of the GbdR regulon in *Pseudomonas aeruginosa*. J. Bacteriol. 2014;196(1):7-15.
[178] Jackson AA, et al., Anr and its activation by PlcH activity in *Pseudomonas aeruginosa* host colonization and virulence. J. Bacteriol. 2013;195(13):3093-3104.
[179] Caiazza NC, et al., Inverse regulation of biofilm formation and swarming motility by *Pseudomonas aeruginosa* PA14. J. Bacteriol. 2007;189(9):3603-3612.